

Hierarchy of bounds in free orthotropic material optimization: From convex relaxations to Hashin–Shtrikman via sequential global programming

Marek Tyburec^{a,*}, Michael Stingl^b, Shenyan Ma^c

^a*Experimental Center, Faculty of Civil Engineering, Czech Technical University in Prague, Czech Republic*

^b*Department of Mathematics, Friedrich-Alexander-University, Erlangen-Nürnberg, Germany*

^c*Department of Mechanics, Faculty of Civil Engineering, Czech Technical University in Prague, Czech Republic*

Abstract

We study free orthotropic material optimization for two-dimensional plane-stress compliance minimization with two well-ordered isotropic phases, motivated by the gap between tensors admissible in classical free-material optimization and tensors realizable by composites. To reduce this gap, we construct a hierarchy of realizability-aware admissible sets induced by zeroth-order, Voigt, and Hashin–Shtrikman (HS) energy bounds, moving from convex relaxations to a tighter nonconvex model. In the convex zeroth-order and Voigt settings, the Voigt set is strictly tighter for intermediate volume fractions and coincides with the zeroth-order set at pure-phase endpoints, and the Voigt model reduces to an isotropic variable-thickness-sheet formulation. In the single-loadcase continuum zeroth-order problem, at least one optimal solution can be chosen orthotropic. For HS constraints, we rewrite the bound as a Voigt term minus a nonnegative correction, clarifying strict tightening for interior volume fractions and local nonconvexity. We further prove that the convex hull of the HS feasible set equals the Voigt set and derive reduced formulations via active-constraint analysis and explicit elementwise volume characterization, including reductions specialized to orthotropic effective tensors. In the single-loadcase continuum setting, the HS relaxation is tight with the Allaire–Kohn relaxed problem, attained in the relaxation sense by sequential laminates, whereas in generic multi-loadcase settings it provides a lower bound on optimal compliance over general microstructures. The resulting nonconvex orthotropic HS problem is solved by sequential global programming, and numerical results confirm the predicted compliance hierarchy and show close agreement with finite-rank laminate references.

Keywords: free material optimization, orthotropic materials, Hashin–Shtrikman bounds, realizability-aware design, sequential global programming, sequential laminates

1. Introduction

Free material optimization (FMO) is a class of topology-optimization methods in which the elasticity tensor field is directly optimized. By treating the local constitutive response as the design variable, FMO offers significantly greater design freedom than density-based topology optimization with prescribed material interpolation laws [43, 13, 14, 54].

Typically, FMO formulations impose positive semidefiniteness of elasticity tensors and invariant-based material-budget constraints. These constraints control stiffness magnitude, but they do not directly characterize phase-wise realizability as effective properties of composites with prescribed constituent phases [52, 49]. A complementary asymptotic result is due to Milton and Cherkaev [38]: in the extreme high-contrast limit, arbitrary positive-definite effective tensors can be realized by hierarchical constructions. However, this asymptotic realizability result does not by itself provide computable finite-contrast admissible sets for fixed constituent phases.

*Corresponding author

This paper addresses the fixed-phase inverse question relevant for material-constrained design: for given well-ordered isotropic phases, which effective tensors are admissible in the model? We pursue this question through computable admissible sets induced by energy bounds and organize them into a hierarchy: zeroth-order, Voigt, and Hashin–Shtrikman bounds. This hierarchy provides progressively tighter, realizability-informed relaxations, but it does not provide a complete characterization of realizability in general. We focus on orthotropy because, in the two-dimensional anisotropic setting, bound-attaining laminate constructions are orthotropic [5, 3], making orthotropy both physically motivated and analytically tractable.

The remainder of this introduction is organized as follows: Section 1.1 reviews FMO, Section 1.2 recalls energy-based bounds, Section 1.3 summarizes homogenization-based optimization, and Section 1.4 states the aims and contributions.

1.1. Free material optimization

Early FMO formulations combined compliance minimization with invariant-based resource constraints on positive-semidefinite constitutive tensors, typically using trace- or Frobenius-type measures. This includes the constitutive-matrix model of Ringertz [43]. Building on that setting, Bendsøe et al. [13] derived analytical local optimal-material laws and a reduced single-loadcase formulation, while Bendsøe et al. [14] extended the framework to multiple independent loadcases via weighted mean compliance. These formulations were later cast in mathematical-programming form for multiple loadcases and contact settings by Zowe et al. [54]. This line culminated in semidefinite-programming formulations of worst-case compliance minimization under multiple loadcases and contact constraints, together with accompanying existence results [10]. Overview articles [29, 33] document this shift from early constitutive formulations to linear and nonlinear semidefinite programming approaches.

The framework was subsequently extended in several practically relevant directions. Formulations with local stress constraints, together with tailored scalable numerical solution methods, were developed in [31, 32]. Vibration requirements were addressed by imposing constraints on the fundamental eigenfrequency [48]. On the theoretical side, Haslinger et al. [26] established existence and convergence results for such multidisciplinary extensions using H -convergence. In parallel, stress-based trace-constrained free material formulations were developed for single and multiple loadcases [22, 23]. These developments were further unified across anisotropic, isotropic, and fixed-Poisson-ratio settings [34] and generalized within admissible-cone frameworks with existence analysis [17]. A recent isotropic specialization reformulates the trace-constrained problem as second-order cone programming [53].

Despite this breadth, most FMO formulations share a common structural feature: admissibility is primarily encoded through positive-semidefiniteness and trace- or Frobenius-norm-based material-resource constraints. These conditions control stiffness levels but do not directly characterize phase-wise realizability for fixed constituent phases.

1.2. Energy-based bounds

To address the realizability gap left by FMO formulations that control material usage through invariant-based measures, one can use admissible sets induced by energy bounds for two-phase composites. Classical interval estimates of Voigt and Reuss type were discussed for reinforced solids by Hill [27], and substantially tightened by the Hashin–Shtrikman variational framework [25]. For two isotropic phases with prescribed volume fractions, Avellaneda [9] established optimal bounds for imposed uniform strain or stress ensembles and proved attainability by finite-rank laminates, making the link between optimal bounds and realizable microgeometries explicit.

This framework was then sharpened in directions directly relevant here. Allaire and Kohn [5] treated mixtures of two possibly anisotropic well-ordered phases and derived optimal upper and lower bounds for elastic and complementary energies (and related sums of energies), with parallel Hashin–Shtrikman and translation-method interpretations. In the two-dimensional isotropic two-phase case, Allaire and Kohn [3] gave explicit optimal formulas and attainability results that also cover non-well-ordered regimes. In the orthotropic setting, Lipton [35] derived optimal correlated bounds for the six independent orthotropic effective moduli of two well-ordered isotropic phases and identified finite-rank orthotropic laminates that attain these bounds.

Later work focused on turning bound theory into optimization-ready ingredients. Bendsøe and Sigmund [12] analyzed interpolation schemes through the lens of energy bounds and realizability constraints, clarifying the modeling role of Voigt-type and Reuss-Voigt-type descriptions versus tighter Hashin–Shtrikman-consistent descriptions. Burazin et al. [20] derived explicit lower Hashin–Shtrikman complementary-energy formulas in 2D well-ordered settings, and later provided explicit 3D Hashin–Shtrikman upper primal and lower complementary bounds together with saturating laminate constructions in [21]. At the opposite end, Lobos and Böhlke [36] revisited constituent-only zeroth-order bounds, provided lower-bound constructions, and derived explicit bounds for individual tensor components. A broad synthesis of variational bounds, translation methods, attainability, and G -closure viewpoints is provided by Milton [37].

1.3. Homogenization-based optimization

Building on these energy bounds and microstructures attaining them, the homogenization literature developed topology optimization formulations in which microstructured composites appear as relaxed design variables. The seminal contribution of Bendsøe and Kikuchi [11] introduced a material-distribution approach on a fixed reference domain, where design variables parameterized effective anisotropic properties of periodic rectangular-hole cells, thereby avoiding repeated remeshing while permitting topology changes. In a related relaxed setting, Allaire and Kohn [4] considered a plane-stress formulation with a weighted objective combining compliance and mass through extremal microstructures and used an alternating-minimization stress-based framework. In a complementary setting, Jog et al. [28] restricted the admissible composites to rank-2 laminates, analytically eliminated microstructural variables through a sequence of reduced optimization problems, and solved the resulting mixed finite-element formulation with coupled macroscopic-microscopic updates.

The same period also established inverse and multi-loadcase perspectives. Sigmund [46] formulated inverse homogenization, namely the optimization of a periodic base cell to match prescribed effective constitutive properties. Allaire et al. [6] extended homogenization-based optimization to multiple loadcases, emphasizing that explicit optimal composite parameters available in single-loadcase settings are not available in the multi-loadcase regime. This direction was strengthened in [7], which proved a general relaxation result in two and three dimensions and introduced a penalized topology-optimization algorithm to recover classical phase-separated designs. Allaire [1] consolidated these developments into a unified framework linking nonexistence of classical minimizers, relaxation by homogenization, and practical numerical algorithms. In the same framework of alternating minimization and sequential laminates, Burazin et al. [20] derived a 2D optimality-criteria method for compliance minimization using explicit lower Hashin–Shtrikman complementary-energy bounds for laminates made of two well-ordered isotropic phases, while Burazin and Crnjac [19] extended this strategy to 3D settings and combined it with penalization to recover classical designs.

Finally, dehomogenization and projection methods have addressed the reconstruction of manufacturable designs from relaxed optima. Pantz and Trabelsi [41] proposed a post-treatment that projects not only density but also lamination information, producing single-scale geometries with controlled detail. Groen and Sigmund [24] simplified and scaled this idea to high-resolution manufacturable lattices with performance close to homogenization-based predictions. Allaire et al. [8] improved optimization-projection consistency for modulated periodic microstructures, including conformal orientation treatment through a harmonic angle field.

1.4. Aims and contributions

The aim of this paper is to develop a realizability-aware free material optimization framework for two well-ordered isotropic phases in plane stress, and to clarify what is gained when moving from zeroth-order constraints to Voigt and then to Hashin–Shtrikman (HS) admissible sets. We make this progression explicit through a pointwise inclusion hierarchy and use it as the organizing principle of both the analysis and the algorithms.

To achieve this aim, the main contributions of this work are:

1. We formulate a realizability-aware free material optimization framework for two-dimensional plane stress, organized as a hierarchy of admissible sets induced by zeroth-order, Voigt, and HS energy bounds. We establish well-posedness by proving existence of minimizers for the zeroth-order and Voigt models and existence in the H -relaxed sense for the HS model.
2. For the convex zeroth-order and Voigt models, we prove strict inclusion of admissible sets for intermediate volume fractions and coincidence at pure-phase endpoints. We also prove that the Voigt model reduces to an isotropic variable-thickness-sheet formulation, and that in the single-loadcase continuum zeroth-order setting an optimal solution can be chosen orthotropic.
3. For HS constraints, we derive an explicit Voigt-minus-correction representation of the energy bound and prove that the convex hull of the HS feasible set equals the Voigt admissible set. We further derive reduced HS formulations via active-constraint analysis and explicit elementwise volume characterization, with dedicated reductions for orthotropic effective tensors.
4. We prove that in the two-dimensional single-loadcase continuum setting with well-ordered isotropic phases, the HS relaxation is tight with respect to the Allaire–Kohn relaxed problem. For generic multi-loadcase configurations, we clarify that the model provides a lower bound on compliance minimization over general microstructures.
5. We develop a sequential global programming method for the resulting nonconvex orthotropic HS problem and validate the hierarchy numerically across phase contrasts and mesh resolutions, confirming the predicted compliance ordering and close agreement with finite-rank laminate references.

The paper is organized as follows. Section 2 introduces notation, and Section 3.1 presents the continuum formulation of the problem together with existence results. Sections 3.2–3.4 then develop the zeroth-order, Voigt, and Hashin–Shtrikman model classes, with inclusion relations, geometric properties, and reduced formulations. Section 3.5 introduces the orthotropic Hashin–Shtrikman formulation. Section 3.6 presents the sequential global programming strategy for the resulting nonconvex optimization problem, while Section 3.7 describes the alternating-minimization laminate-based method used for single-loadcase comparison. Finally, Section 4 reports numerical experiments, and Section 5 concludes.

2. Notation

We focus on the planar setting, $d = 2$, and adopt the following conventions for the notation used throughout the paper. Vectors and matrices are written in boldface sans-serif font. Vectors are written in lowercase, e.g., $\mathbf{u} \in \mathbb{R}^n$, and matrices in uppercase, e.g., $\mathbf{A} \in \mathbb{R}^{m \times n}$. Tensors are written in boldface serif font. First-order tensors are written in lowercase italics, e.g., \boldsymbol{x} . For second-order tensors we use lowercase upright, e.g., $\boldsymbol{\varepsilon} \in \mathbb{R}^{d \times d}$, while fourth-order tensors are written in uppercase upright, e.g., $\mathbf{E} \in \mathbb{R}^{d \times d \times d \times d}$.

For vectors and tensors of compatible sizes, $\langle \cdot, \cdot \rangle$ denotes the Frobenius inner product. We write $|\cdot|$ for the associated norm and use $\|\cdot\|_F$ when emphasizing the Frobenius norm. For $\mathbf{a} \in \mathbb{R}^{d \times d}$ we write $\text{Tr}(\mathbf{a})$ for its trace and $\text{Det}(\mathbf{a})$ for its determinant. Moreover, for $\mathbf{a}, \mathbf{b} \in \mathbb{R}^{d \times d}$ we denote by $\mathbf{a} \otimes \mathbf{b}$ the tensor product defined by $(\mathbf{a} \otimes \mathbf{b})_{ijkl} := a_{ij}b_{kl}$. For a fourth-order tensor \mathbf{E} acting on a second-order tensor \mathbf{a} , we write $\mathbf{E} : \mathbf{a}$, and also use the shorthand $\mathbf{E}\mathbf{a}$. In particular, $\langle \mathbf{E}\boldsymbol{\varepsilon}, \boldsymbol{\varepsilon} \rangle := \langle \mathbf{E} : \boldsymbol{\varepsilon}, \boldsymbol{\varepsilon} \rangle$.

By $\mathbb{S}^{n \times n}$ we denote the space of real symmetric $n \times n$ matrices and by $\mathbb{S}_{\geq 0}^{n \times n}$ the cone of symmetric positive semidefinite matrices. More generally, let V be a finite-dimensional real inner product space with inner product $\langle \cdot, \cdot \rangle$. For self-adjoint linear maps $A, B : V \rightarrow V$ we write $A \succeq 0$ if $\langle Au, u \rangle \geq 0$ for all $u \in V$ and define the (Loewner) order $A \preceq B$ by $B - A \succeq 0$ (strict inequalities \prec, \succ analogously). This convention applies, in particular, to symmetric matrices ($V = \mathbb{R}^n$) and to fourth-order elasticity tensors acting as self-adjoint maps on $V = \mathbb{S}^{d \times d}$. In this sense, $\mathbb{S}_{>0}^{d \times d \times d \times d}$ denotes the subset of $\mathbb{S}^{d \times d \times d \times d}$ that is positive definite as a self-adjoint linear map on $\mathbb{S}^{d \times d}$.

Let $\mathbf{I}_{d \times d}$ denote the identity matrix in $\mathbb{R}^{d \times d}$. Moreover, let $\mathbf{I}_{d \times d \times d \times d}$ denote the fourth-order identity on $\mathbb{S}^{d \times d}$, i.e., $(\mathbf{I}_{d \times d \times d \times d} : \boldsymbol{\varepsilon}) = \boldsymbol{\varepsilon}$ for all $\boldsymbol{\varepsilon} \in \mathbb{S}^{d \times d}$. For a fourth-order tensor $\mathbf{E} \in \mathbb{S}^{d \times d \times d \times d}$ acting as a self-adjoint linear map on $\mathbb{S}^{d \times d}$, we define its trace by $\text{Tr}(\mathbf{E}) := \mathbf{E} : \mathbf{I}_{d \times d \times d \times d}$. Equivalently, $\text{Tr}(\mathbf{E})$ coincides with the trace of the Kelvin–Mandel matrix representation of \mathbf{E} on $\mathbb{S}^{d \times d}$.

For an isotropic fourth-order tensor \mathbf{E} with shear modulus μ and bulk modulus κ , the constitutive law $\boldsymbol{\sigma} = \mathbf{E} : \boldsymbol{\varepsilon}$ takes the volumetric–deviatoric form

$$\forall \boldsymbol{\varepsilon} \in \mathbb{S}^{d \times d}, \quad \mathbf{E} : \boldsymbol{\varepsilon} = \kappa \operatorname{Tr}(\boldsymbol{\varepsilon}) \mathbf{I}_{d \times d} + 2\mu \left(\boldsymbol{\varepsilon} - \frac{1}{d} \operatorname{Tr}(\boldsymbol{\varepsilon}) \mathbf{I}_{d \times d} \right). \quad (1)$$

The inverse tensor is then

$$\forall \boldsymbol{\sigma} \in \mathbb{S}^{d \times d}, \quad \mathbf{E}^{-1} : \boldsymbol{\sigma} = \frac{1}{\kappa d} \operatorname{Tr}(\boldsymbol{\sigma}) \mathbf{I}_{d \times d} + \frac{1}{2\mu} \left(\boldsymbol{\sigma} - \frac{1}{d} \operatorname{Tr}(\boldsymbol{\sigma}) \mathbf{I}_{d \times d} \right). \quad (2)$$

Given two isotropic tensors $\mathbf{E}^-, \mathbf{E}^+$, we say they are well ordered if $\mathbf{E}^- \prec \mathbf{E}^+$, equivalently $\mu^- < \mu^+$ and $\kappa^- < \kappa^+$.

3. Methods

This section formulates the free material optimization problem and the corresponding energy bounds. We work in plane stress ($d = 2$) with two isotropic constituent tensors $\mathbf{E}^-, \mathbf{E}^+ \in \mathbb{S}_{>0}^{d \times d \times d \times d}$ satisfying $\mathbf{E}^- \prec \mathbf{E}^+$. For a local stiff-phase volume fraction $v^+ \in [0, 1]$, mixtures of these phases generate effective tensors, and our goal is to characterize as tightly as possible the admissible set of orthotropic effective tensors through energy bounds. The design variables are the effective tensor field $\mathbf{E}(\mathbf{x})$ and the local volume fraction $v^+(\mathbf{x})$, coupled by pointwise bound constraints.

We start from a continuum multi-loadcase compliance-minimization problem and a unified strain-energy representation of admissibility of the energy bounds (Section 3.1). We then derive discrete models with increasing tightness: zeroth-order bounds (Section 3.2), Voigt upper bounds (Section 3.3), and Hashin–Shtrikman-type upper bounds (Section 3.4). Next, we specialize to orthotropic effective tensors (Section 3.5) and solve the resulting nonconvex problems by sequential global programming (Section 3.6). Section 3.7 recalls the alternating-minimization laminate method of Burazin et al. [20], used as a comparison reference.

3.1. Continuum formulation and solution existence

Let $\Omega \subset \mathbb{R}^d$ be a bounded Lipschitz domain. Its boundary is decomposed as $\partial\Omega = \overline{\Gamma_D} \cup \overline{\Gamma_N}$ with $\Gamma_D \cap \Gamma_N = \emptyset$ and $|\Gamma_D| > 0$. We prescribe homogeneous Dirichlet conditions on Γ_D and set

$$\mathcal{U}_0 := \{ \mathbf{v} \in H^1(\Omega; \mathbb{R}^d) : \mathbf{v} = \mathbf{0} \text{ on } \Gamma_D \}. \quad (3)$$

For $\mathbf{u} \in \mathcal{U}_0$ we set the linearized strain

$$\boldsymbol{\varepsilon}(\mathbf{u}) := \frac{1}{2} (\nabla \mathbf{u} + \nabla \mathbf{u}^\top) \in \mathbb{S}^{d \times d}. \quad (4)$$

Let $n_{lc} \in \mathbb{N}$ denote the number of load cases. For each $j = 1, \dots, n_{lc}$, we prescribe a traction $\mathbf{f}_j \in L^2(\Gamma_N; \mathbb{R}^d)$ and define

$$\ell_j(\mathbf{v}) := \int_{\Gamma_N} \langle \mathbf{f}_j, \mathbf{v} \rangle \, d\Gamma, \quad \forall \mathbf{v} \in \mathcal{U}_0. \quad (5)$$

Given a design $\mathbf{E} \in L^\infty(\Omega; \mathbb{S}_{>0}^{d \times d \times d \times d})$, we introduce the bilinear form

$$a_{\mathbf{E}}(\mathbf{u}, \mathbf{v}) := \int_{\Omega} \langle \mathbf{E}(\mathbf{x}) \boldsymbol{\varepsilon}(\mathbf{u}(\mathbf{x})), \boldsymbol{\varepsilon}(\mathbf{v}(\mathbf{x})) \rangle \, d\mathbf{x}, \quad (6)$$

where $\mathbf{E}(\mathbf{x})$ has the usual minor and major symmetries and acts as a self-adjoint linear map on $\mathbb{S}^{d \times d}$. For each loadcase j , we define $\mathbf{u}_j = \mathbf{u}_j(\mathbf{E}) \in \mathcal{U}_0$ as the solution of the weak equilibrium problem

$$a_{\mathbf{E}}(\mathbf{u}_j, \mathbf{v}) = \ell_j(\mathbf{v}), \quad \forall \mathbf{v} \in \mathcal{U}_0. \quad (7)$$

The compliance associated with the j -th loadcase is defined as the work done by the external loads,

$$c_j(\mathbf{E}) := \ell_j(\mathbf{u}_j(\mathbf{E})) = a_{\mathbf{E}}(\mathbf{u}_j(\mathbf{E}), \mathbf{u}_j(\mathbf{E})), \quad (8)$$

and the objective functional is the sum of the individual compliance terms

$$J(\mathbf{E}) := \sum_{j=1}^{n_{lc}} c_j(\mathbf{E}). \quad (9)$$

To encode energy bounds on the effective tensors, we introduce a local volume fraction $v^+ : \Omega \rightarrow [0, 1]$ of the stiffer isotropic phase \mathbf{E}^+ and restrict the effective elasticity tensors through pointwise strain-energy inequalities. Specifically, for a.e. $\mathbf{x} \in \Omega$, we require

$$\Phi_{lb}(\boldsymbol{\varepsilon}; v^+(\mathbf{x})) \leq \langle \mathbf{E}(\mathbf{x}) \boldsymbol{\varepsilon}, \boldsymbol{\varepsilon} \rangle \leq \Phi_{ub}(\boldsymbol{\varepsilon}; v^+(\mathbf{x})), \quad \forall \boldsymbol{\varepsilon} \in \mathbb{S}^{d \times d}. \quad (10)$$

We assume the chosen energy bounds satisfy the sandwich condition

$$\langle \mathbf{E}^- \boldsymbol{\varepsilon}, \boldsymbol{\varepsilon} \rangle \leq \Phi_{lb}(\boldsymbol{\varepsilon}; v) \leq \Phi_{ub}(\boldsymbol{\varepsilon}; v) \leq \langle \mathbf{E}^+ \boldsymbol{\varepsilon}, \boldsymbol{\varepsilon} \rangle, \quad \forall \boldsymbol{\varepsilon} \in \mathbb{S}^{d \times d}, \forall v \in [0, 1], \quad (11)$$

with fixed $0 \prec \mathbf{E}^- \prec \mathbf{E}^+$. In particular, there exist constants $0 < \alpha \leq \beta < \infty$ such that every admissible design satisfies

$$\alpha |\boldsymbol{\varepsilon}|^2 \leq \langle \mathbf{E}(\mathbf{x}) \boldsymbol{\varepsilon}, \boldsymbol{\varepsilon} \rangle \leq \beta |\boldsymbol{\varepsilon}|^2, \quad \forall \boldsymbol{\varepsilon} \in \mathbb{S}^{d \times d}, \text{ for a.e. } \mathbf{x} \in \Omega. \quad (12)$$

For instance, one may take $\alpha := \lambda_{\min}(\mathbf{E}^-)$ and $\beta := \lambda_{\max}(\mathbf{E}^+)$ with respect to the Frobenius inner product on $\mathbb{S}^{d \times d}$.

Different choices of (Φ_{lb}, Φ_{ub}) correspond to increasingly tight descriptions of realizable effective tensors. Denoting by $\mathcal{A}^{(0)}(v^+)$, $\mathcal{A}^{(1)}(v^+)$, $\mathcal{A}^{(2)}(v^+)$ the admissible sets induced, respectively, by the zeroth-, first-, and second-order bounds used in this work, we have the pointwise hierarchy

$$\mathcal{A}^{(0)}(v^+) \supseteq \mathcal{A}^{(1)}(v^+) \supseteq \mathcal{A}^{(2)}(v^+), \quad \text{for all } v^+ \in [0, 1]. \quad (13)$$

The explicit expressions for these bounds and their inclusion relations are developed in Sections 3.2–3.4.

After imposing the global volume constraint

$$\int_{\Omega} v^+(\mathbf{x}) \, d\mathbf{x} \leq \bar{V} |\Omega|, \quad \bar{V} \in [0, 1], \quad (14)$$

the continuum free material optimization problem reads as

$$\inf_{\mathbf{E}, v^+} J(\mathbf{E}) \quad (15a)$$

$$\text{s.t. } \mathbf{u}_j(\mathbf{E}) \in \mathcal{U}_0 \text{ solves (7) for } j = 1, \dots, n_{lc}, \quad (15b)$$

$$\mathbf{E}(\mathbf{x}) \text{ satisfies (10) for a.e. } \mathbf{x} \in \Omega, \quad (15c)$$

$$0 \leq v^+(\mathbf{x}) \leq 1 \text{ for a.e. } \mathbf{x} \in \Omega, \quad (15d)$$

$$\int_{\Omega} v^+(\mathbf{x}) \, d\mathbf{x} \leq \bar{V} |\Omega|. \quad (15e)$$

By (12), the bilinear form $a_{\mathbf{E}}$ is continuous and coercive on \mathcal{U}_0 . Indeed, for all $\mathbf{u}, \mathbf{v} \in \mathcal{U}_0$,

$$|a_{\mathbf{E}}(\mathbf{u}, \mathbf{v})| \leq \beta \|\boldsymbol{\varepsilon}(\mathbf{u})\|_{L^2(\Omega)} \|\boldsymbol{\varepsilon}(\mathbf{v})\|_{L^2(\Omega)}. \quad (16)$$

Moreover, Korn's inequality [40, Definition 3.1] on \mathcal{U}_0 (using $|\Gamma_D| > 0$) yields a constant $C_K > 0$ such that

$$a_{\mathbf{E}}(\mathbf{u}, \mathbf{u}) \geq \alpha \|\boldsymbol{\varepsilon}(\mathbf{u})\|_{L^2(\Omega)}^2 \geq \frac{\alpha}{C_K^2} \|\mathbf{u}\|_{H^1(\Omega)}^2 \quad \forall \mathbf{u} \in \mathcal{U}_0. \quad (17)$$

Hence, (7) has a unique solution $\mathbf{u}_j(\mathbf{E}) \in \mathcal{U}_0$ for each j due to the Lax–Milgram theorem [18, Corollary 5.8].

To discuss existence of minimizers of (15), we introduce the admissible set

$$\mathcal{D} := \left\{ (\mathbf{E}, v^+) \in L^\infty(\Omega; \mathbb{S}^{d \times d \times d \times d}) \times L^\infty(\Omega) : 0 \leq v^+ \leq 1 \text{ a.e., (14) holds, and } \mathbf{E} \text{ satisfies (10)} \right\}. \quad (18)$$

For each fixed $v \in [0, 1]$, define the local (pointwise) admissible set of tensors by

$$\mathcal{A}(v) := \left\{ \mathbf{E} \in \mathbb{S}^{d \times d \times d \times d} : \Phi_{\text{lb}}(\boldsymbol{\varepsilon}; v) \leq \langle \mathbf{E} \boldsymbol{\varepsilon}, \boldsymbol{\varepsilon} \rangle \leq \Phi_{\text{ub}}(\boldsymbol{\varepsilon}; v) \quad \forall \boldsymbol{\varepsilon} \in \mathbb{S}^{d \times d} \right\}, \quad (19)$$

so that (10) is equivalently the pointwise constraint $\mathbf{E}(\mathbf{x}) \in \mathcal{A}(v^+(\mathbf{x}))$ for a.e. $\mathbf{x} \in \Omega$.

The upper bound in (12) implies $\|\mathbf{E}(\mathbf{x})\|_{\text{op}} \leq \beta$ for a.e. $\mathbf{x} \in \Omega$, where $\|\mathbf{E}\|_{\text{op}} := \sup_{\boldsymbol{\varepsilon} \in \mathbb{S}^{d \times d} \setminus \{0\}} \langle \mathbf{E} \boldsymbol{\varepsilon}, \boldsymbol{\varepsilon} \rangle / |\boldsymbol{\varepsilon}|^2$. Consequently $\|\mathbf{E}\|_{L^\infty(\Omega; \text{op})} \leq \beta$ for all admissible designs, and together with $0 \leq v^+ \leq 1$ this yields boundedness of \mathcal{D} in $L^\infty(\Omega; \mathbb{S}^{d \times d \times d \times d}) \times L^\infty(\Omega)$. Hence, by the Banach–Alaoglu theorem [18, Theorem 3.16], any minimizing sequence admits a subsequence

$$(\mathbf{E}_k, v_k^+) \xrightarrow{*} (\mathbf{E}, v^+) \quad \text{in } L^\infty(\Omega; \mathbb{S}^{d \times d \times d \times d}) \times L^\infty(\Omega). \quad (20)$$

The simple constraints $0 \leq v^+ \leq 1$ and the volume constraint (14) are weak- \star closed. It remains to discuss the weak- \star lower semicontinuity of the objective and the stability of the pointwise realizability constraint $\mathbf{E}(\mathbf{x}) \in \mathcal{A}(v^+(\mathbf{x}))$.

3.1.1. Zeroth-order and Voigt bounds

For the zeroth-order and Voigt admissible sets defined later in (28) and (43), respectively, the graph

$$\mathcal{G} := \{(v, \mathbf{E}) \in [0, 1] \times \mathbb{S}^{d \times d \times d \times d} : \mathbf{E} \in \mathcal{A}(v)\} \quad (21)$$

is a closed convex subset of a finite-dimensional space. Consider the induced set of admissible fields

$$\mathcal{K}_{\mathcal{G}} := \{(\mathbf{E}, v^+) \in L^\infty(\Omega; \mathbb{S}^{d \times d \times d \times d}) \times L^\infty(\Omega) : (v^+(\mathbf{x}), \mathbf{E}(\mathbf{x})) \in \mathcal{G} \text{ for a.e. } \mathbf{x} \in \Omega\}. \quad (22)$$

Let $\text{dist}_{\mathcal{G}}$ be the Euclidean distance to \mathcal{G} . Since \mathcal{G} is closed and convex, $\text{dist}_{\mathcal{G}}$ is convex and continuous, and, therefore, the functional

$$(\mathbf{E}, v^+) \mapsto \int_{\Omega} \text{dist}_{\mathcal{G}}(v^+(\mathbf{x}), \mathbf{E}(\mathbf{x})) \, d\mathbf{x} \quad (23)$$

is weak- \star lower semicontinuous on $L^\infty \times L^\infty$. Hence, if $(\mathbf{E}_k, v_k^+) \in \mathcal{K}_{\mathcal{G}}$ and $(\mathbf{E}_k, v_k^+) \rightharpoonup^* (\mathbf{E}, v^+)$, then the above integral is 0 along the sequence and thus also at the limit, which implies $(\mathbf{E}, v^+) \in \mathcal{K}_{\mathcal{G}}$. Consequently, for these convex bound choices, the full admissible set \mathcal{D} in (18) is weak- \star closed, and since it is bounded it is weak- \star compact by the Banach–Alaoglu theorem.

It remains to verify lower semicontinuity of the objective. For each loadcase j , the compliance admits the dual representation

$$c_j(\mathbf{E}) = \sup_{\mathbf{u} \in \mathcal{U}_0} \left(2\ell_j(\mathbf{u}) - a_{\mathbf{E}}(\mathbf{u}, \mathbf{u}) \right), \quad (24)$$

obtained from the minimum principle for the potential energy. For fixed \mathbf{u} , the map $\mathbf{E} \mapsto a_{\mathbf{E}}(\mathbf{u}, \mathbf{u})$ is weak- \star continuous (it is linear in \mathbf{E}), hence (24) is the supremum of weak- \star continuous affine functionals and, therefore, weak- \star lower semicontinuous. Thus, $J = \sum_{j=1}^{m_{\text{lc}}} c_j$ is weak- \star lower semicontinuous as well, and the direct method yields existence of a minimizer $(\mathbf{E}^*, v^{*+}) \in \mathcal{D}$. The associated states $\mathbf{u}_j(\mathbf{E}^*)$ exist uniquely by the Lax–Milgram theorem.

3.1.2. Hashin–Shtrikman-type bounds

For Hashin–Shtrikman-type constraints (with the pointwise admissible set $\mathcal{A}^{(2)}(v)$ defined in (56)), the feasible set is convex in \mathbf{E} for fixed v^+ but in general not jointly convex in (v^+, \mathbf{E}) (cf. Lemma 3.1). In particular, the pointwise constraint set (22) need not be weak- \star closed. Moreover, even under the uniform ellipticity bounds (12), weak- \star convergence of coefficients is in general not compatible with passing to the limit in the state equation; see, e.g., the discussion in [26, Sections 2.2–2.3].

Following [26], we, therefore, formulate an existence statement in the homogenization topology of H -convergence for the stiffness field. Let

$$\mathcal{E}_{\alpha,\beta} := \{\mathbf{E} \in L^\infty(\Omega; \mathbb{S}^{d \times d \times d \times d}) : \alpha \mathbf{I}_{d \times d \times d \times d} \preceq \mathbf{E}(\mathbf{x}) \preceq \beta \mathbf{I}_{d \times d \times d \times d} \text{ a.e. in } \Omega\}, \quad (25)$$

where α, β are as in (12). Then any admissible stiffness field belongs to $\mathcal{E}_{\alpha,\beta}$, and $\mathcal{E}_{\alpha,\beta}$ is sequentially compact with respect to H -convergence (cf. [26, Theorem 2.2]).

Define the H -relaxed admissible set as the closure of \mathcal{D} in the product topology $(\mathbf{E}_k \rightarrow_H \mathbf{E}) \times (v_k^+ \rightharpoonup^* v^+)$, i.e.,

$$\mathcal{D}^H := \overline{\mathcal{D}}^{(\rightarrow_H) \times (\rightharpoonup^*)}. \quad (26)$$

Let $(\mathbf{E}_k, v_k^+) \subset \mathcal{D}$ be a minimizing sequence. By the Banach–Alaoglu theorem, we may assume (up to a subsequence) $v_k^+ \rightharpoonup^* v^{+*}$ in L^∞ . By H -compactness of $\mathcal{E}_{\alpha,\beta}$ we may further assume $\mathbf{E}_k \rightarrow_H \mathbf{E}^*$. Hence $(\mathbf{E}^*, v^{+*}) \in \mathcal{D}^H$ by definition.

Finally, along any H -convergent sequence $\mathbf{E}_k \xrightarrow{H} \mathbf{E}^*$, the corresponding state solutions satisfy

$$\mathbf{u}_j(\mathbf{E}_k) \rightharpoonup \mathbf{u}_j(\mathbf{E}^*) \quad \text{in } \mathcal{U}_0, \quad j = 1, \dots, n_{\text{lc}},$$

and the compliance is lower semicontinuous with respect to this convergence; see the H -lower semicontinuity condition [26, (2.14)] and the fact that the compliance is a typical example satisfying it. Therefore,

$$J(\mathbf{E}^*) \leq \liminf_{k \rightarrow \infty} J(\mathbf{E}_k), \quad (27)$$

and the direct-method existence argument (cf. [26, Theorem 2.8]) yields existence of a minimizer of the relaxed problem (15) posed over \mathcal{D}^H . We emphasize that (\mathbf{E}^*, v^{+*}) is an H -relaxed limit of admissible designs; in general, it need not satisfy the original Hashin–Shtrikman pointwise constraints in a strongly closed sense under weak- \star convergence.

Remark 3.1 (Orthotropic restriction). *If we further restrict admissible tensors to the orthotropic symmetry class with free rotations, we mean fields \mathbf{E} such that, for a.e. $\mathbf{x} \in \Omega$, there exist an angle $\varphi(\mathbf{x})$ and an orthotropic base tensor $\mathbf{E}^b(\mathbf{x})$ with $(\mathbf{E}^b)_{1112} = (\mathbf{E}^b)_{2212} = 0$, and $\mathbf{E}(\mathbf{x})$ is obtained from $\mathbf{E}^b(\mathbf{x})$ by planar rotation; see Section 3.5. This pointwise admissible set is, in general, not weak- \star closed: weak- \star limits may average rapidly oscillating orientation fields, while convex combinations of differently rotated orthotropic tensors need not remain orthotropic. Existence is, therefore, understood in the relaxed sense, i.e., by minimizing over the closure of orthotropic-admissible designs in $(\rightarrow_H) \times (\rightharpoonup^*)$.*

For the model classes considered in this paper:

- *Zeroth-order bounds: in the single-loadcase continuum setting, at least one minimizer of (34) can be chosen orthotropic (Proposition 3.1). This is a property of the original model without imposing orthotropy a priori; consequently, adding an orthotropic restriction does not increase the optimal value in that setting.*
- *Voigt bounds: isotropic optimal minimizers exist both in the discrete model (47) and in the continuum Voigt setting (Proposition 3.3). Thus, without imposing symmetry a priori, one can choose an isotropic (hence orthotropic) minimizer, and adding an orthotropic restriction does not change the optimal value.*
- *Hashin–Shtrikman bounds: here the orthotropic class is not weak- \star closed, so existence is interpreted via the relaxed closure in $(\rightarrow_H) \times (\rightharpoonup^*)$. Theorem 3.1 shows that, in the two-dimensional single-loadcase continuum setting with well-ordered isotropic phases, the relaxed value is attained in the relaxation sense by rank-one and rank-two sequential laminates, which are orthotropic. Therefore, imposing orthotropy does not change the continuum relaxed optimal value.*

For numerical solution, we discretize the state space by $\mathcal{U}_h \subset \mathcal{U}_0$ and parametrize (\mathbf{E}, v^+) by elementwise constants. Then (10) becomes a collection of local constraints on the element variables. For the zeroth-order and Voigt bounds, these constraints are jointly convex and can be written as linear matrix inequalities, while Hashin–Shtrikman-type bounds are convex in \mathbf{E} for fixed v^+ but not jointly convex in (\mathbf{E}, v^+) . The resulting discrete formulations are given in Sections 3.2–3.4.

3.2. FMO problem under zeroth-order bounds

We start with the weakest pointwise admissible set $\mathcal{A}^{(0)}(v)$, obtained by imposing only uniform bounds on the effective elasticity tensor [36, 43],

$$\mathcal{A}^{(0)}(v) := \{ \mathbf{E} \in \mathbb{S}_{>0}^{d \times d \times d \times d} : \mathbf{E}^- \preceq \mathbf{E} \preceq \mathbf{E}^+ \}, \quad v \in [0, 1], \quad (28)$$

where $\mathbf{E}^-, \mathbf{E}^+$ are the (isotropic) tensors of the soft and stiff constituents such that $0 \prec \mathbf{E}^- \prec \mathbf{E}^+$. In contrast to the Voigt and Hashin–Shtrikman bounds considered later, (28) does not couple \mathbf{E} to a local volume-fraction variable v^+ . We therefore first derive the discrete FMO formulation under zeroth-order bounds for computation and then return to the single-loadcase continuum setting to show that an orthotropic minimizer exists.

For numerical treatment, we now pass to a finite-element discretization of Ω into n_e elements and approximate the effective tensor field by elementwise constants \mathbf{E}_i . Following the standard trace-constrained resource modeling in free material design [43, 14, 54, 10, 22, 23], and since (28) does not include an explicit local volume fraction variable, we introduce auxiliary elementwise volume fractions $v_i^+ \in [0, 1]$ and enforce a local trace-level mixture inequality

$$\text{Tr}(\mathbf{E}_i) \leq (1 - v_i^+) \text{Tr}(\mathbf{E}^-) + v_i^+ \text{Tr}(\mathbf{E}^+), \quad i = 1, \dots, n_e. \quad (29)$$

Assuming equisized elements and imposing the average volume-fraction bound $\frac{1}{n_e} \sum_{i=1}^{n_e} v_i^+ \leq \bar{V}$, summing (29) over all elements gives

$$\frac{1}{n_e} \sum_{i=1}^{n_e} \text{Tr}(\mathbf{E}_i) \leq \bar{V} \text{Tr}(\mathbf{E}^+) + (1 - \bar{V}) \text{Tr}(\mathbf{E}^-). \quad (30)$$

Conversely, if $\mathbf{E}^- \preceq \mathbf{E}_i \preceq \mathbf{E}^+$ and the global trace bound above holds, then defining

$$v_i^+ := \frac{\text{Tr}(\mathbf{E}_i) - \text{Tr}(\mathbf{E}^-)}{\text{Tr}(\mathbf{E}^+) - \text{Tr}(\mathbf{E}^-)} \in [0, 1] \quad (31)$$

yields (29) with equality, and $\frac{1}{n_e} \sum_i v_i^+ \leq \bar{V}$. Hence, after eliminating $\{v_i^+\}$, this auxiliary formulation is equivalent to the global trace constraint (32d).

For each loadcase $j = 1, \dots, n_{lc}$, let $\mathbf{f}_j \in \mathbb{R}^{n_{\text{dof},j}}$ be the discrete load vector and $\mathbf{K}_j(\{\mathbf{E}_i\}) \in \mathbb{S}_{>0}^{n_{\text{dof},j} \times n_{\text{dof},j}}$ the assembled stiffness matrix. The multi-loadcase compliance admits the standard Schur-complement epigraph reformulation as a semidefinite program [16, Appendix A], as commonly used in free material and compliance optimization [10, 30]. The resulting minimum-compliance free material optimization problem reads

$$\min_{\{c_j\}, \{\mathbf{E}_i\}} \sum_{j=1}^{n_{lc}} c_j \quad (32a)$$

$$\text{s.t.} \quad \begin{pmatrix} c_j & -\mathbf{f}_j^\top \\ -\mathbf{f}_j & \mathbf{K}_j(\{\mathbf{E}_i\}) \end{pmatrix} \succeq 0, \quad j = 1, \dots, n_{lc}, \quad (32b)$$

$$\mathbf{E}^- \preceq \mathbf{E}_i \preceq \mathbf{E}^+, \quad i = 1, \dots, n_e, \quad (32c)$$

$$\frac{1}{n_e} \sum_{i=1}^{n_e} \text{Tr}(\mathbf{E}_i) \leq \bar{V} \text{Tr}(\mathbf{E}^+) + (1 - \bar{V}) \text{Tr}(\mathbf{E}^-). \quad (32d)$$

The linear matrix inequality (32b) enforces $c_j \geq \mathbf{f}_j^\top \mathbf{K}_j(\{\mathbf{E}_i\})^{-1} \mathbf{f}_j$ by the Schur complement, so that at optimality c_j equals the compliance of loadcase j . The tensor bound (32c) is equivalent to the strain-energy inequalities

$$\langle \mathbf{E}^- \boldsymbol{\varepsilon}, \boldsymbol{\varepsilon} \rangle \leq \langle \mathbf{E}_i \boldsymbol{\varepsilon}, \boldsymbol{\varepsilon} \rangle \leq \langle \mathbf{E}^+ \boldsymbol{\varepsilon}, \boldsymbol{\varepsilon} \rangle, \quad \forall \boldsymbol{\varepsilon} \in \mathbb{S}^{d \times d}, \quad (33)$$

i.e., no element can be stiffer than \mathbf{E}^+ or softer than \mathbf{E}^- in any direction.

Problem (32) is a convex finite-dimensional semidefinite program and can, therefore, be solved to global optimality. We refer to (32) as the zeroth-order free material optimization model (ZO-FMO). Its main drawback is that the admissible set (32c) is typically very large; in particular, it does not encode any microstructural information beyond the uniform ellipticity range $\mathbf{E}^- \preceq \mathbf{E}_i \preceq \mathbf{E}^+$.

Before introducing tighter bounds, we record a structural property that connects the zeroth-order (ZO) model to our orthotropic focus at the continuum level. In the single-loadcase setting, the continuum ZO problem

$$\inf_{\mathbf{E} \in L^\infty(\Omega; \mathbb{S}_{>0}^{d \times d \times d \times d})} c_1(\mathbf{E}) \quad (34a)$$

$$\text{s.t. } \mathbf{E}^- \preceq \mathbf{E}(\mathbf{x}) \preceq \mathbf{E}^+ \text{ for a.e. } \mathbf{x} \in \Omega, \quad (34b)$$

$$\frac{1}{|\Omega|} \int_{\Omega} \text{Tr}(\mathbf{E}(\mathbf{x})) \, d\mathbf{x} \leq \bar{V} \text{Tr}(\mathbf{E}^+) + (1 - \bar{V}) \text{Tr}(\mathbf{E}^-) \quad (34c)$$

is the reference model below; we will show that it admits an orthotropic optimal solution.

For later use, recall the complementary-energy representation (minimum complementary energy principle): for $n_{lc} = 1$ and any admissible \mathbf{E} ,

$$c_1(\mathbf{E}) = \min_{\boldsymbol{\sigma} \in \Sigma_{\text{ad},1}} \int_{\Omega} \langle \mathbf{E}(\mathbf{x})^{-1} \boldsymbol{\sigma}(\mathbf{x}), \boldsymbol{\sigma}(\mathbf{x}) \rangle \, d\mathbf{x}, \quad (35)$$

where

$$\Sigma_{\text{ad},1} := \left\{ \boldsymbol{\sigma} \in L^2(\Omega; \mathbb{S}^{d \times d}) : \int_{\Omega} \langle \boldsymbol{\sigma}, \boldsymbol{\varepsilon}(\mathbf{v}) \rangle \, d\mathbf{x} = \ell_1(\mathbf{v}) \quad \forall \mathbf{v} \in \mathcal{U}_0 \right\}. \quad (36)$$

The minimum in (35) is attained: $\Sigma_{\text{ad},1}$ is a closed affine subspace of $L^2(\Omega; \mathbb{S}^{d \times d})$, and the functional $\boldsymbol{\sigma} \mapsto \int_{\Omega} \langle \mathbf{E}^{-1} \boldsymbol{\sigma}, \boldsymbol{\sigma} \rangle \, d\mathbf{x}$ is coercive and strictly convex for admissible \mathbf{E} .

The structural role of principal directions in compliance-driven design is classical in orientation optimization of orthotropic materials [42] and in homogenization-based laminate constructions [3, 1]. The next proposition gives a corresponding representative-minimizer statement directly for the single-loadcase continuum zeroth-order FMO model (34).

Proposition 3.1 (Orthotropic minimizer for the single-loadcase continuum ZO problem). *Assume $n_{lc} = 1$ and $d = 2$. Then (34) admits a minimizer, and at least one minimizer $\mathbf{E}^{\text{ortho}}$ can be chosen such that, for a.e. $\mathbf{x} \in \Omega$, $\mathbf{E}^{\text{ortho}}(\mathbf{x})$ is orthotropic in a principal basis of an optimal stress field for (35).*

Proof. Existence of a minimizer for (34) follows from Section 3.1. Let \mathbf{E}^* be such a minimizer.

Pick $\boldsymbol{\sigma}^* \in \Sigma_{\text{ad},1}$ minimizing (35) for \mathbf{E}^* . Using the spectral decomposition in 2D, choose a measurable orthogonal field $\mathbf{U}(\mathbf{x})$ that diagonalizes $\boldsymbol{\sigma}^*(\mathbf{x})$ for a.e. \mathbf{x} (and set $\mathbf{U} = \mathbf{I}$ on repeated-eigenvalue points). Set $\mathbf{M} := \text{Diag}(1, -1)$ and $\mathbf{Q} := \mathbf{U}\mathbf{M}\mathbf{U}^\top$. For any fourth-order tensor \mathbf{A} , denote by $\mathcal{T}_{\mathbf{Q}}(\mathbf{A})$ its orthogonal transform: $(\mathcal{T}_{\mathbf{Q}}(\mathbf{A}))_{ijkl} := \sum_{p,q,r,s=1}^d (\mathbf{Q})_{ip}(\mathbf{Q})_{jq}(\mathbf{Q})_{kr}(\mathbf{Q})_{ls}(\mathbf{A})_{pqrs}$. Define

$$\mathbf{E}^{\text{ortho}} := \frac{1}{2}(\mathbf{E}^* + \mathcal{T}_{\mathbf{Q}}(\mathbf{E}^*)) \quad \text{pointwise in } \Omega. \quad (37)$$

Because $\mathbf{E}^-, \mathbf{E}^+$ are isotropic, $\mathcal{T}_{\mathbf{Q}}$ preserves the bounds $\mathbf{E}^- \preceq \cdot \preceq \mathbf{E}^+$; by convexity, $\mathbf{E}^{\text{ortho}}$ is feasible for (34). Also $\text{Tr}(\mathcal{T}_{\mathbf{Q}}(\mathbf{A})) = \text{Tr}(\mathbf{A})$, so the trace constraint is unchanged.

For fixed $\boldsymbol{\sigma}^*(\mathbf{x})$, the map $\mathbf{A} \mapsto \langle \mathbf{A}^{-1} \boldsymbol{\sigma}^*, \boldsymbol{\sigma}^* \rangle$ is convex on positive-definite tensors. Moreover, by orthogonality and $\mathbf{Q}^\top \boldsymbol{\sigma}^* \mathbf{Q} = \boldsymbol{\sigma}^*$, so that $(\mathcal{T}_\mathbf{Q}(\mathbf{A}))^{-1} = \mathcal{T}_\mathbf{Q}(\mathbf{A}^{-1})$ and

$$\langle (\mathcal{T}_\mathbf{Q}(\mathbf{E}^*))^{-1} \boldsymbol{\sigma}^*, \boldsymbol{\sigma}^* \rangle = \langle (\mathbf{E}^*)^{-1} \boldsymbol{\sigma}^*, \boldsymbol{\sigma}^* \rangle. \quad (38)$$

Hence, pointwise in Ω ,

$$\langle (\mathbf{E}^{\text{ortho}})^{-1} \boldsymbol{\sigma}^*, \boldsymbol{\sigma}^* \rangle \leq \frac{1}{2} \langle (\mathbf{E}^*)^{-1} \boldsymbol{\sigma}^*, \boldsymbol{\sigma}^* \rangle + \frac{1}{2} \langle (\mathcal{T}_\mathbf{Q}(\mathbf{E}^*))^{-1} \boldsymbol{\sigma}^*, \boldsymbol{\sigma}^* \rangle = \langle (\mathbf{E}^*)^{-1} \boldsymbol{\sigma}^*, \boldsymbol{\sigma}^* \rangle. \quad (39)$$

Integrating gives

$$\int_\Omega \langle (\mathbf{E}^{\text{ortho}})^{-1} \boldsymbol{\sigma}^*, \boldsymbol{\sigma}^* \rangle \, d\mathbf{x} \leq \int_\Omega \langle (\mathbf{E}^*)^{-1} \boldsymbol{\sigma}^*, \boldsymbol{\sigma}^* \rangle \, d\mathbf{x} = c_1(\mathbf{E}^*). \quad (40)$$

By (35),

$$c_1(\mathbf{E}^{\text{ortho}}) \leq \int_\Omega \langle (\mathbf{E}^{\text{ortho}})^{-1} \boldsymbol{\sigma}^*, \boldsymbol{\sigma}^* \rangle \, d\mathbf{x} \leq c_1(\mathbf{E}^*). \quad (41)$$

Since \mathbf{E}^* is optimal for (34), we conclude $c_1(\mathbf{E}^{\text{ortho}}) = c_1(\mathbf{E}^*)$, so $\mathbf{E}^{\text{ortho}}$ is also optimal. In the principal basis of $\boldsymbol{\sigma}^*$, averaging with \mathbf{M} cancels the shear-coupling terms, hence $\mathbf{E}^{\text{ortho}}$ is orthotropic. \square

Proposition 3.1 is a global continuum statement for single-loadcase ZO-FMO: at least one minimizer can be chosen orthotropic. This argument is continuum-level and does not transfer directly to fixed finite-element discretizations. For low-order elements, stresses can be elementwise constant, but such discretizations are prone to checkerboarding unless regularized; this regularization averages neighboring tensors and generally destroys local orthotropic structure. Using higher-order elements mitigates these artifacts, but stresses are then no longer elementwise constant, so local tensors must be optimal with respect to multiple stress states, which again typically breaks orthotropy.

We now tighten ZO-FMO by adding Voigt upper bounds; in that case, we obtain an even stronger structural result (existence of isotropic optimal minimizers, Proposition 3.3).

3.3. FMO problem under Voigt upper bounds

To strengthen the connection between the FMO problem and the realizable elasticity tensors without sacrificing convexity, we proceed by exploiting the Voigt upper bound [27] for effective elasticity tensors of composites

$$\mathbf{E}_i \preceq \mathbf{E}_i^{\text{V}}(v_i^+) := (1 - v_i^+) \mathbf{E}^- + v_i^+ \mathbf{E}^+, \quad (42)$$

where v_i^+ is the volume fraction of the stiffer material \mathbf{E}^+ in the i -th element. The inequality (42) is equivalent to the strain-energy bound $\langle \mathbf{E}_i \boldsymbol{\varepsilon}, \boldsymbol{\varepsilon} \rangle \leq \langle \mathbf{E}_i^{\text{V}}(v_i^+) \boldsymbol{\varepsilon}, \boldsymbol{\varepsilon} \rangle$ for all $\boldsymbol{\varepsilon} \in \mathbb{S}^{d \times d}$. Moreover, since $v_i^+ \in [0, 1]$ and $\mathbf{E}^- \preceq \mathbf{E}^+$, we also have $\mathbf{E}_i^{\text{V}}(v_i^+) \preceq \mathbf{E}^+$. The Voigt constraint (42) thus induces the first-order admissible set

$$\mathcal{A}^{(1)}(v) := \left\{ \mathbf{E} \in \mathbb{S}^{d \times d \times d \times d} : \mathbf{E}^- \preceq \mathbf{E} \preceq (1 - v) \mathbf{E}^- + v \mathbf{E}^+ \right\}, \quad v \in [0, 1]. \quad (43)$$

In what follows, we exploit the Voigt upper bound (42) to provide a better estimate of the microstructural relative volume. In particular, due to the Loewner ordering, we have

$$\text{Tr}(\mathbf{E}_i) \leq \text{Tr}((1 - v_i^+) \mathbf{E}^- + v_i^+ \mathbf{E}^+) \leq \text{Tr}(\mathbf{E}^+), \quad (44)$$

and, thus, also for the average of the elasticity tensors \mathbf{E}_i over all elements, assuming equisized elements for simplicity,

$$\frac{1}{n_e} \sum_{i=1}^{n_e} \text{Tr}(\mathbf{E}_i) \leq \text{Tr}(\mathbf{E}^-) + \frac{1}{n_e} [\text{Tr}(\mathbf{E}^+) - \text{Tr}(\mathbf{E}^-)] \sum_{i=1}^{n_e} v_i^+ \leq \text{Tr}(\mathbf{E}^+). \quad (45)$$

Now, allowing the average trace to be at most $\bar{V} \text{Tr}(\mathbf{E}^+) + (1 - \bar{V}) \text{Tr}(\mathbf{E}^-)$ as in (32d), the tighter volume estimator reads as

$$\text{Tr}(\mathbf{E}^-) + \frac{1}{n_e} [\text{Tr}(\mathbf{E}^+) - \text{Tr}(\mathbf{E}^-)] \sum_{i=1}^{n_e} v_i^+ \leq \bar{V} \text{Tr}(\mathbf{E}^+) + (1 - \bar{V}) \text{Tr}(\mathbf{E}^-), \quad (46)$$

which, after simplification, provides the Voigt free material optimization problem (V-FMO)

$$\min_{\{c_j\}, \{\mathbf{E}_i\}, \{v_i^+\}} \sum_{j=1}^{n_{lc}} c_j \quad (47a)$$

$$\text{s.t.} \quad \begin{pmatrix} c_j & -f_j^\top \\ -f_j & \mathbf{K}_j(\{\mathbf{E}_i\}) \end{pmatrix} \succeq 0, \quad j = 1, \dots, n_{lc}, \quad (47b)$$

$$\mathbf{E}^- \preceq \mathbf{E}_i \preceq (1 - v_i^+) \mathbf{E}^- + v_i^+ \mathbf{E}^+, \quad i = 1, \dots, n_e, \quad (47c)$$

$$\frac{1}{n_e} \sum_{i=1}^{n_e} v_i^+ \leq \bar{V}, \quad (47d)$$

$$0 \leq v_i^+ \leq 1, \forall i \in 1, \dots, n_e. \quad (47e)$$

Notice that the constraint (47d) now directly limits the average volume fraction of the stiffer material \mathbf{E}^+ .

The V-FMO problem (47) is indeed tighter than the FMO problem under zeroth-order bounds (32). In particular, for $\bar{V} \in (0, 1)$ and after projecting out the auxiliary variables $\{v_i^+\}$, the feasible set in $(\{c_j\}, \{\mathbf{E}_i\})$ -

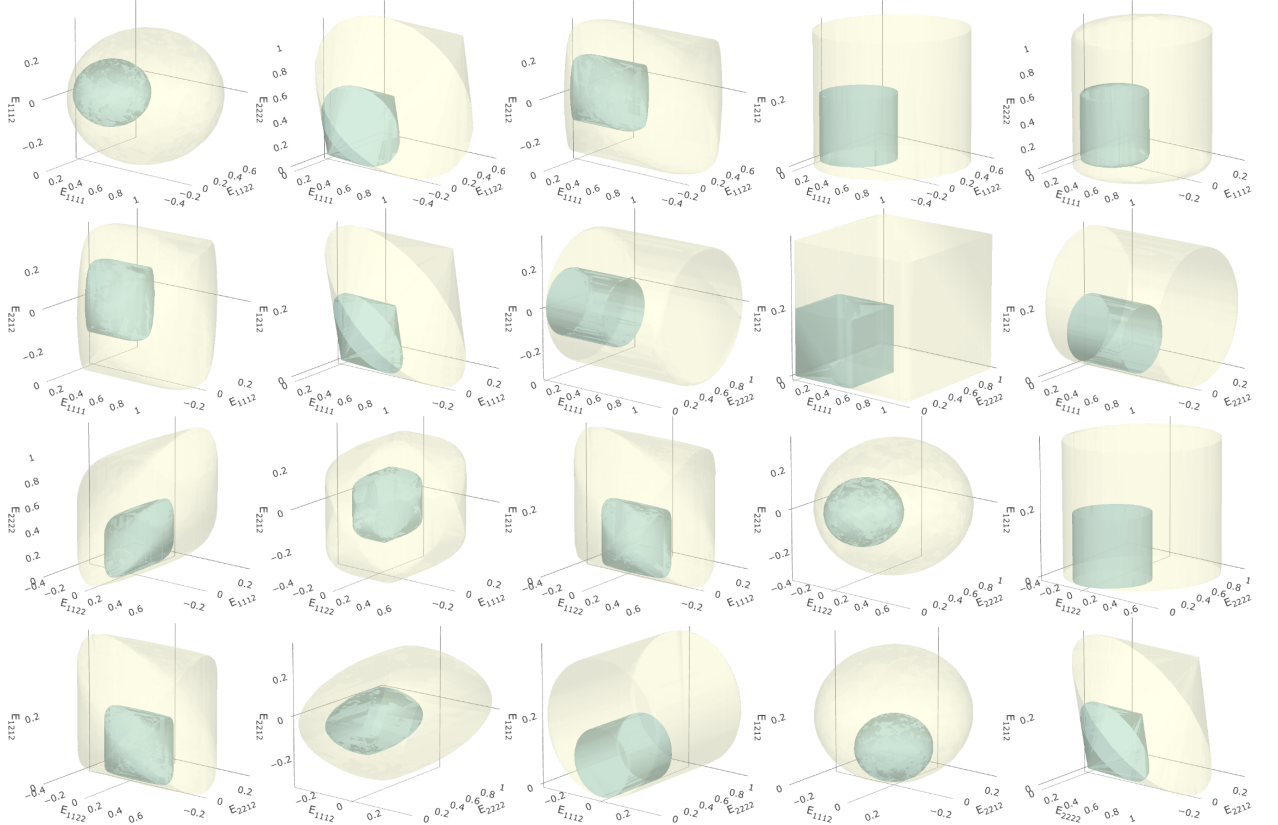


Figure 1: Comparison of the admissible sets $\mathcal{A}^{(0)}(0.5)$ (zeroth-order, yellow) and $\mathcal{A}^{(1)}(0.5)$ (Voigt, blue). The sets are shown in a selected three-dimensional projection of \mathbf{E}_i as outer-envelope boundary surfaces, obtained from 750 sampled strains $\boldsymbol{\varepsilon}$ with Frobenius norm $\sqrt{2}/2$. Material parameters: $\kappa^- = 0.714 \times 10^{-9}$, $\kappa^+ = 0.714$, $\mu^- = 0.385 \times 10^{-9}$, and $\mu^+ = 0.385$.

space induced by (47) is strictly contained in the feasible set of (32). Figure 1 provides pointwise geometric intuition at fixed v_i^+ .

Proposition 3.2 (Strict feasible-set inclusion of V-FMO in ZO-FMO). *Assume $0 < \bar{V} < 1$ and $\mathbf{E}^- \prec \mathbf{E}^+$, i.e., the phase bulk and shear moduli satisfying $0 < \kappa^- < \kappa^+$ and $0 < \mu^- < \mu^+$. With $\mathcal{F}_{\text{ZO}} := \{(\{c_j\}, \{\mathbf{E}_i\}) : (\{c_j\}, \{\mathbf{E}_i\}) \text{ feasible for (32)}\}$, and $\mathcal{F}_{\text{FO}} := \{(\{c_j\}, \{\mathbf{E}_i\}) : \exists \{v_i^+\} \text{ s.t. } (\{c_j\}, \{\mathbf{E}_i\}, \{v_i^+\}) \text{ feasible for (47)}\}$, it holds that $\mathcal{F}_{\text{FO}} \subsetneq \mathcal{F}_{\text{ZO}}$.*

Proof. Inclusion $\mathcal{F}_{\text{FO}} \subseteq \mathcal{F}_{\text{ZO}}$ is immediate: (47b) is the same as (32b), (47c) with $v_i^+ \in [0, 1]$ implies (32c), and

$$\frac{1}{n_e} \sum_{i=1}^{n_e} \text{Tr}(\mathbf{E}_i) \leq \text{Tr}(\mathbf{E}^-) + \frac{\text{Tr}(\mathbf{E}^+) - \text{Tr}(\mathbf{E}^-)}{n_e} \sum_{i=1}^{n_e} v_i^+ \leq \bar{V} \text{Tr}(\mathbf{E}^+) + (1 - \bar{V}) \text{Tr}(\mathbf{E}^-), \quad (48)$$

so (32d) holds.

For strictness, write the bulk and shear moduli differences as $\Delta\kappa := \kappa^+ - \kappa^- > 0$, $\Delta\mu := \mu^+ - \mu^- > 0$, and

$$\alpha := \frac{\Delta\kappa}{\Delta\kappa + 2\Delta\mu} \in (0, 1), \quad \theta := \min\{1, \bar{V}/\alpha\}, \quad (49)$$

so $\theta > \bar{V}$ and $\alpha\theta \leq \bar{V}$. Define an isotropic tensor $\hat{\mathbf{E}}$ by $\hat{\kappa} := \kappa^- + \theta\Delta\kappa$ and $\hat{\mu} := \mu^-$, and set $\mathbf{E}_i = \hat{\mathbf{E}}$ for all i . Then $\mathbf{E}^- \preceq \mathbf{E}_i \preceq \mathbf{E}^+$. Moreover, for $d = 2$,

$$\frac{\text{Tr}(\mathbf{E}_i) - \text{Tr}(\mathbf{E}^-)}{\text{Tr}(\mathbf{E}^+) - \text{Tr}(\mathbf{E}^-)} = \frac{2\theta\Delta\kappa}{2\Delta\kappa + 4\Delta\mu} = \alpha\theta \leq \bar{V}, \quad (50)$$

hence (32d) holds. Choosing $c_j := \mathbf{f}_j^T \mathbf{K}_j(\{\mathbf{E}_i\})^{-1} \mathbf{f}_j$ gives (32b), so $(\{c_j\}, \{\mathbf{E}_i\}) \in \mathcal{F}_{\text{ZO}}$.

If $(\{c_j\}, \{\mathbf{E}_i\}) \in \mathcal{F}_{\text{FO}}$, then for some $\{v_i^+\}$, (47c) implies $\kappa^- + \theta\Delta\kappa = \hat{\kappa} \leq \kappa^- + v_i^+ \Delta\kappa$, hence $v_i^+ \geq \theta$ for all i . Therefore $\frac{1}{n_e} \sum_i v_i^+ \geq \theta > \bar{V}$, contradicting (47d). Thus, $(\{c_j\}, \{\mathbf{E}_i\}) \notin \mathcal{F}_{\text{FO}}$, and $\mathcal{F}_{\text{FO}} \subsetneq \mathcal{F}_{\text{ZO}}$. \square

The endpoint cases satisfy $\mathcal{F}_{\text{FO}} = \mathcal{F}_{\text{ZO}}$ for $\bar{V} \in \{0, 1\}$. Indeed, for $\bar{V} = 0$, the Voigt volume constraint (47d) forces $v_i^+ = 0$ for all i , hence (47c) reduces to $\mathbf{E}^- \preceq \mathbf{E}_i \preceq \mathbf{E}^-$, i.e., $\mathbf{E}_i = \mathbf{E}^-$, which is exactly what (32d) enforces in the zeroth-order formulation. For $\bar{V} = 1$, the volume constraints are inactive in both models, and any zeroth-order-feasible tensor field also satisfies the Voigt bounds by taking $v_i^+ = 1$ for all i .

For the Voigt-constrained problem (47), we now show that isotropic optimal minimizers exist in both the discrete and continuum settings.

Proposition 3.3 (Existence of isotropic minimizers for V-FMO (discrete and continuum)). *Let \mathbf{E}^- and \mathbf{E}^+ be well-ordered isotropic elasticity tensors with $\mathbf{E}^- \preceq \mathbf{E}^+$. Then:*

1. *The discrete V-FMO problem (47) admits an optimal solution in which each elasticity tensor saturates the upper bound in (47c), i.e.,*

$$\mathbf{E}_i^* = \mathbf{E}_i^{\text{V}}(v_i^{+\star}) := (1 - v_i^{+\star})\mathbf{E}^- + v_i^{+\star}\mathbf{E}^+, \quad \text{for all } i = 1, \dots, n_e.$$

In particular, there always exists an optimal discrete solution consisting entirely of isotropic tensors.

2. *In the continuum setting of Section 3.1, if (\mathbf{E}, v^+) satisfies the Voigt pointwise admissibility $\mathbf{E}(\mathbf{x}) \in \mathcal{A}^{(1)}(v^+(\mathbf{x}))$ for a.e. $\mathbf{x} \in \Omega$, with $\mathcal{A}^{(1)}$ from (43), and*

$$\tilde{\mathbf{E}}(\mathbf{x}) := (1 - v^+(\mathbf{x}))\mathbf{E}^- + v^+(\mathbf{x})\mathbf{E}^+,$$

then $(\tilde{\mathbf{E}}, v^+)$ is Voigt-admissible and $J(\tilde{\mathbf{E}}) \leq J(\mathbf{E})$. In particular, one may always choose an isotropic minimizer in the continuum Voigt-constrained model.

Proof. For part 1, existence of a discrete minimizer for (47) follows from finite-dimensional compactness: by (47c) and $0 \leq v_i^+ \leq 1$, all \mathbf{E}_i are uniformly bounded between \mathbf{E}^- and \mathbf{E}^+ , and for fixed $(\{\mathbf{E}_i\}, \{v_i^+\})$ the minimal admissible c_j is given by the Schur-complement value $\mathbf{f}_j^\top \mathbf{K}_j(\{\mathbf{E}_i\})^{-1} \mathbf{f}_j$. Let $(\{\mathbf{E}_i^*\}, \{c_j^*\}, \{v_i^{+*}\})$ be such an optimal solution, and suppose that for some index i we have $\mathbf{E}_i^* \neq \mathbf{E}_i^{\text{V}}(v_i^{+*})$. Since $\mathbf{E}_i^* \preceq \mathbf{E}_i^{\text{V}}(v_i^{+*})$, there exists a symmetric positive semidefinite tensor $\mathbf{F}_i \succeq 0$, $\mathbf{F}_i \neq \mathbf{0}$ such that $\mathbf{E}_i^{\text{V}}(v_i^{+*}) = \mathbf{E}_i^* + \mathbf{F}_i$.

Define now a modified design by replacing \mathbf{E}_i^* with $\tilde{\mathbf{E}}_i := \mathbf{E}_i^{\text{V}}(v_i^{+*})$ while keeping all other variables unchanged. The constraints (47c) and (47d) remain satisfied by construction. Since the element stiffness contributions are linear in \mathbf{E}_i , the assembled matrix \mathbf{K}_j is linear in $\{\mathbf{E}_i\}$. Therefore, $\tilde{\mathbf{E}}_i \succeq \mathbf{E}_i^*$ implies $\mathbf{K}_j(\{\tilde{\mathbf{E}}_i\}) \succeq \mathbf{K}_j(\{\mathbf{E}_i^*\})$ and, thus,

$$\begin{pmatrix} c_j^* & -\mathbf{f}_j^\top \\ -\mathbf{f}_j & \mathbf{K}_j(\{\mathbf{E}_i^*\}) \end{pmatrix} \succeq \begin{pmatrix} c_j^* & -\mathbf{f}_j^\top \\ -\mathbf{f}_j & \mathbf{K}_j(\{\tilde{\mathbf{E}}_i\}) \end{pmatrix} \succeq 0. \quad (51)$$

By the Schur complement lemma, this implies $c_j^* \geq \mathbf{f}_j^\top \mathbf{K}_j(\{\tilde{\mathbf{E}}_i\})^{-1} \mathbf{f}_j$, so the compliance remains at most c_j^* , and the updated design is feasible. Repeating this replacement for all i such that $\mathbf{E}_i^* \neq \mathbf{E}_i^{\text{V}}(v_i^{+*})$ yields a fully isotropic design, in which all elasticity tensors lie on the Voigt upper bound.

For part 2, from $\mathbf{E}(\mathbf{x}) \in \mathcal{A}^{(1)}(v^+(\mathbf{x}))$ and (43), we have $\mathbf{E}^- \preceq \mathbf{E}(\mathbf{x}) \preceq \tilde{\mathbf{E}}(\mathbf{x})$ for a.e. \mathbf{x} , so $(\tilde{\mathbf{E}}, v^+)$ is feasible. Moreover, for every loadcase j and every $\mathbf{u} \in \mathcal{U}_0$, $a_{\tilde{\mathbf{E}}}(\mathbf{u}, \mathbf{u}) \geq a_{\mathbf{E}}(\mathbf{u}, \mathbf{u})$. Using the dual representation (24),

$$c_j(\tilde{\mathbf{E}}) = \sup_{\mathbf{u} \in \mathcal{U}_0} (2\ell_j(\mathbf{u}) - a_{\tilde{\mathbf{E}}}(\mathbf{u}, \mathbf{u})) \leq \sup_{\mathbf{u} \in \mathcal{U}_0} (2\ell_j(\mathbf{u}) - a_{\mathbf{E}}(\mathbf{u}, \mathbf{u})) = c_j(\mathbf{E}). \quad (52)$$

Summing over $j = 1, \dots, n_{lc}$ yields $J(\tilde{\mathbf{E}}) \leq J(\mathbf{E})$. Since existence of a continuum minimizer for the Voigt model is established in Section 3.1, applying this isotropic replacement to any minimizer yields an isotropic minimizer. \square

Using the discrete part of Proposition 3.3, optimal elasticities can be parameterized directly by the Voigt mixture. Hence, we reparametrize the optimized elasticities as

$$\mathbf{E}_i(v_i^+) := \mathbf{E}^- + (\mathbf{E}^+ - \mathbf{E}^-)v_i^+ \quad (53)$$

so that the constraint (47c) is always satisfied. This allows us to eliminate the tensor variables and parametrize the tensors only using the scalars $\{v_i^+\}$. Then, the reduced version of the free material optimization problem under Voigt upper bounds reads as

$$\min_{\{c_j\}, \{v_i^+\}} \sum_{j=1}^{n_{lc}} c_j \quad (54a)$$

$$\text{s.t.} \quad \begin{pmatrix} c_j & -\mathbf{f}_j^\top \\ -\mathbf{f}_j & \mathbf{K}_j(\{\mathbf{E}_i(v_i^+)\}) \end{pmatrix} \succeq 0, \quad j = 1, \dots, n_{lc}, \quad (54b)$$

$$\frac{1}{n_e} \sum_{i=1}^{n_e} v_i^+ \leq \bar{V}, \quad (54c)$$

$$0 \leq v_i^+ \leq 1, \forall i \in 1, \dots, n_e. \quad (54d)$$

This corresponds to the standard variable-thickness-sheet problem [44] as also observed by Bendsøe and Sigmund [12]. We refer to (54) as the reduced (equivalent) V-FMO formulation.

3.4. FMO problem under Hashin–Shtrikman upper bounds

Although the Voigt upper bound presented in the previous section tightened the space of elasticity tensors \mathbf{E}_i , it can be further sharpened by exploiting the second-order microstructure characteristics, provided by the Hashin–Shtrikman (upper) bounds. Nevertheless, there is an associated cost: loss of convexity of the optimization problem (Lemma 3.1).

3.4.1. Finite-dimensional semi-infinite formulation

The Hashin–Shtrikman upper bounds on elastic energy take the form

$$\forall \boldsymbol{\varepsilon} \in \mathbb{S}^{2 \times 2} : \langle \mathbf{E}_i \boldsymbol{\varepsilon}, \boldsymbol{\varepsilon} \rangle \leq f^{\text{HS}}(\boldsymbol{\varepsilon}; v_i^+), \quad f^{\text{HS}}(\boldsymbol{\varepsilon}; v_i^+) := \langle [(1 - v_i^+) \mathbf{E}^- + v_i^+ \mathbf{E}^+] \boldsymbol{\varepsilon}, \boldsymbol{\varepsilon} \rangle - q(\boldsymbol{\varepsilon}; v_i^+), \quad (55)$$

where $\boldsymbol{\varepsilon}$ is the strain tensor and $q(\boldsymbol{\varepsilon}; v_i^+)$ is a nonnegative scalar (which we show in Proposition 3.4) that serves as a correction from the Voigt upper bound (42): by setting $q(\boldsymbol{\varepsilon}; v_i^+) = 0$, the inequality $\forall \boldsymbol{\varepsilon} \in \mathbb{S}^{2 \times 2} : \langle \mathbf{E}_i \boldsymbol{\varepsilon}, \boldsymbol{\varepsilon} \rangle \leq \langle [(1 - v_i^+) \mathbf{E}^- + v_i^+ \mathbf{E}^+] \boldsymbol{\varepsilon}, \boldsymbol{\varepsilon} \rangle$ is equivalent to $\mathbf{E}_i \preceq (1 - v_i^+) \mathbf{E}^- + v_i^+ \mathbf{E}^+$. In the notation of (13), the Hashin–Shtrikman-type admissible set reads

$$\mathcal{A}^{(2)}(v) := \left\{ \mathbf{E} \in \mathbb{S}^{2 \times 2 \times 2 \times 2} : \mathbf{E}^- \preceq \mathbf{E}, \langle \mathbf{E} \boldsymbol{\varepsilon}, \boldsymbol{\varepsilon} \rangle \leq f^{\text{HS}}(\boldsymbol{\varepsilon}; v), \quad \forall \boldsymbol{\varepsilon} \in \mathbb{S}^{2 \times 2} \right\}. \quad (56)$$

Thus, (57d) is the elementwise constraint $\mathbf{E}_i \in \mathcal{A}^{(2)}(v_i^+)$.

In contrast to the Voigt upper bound, Hashin–Shtrikman upper bounds are tight in the sense that, for each strain $\boldsymbol{\varepsilon}$, there exists a sequentially laminated composite whose effective tensor attains equality in (55) [5, 3]. The corresponding optimization FMO problem then writes as

$$\min_{\{c_j\}, \{\mathbf{E}_i\}, \{v_i^+\}} \sum_{j=1}^{n_{\text{lc}}} c_j \quad (57a)$$

$$\text{s.t.} \quad \begin{pmatrix} c_j & -\mathbf{f}_j^{\text{T}} \\ -\mathbf{f}_j & \mathbf{K}_j(\{\mathbf{E}_i\}) \end{pmatrix} \succeq 0, \quad j = 1, \dots, n_{\text{lc}}, \quad (57b)$$

$$\mathbf{E}^- \preceq \mathbf{E}_i, \quad i = 1, \dots, n_e, \quad (57c)$$

$$\langle \mathbf{E}_i \boldsymbol{\varepsilon}, \boldsymbol{\varepsilon} \rangle \leq \langle [(1 - v_i^+) \mathbf{E}^- + v_i^+ \mathbf{E}^+] \boldsymbol{\varepsilon}, \boldsymbol{\varepsilon} \rangle - q(\boldsymbol{\varepsilon}; v_i^+) \quad i = 1, \dots, n_e, \forall \boldsymbol{\varepsilon} \in \mathbb{S}^{2 \times 2}, \quad (57d)$$

$$\frac{1}{n_e} \sum_{i=1}^{n_e} v_i^+ \leq \bar{V}, \quad (57e)$$

$$0 \leq v_i^+ \leq 1, \forall i \in 1, \dots, n_e. \quad (57f)$$

Define now $t = |\text{Tr}(\boldsymbol{\varepsilon})|$ and $s = \sqrt{\text{Tr}(\boldsymbol{\varepsilon})^2 - 4 \text{Det}(\boldsymbol{\varepsilon})} = \sqrt{(\varepsilon_{11} - \varepsilon_{22})^2 + 4\varepsilon_{12}^2}$. In addition, let $\Delta\kappa = \kappa^+ - \kappa^- > 0$ and $\Delta\mu = \mu^+ - \mu^- > 0$ be the contrast of the bulk and shear moduli of the isotropic constituents. Then, based on the result of Allaire and Kohn [3, Proposition 2.3], for anisotropic composites made of well-ordered isotropic constituents, q has the explicit form:

$$q(\boldsymbol{\varepsilon}; v_i^+) = \begin{cases} q_1(\boldsymbol{\varepsilon}; v_i^+) := \frac{v_i^+ (1 - v_i^+) (\Delta\kappa t - \Delta\mu s)^2}{\kappa^+ + \mu^+ - (\Delta\kappa + \Delta\mu) v_i^+} & \text{if } v_i^+ t \Delta\kappa \leq (\kappa^+ + \mu^+ - \Delta\kappa v_i^+) s \text{ and } v_i^+ s \Delta\mu \leq (\kappa^+ + \mu^+ - \Delta\mu v_i^+) t, \\ q_2(\boldsymbol{\varepsilon}; v_i^+) := (1 - v_i^+) \left[\frac{v_i^+ t^2 \Delta\kappa^2}{\kappa^+ + \mu^+ - \Delta\kappa v_i^+} - s^2 \Delta\mu \right] & \text{if } v_i^+ t \Delta\kappa > (\kappa^+ + \mu^+ - \Delta\kappa v_i^+) s, \\ q_3(\boldsymbol{\varepsilon}; v_i^+) := (1 - v_i^+) \left[\frac{v_i^+ s^2 \Delta\mu^2}{\kappa^+ + \mu^+ - \Delta\mu v_i^+} - t^2 \Delta\kappa \right] & \text{if } v_i^+ s \Delta\mu > (\kappa^+ + \mu^+ - \Delta\mu v_i^+) t. \end{cases} \quad (58)$$

The correction term $q(\boldsymbol{\varepsilon}; v_i^+)$ in (58) is given by three explicit formulas chosen via two inequalities. These cases form a consistent partition (there is no overlap where both strict inequalities hold), and the expressions coincide on the branch boundaries (in particular $q_1 = q_2$ on Γ_{12} and $q_1 = q_3$ on Γ_{13}), so that q (and hence f^{HS}) is continuous across branch transitions; see Proposition A.1 in the Appendix.

With $q(\boldsymbol{\varepsilon}; v_i^+)$ defined in (58), (55) is invariant under scalar scaling of the strain tensor. Indeed, for any $\alpha \neq 0$ we have $\langle \mathbf{E}_i(\alpha \boldsymbol{\varepsilon}), \alpha \boldsymbol{\varepsilon} \rangle = \alpha^2 \langle \mathbf{E}_i \boldsymbol{\varepsilon}, \boldsymbol{\varepsilon} \rangle$, $|\text{Tr}(\alpha \boldsymbol{\varepsilon})| = |\alpha| |\text{Tr}(\boldsymbol{\varepsilon})|$, and $\text{Det}(\alpha \boldsymbol{\varepsilon}) = \alpha^2 \text{Det}(\boldsymbol{\varepsilon})$. Since the Hashin–Shtrikman envelope $f^{\text{HS}}(\boldsymbol{\varepsilon}; v)$ is positively 2-homogeneous in $\boldsymbol{\varepsilon}$, both sides of (55) scale quadratically with α and the inequality is equivalent for all $\alpha \neq 0$. Hence, it suffices to enforce (55) on any fixed sphere in $\mathbb{S}^{2 \times 2}$. We choose the normalization $\|\boldsymbol{\varepsilon}\|_F = \sqrt{2}/2$, and introduce the invariants

$$t := |\text{Tr}(\boldsymbol{\varepsilon})|, \quad s := \sqrt{\text{Tr}(\boldsymbol{\varepsilon})^2 - 4 \text{Det}(\boldsymbol{\varepsilon})} = \sqrt{(\varepsilon_{11} - \varepsilon_{22})^2 + 4\varepsilon_{12}^2}. \quad (59)$$

For $\|\varepsilon\|_F = \sqrt{2}/2$ these satisfy $t \in [0, 1]$, $s \in [0, 1]$, and the identity $t^2 + s^2 = 2\|\varepsilon\|_F^2 = 1$. Consequently, we may eliminate $s = \sqrt{1 - t^2}$ and parameterize the constraint solely by $t \in [0, 1]$

$$q(t; v_i^+) = \begin{cases} q_1(t; v_i^+) := \frac{v_i^+(1 - v_i^+) (\Delta\kappa t - \Delta\mu\sqrt{1 - t^2})^2}{\kappa^+ + \mu^+ - (\Delta\kappa + \Delta\mu)v_i^+} \\ \quad \text{if } v_i^+ t \Delta\kappa \leq (\kappa^+ + \mu^+ - \Delta\kappa v_i^+) \sqrt{1 - t^2} \text{ and } v_i^+ \Delta\mu \sqrt{1 - t^2} \leq (\kappa^+ + \mu^+ - \Delta\mu v_i^+) t, \\ q_2(t; v_i^+) := (1 - v_i^+) \left[\frac{v_i^+ t^2 \Delta\kappa^2}{\kappa^+ + \mu^+ - \Delta\kappa v_i^+} - (1 - t^2) \Delta\mu \right] \\ \quad \text{if } v_i^+ t \Delta\kappa > (\kappa^+ + \mu^+ - \Delta\kappa v_i^+) \sqrt{1 - t^2}, \\ q_3(t; v_i^+) := (1 - v_i^+) \left[\frac{v_i^+ \Delta\mu^2 (1 - t^2)}{\kappa^+ + \mu^+ - \Delta\mu v_i^+} - t^2 \Delta\kappa \right] \\ \quad \text{if } v_i^+ \Delta\mu \sqrt{1 - t^2} > (\kappa^+ + \mu^+ - \Delta\mu v_i^+) t, \end{cases} \quad (60)$$

which shows that the correction term q depends only on $t = |\text{Tr}(\varepsilon)|$ and the volume fraction v_i^+ . In contrast, the full Hashin–Shtrikman upper bound (55) still depends on the whole strain tensor ε through the Voigt part $\langle [(1 - v_i^+) \mathbf{E}^- + v_i^+ \mathbf{E}^+] \varepsilon, \varepsilon \rangle$. At this stage, the t -parameterization is used only for the correction term; the corresponding one-parameter reduction of the activating-volume map is obtained later for orthotropic tensors in Section 3.5 (Proposition 3.6).

Using this form, we now prove that $q(t; v_i^+) \geq 0$ for all $v_i^+ \in [0, 1]$ and ε , which shows that the Hashin–Shtrikman upper bound (55) is tighter than the Voigt upper bound (42) (see also Figure 2 for a graphical illustration).

Proposition 3.4 (Nonnegativity and equality cases of the HS correction term). *For the Hashin–Shtrikman upper bounds (55) with $q(t; v_i^+)$ defined in (60), it holds for all $v_i^+ \in [0, 1]$ and $\varepsilon \in \mathbb{S}^{2 \times 2}$ with the Frobenius norm $\sqrt{2}/2$ and $t = |\text{Tr}(\varepsilon)|$ that $q(t; v_i^+) \geq 0$. Moreover, $q(t; v_i^+) = 0$ if and only if $v_i^+ \in \{0, 1\}$ or $\Delta\kappa t = \Delta\mu\sqrt{1 - t^2}$.*

Proof. We prove the statement by first analyzing the boundary values $v_i^+ \in \{0, 1\}$ and then showing positivity or nonnegativity of each branch in (60) for $v_i^+ \in (0, 1)$.

Consider now $v_i^+ \in \{0, 1\}$. For $v_i^+ = 0$, the conditions of the first branch are satisfied for all $t \in [0, 1]$ and hence for all strains ε , because the left-hand side of the inequalities are zero and the right-hand sides nonnegative. Using arbitrary t , $q(t; 0) = q_1(t; 0) = 0$ and, therefore, the Voigt upper bound is tight for $v_i^+ = 0$. For $v_i^+ = 1$, all three branches in (60) evaluate as zero due to the $(1 - v_i^+)$ prefactor. Hence, $q(t; 1) = 0$, so the Voigt upper bound is also tight in this case.

Let us further proceed with the branches of $q(t; v_i^+)$ for $v_i^+ \in (0, 1)$. The first branch in (60) is nonnegative due to $v_i^+ \in (0, 1)$, $0 \leq \mu^- < \mu^+$, $0 \leq \kappa^- < \kappa^+$, hence $v_i^+ \Delta\kappa < \kappa^+$ and $v_i^+ \Delta\mu < \mu^+$. Moreover, $q_1(t; v_i^+) = 0$ if and only if $\Delta\kappa t = \Delta\mu\sqrt{1 - t^2}$, i.e., $t = \Delta\mu / \sqrt{\Delta\mu^2 + \Delta\kappa^2}$. Under this equality, the two branch conditions reduce to $\kappa^+ + \mu^+ - v_i^+ (\Delta\kappa + \Delta\mu) \geq 0$, which holds for all $v_i^+ \in (0, 1)$, so the related strains are indeed in this branch. For any other strains $\mathcal{E} := \{\varepsilon \in \mathbb{S}^{2 \times 2} : \text{Tr}(\varepsilon) \neq \Delta\mu / \sqrt{\Delta\mu^2 + \Delta\kappa^2}\}$ satisfying the branch conditions (for example, set $t = 1 / \sqrt{1 + (v_i^+ \Delta\kappa / d_2)^2}$), $q_1(t; v_i^+) > 0$ for all $v_i^+ \in (0, 1)$.

For the second branch in (60), the denominator $d_2 := \kappa^+ + \mu^+ - \Delta\kappa v_i^+$ is positive due to ordered materials, so we only need to show positivity of

$$(1 - v_i^+) [v_i^+ t^2 \Delta\kappa^2 - \Delta\mu d_2 (1 - t^2)] \quad \text{for } v_i^+ t \Delta\kappa \geq d_2 \sqrt{1 - t^2}. \quad (61)$$

Since both sides are nonnegative, squaring preserves inequality and yields $(v_i^+)^2 t^2 \Delta\kappa^2 > d_2^2 (1 - t^2)$, hence $d_2 (1 - t^2) < (v_i^+)^2 t^2 \Delta\kappa^2 / d_2$. Substituting this upper bound into the negative term in (61) gives the lower bound

$$(1 - v_i^+) v_i^+ t^2 \Delta\kappa^2 \frac{\kappa^+ + \mu^+ - (\Delta\kappa + \Delta\mu) v_i^+}{d_2} > 0, \quad (62)$$

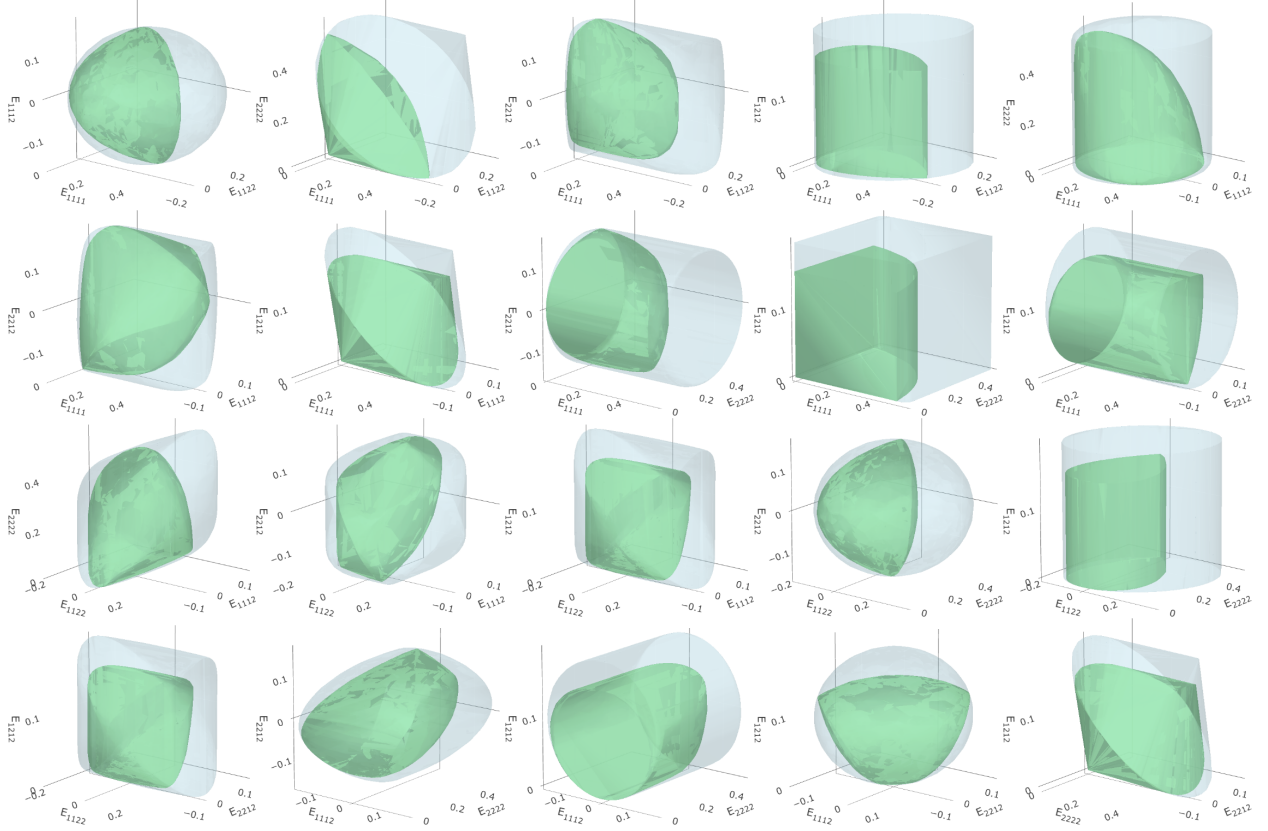


Figure 2: Comparison of the admissible sets $\mathcal{A}^{(2)}(0.5)$ (Hashin–Shtrikman, green) and $\mathcal{A}^{(1)}(0.5)$ (Voigt, blue). The sets are shown in a selected three-dimensional projection of \mathbf{E}_i as outer-envelope boundary surfaces, obtained from 750 sampled strains $\boldsymbol{\varepsilon}$ with Frobenius norm $\sqrt{2}/2$. Material parameters: $\kappa^- = 0.714 \times 10^{-9}$, $\kappa^+ = 0.714$, $\mu^- = 0.385 \times 10^{-9}$, and $\mu^+ = 0.385$.

which is positive due to $v_i^+ \in (0, 1)$ and because $t^2 = 0$ violates the branch condition.

For the third case in (60), the denominator $d_3 = \kappa^+ + \mu^+ - \Delta\mu v_i^+$ is again positive, so we only need to show positivity of

$$(1 - v_i^+) [v_i^+ \Delta\mu^2 (1 - t^2) - \Delta\kappa d_3 t^2] \quad \text{for } v_i^+ \Delta\mu \sqrt{1 - t^2} > d_3 t. \quad (63)$$

Both sides of the right inequality are nonnegative, so it is after squaring equivalent to $(v_i^+)^2 (1 - t^2) \Delta\mu^2 / d_3 > d_3 t^2$. Inserting this upper bound into the negative term in (63), we obtain

$$(1 - v_i^+) v_i^+ (1 - t^2) \Delta\mu^2 \frac{\kappa^+ + \mu^+ - (\Delta\kappa + \Delta\mu) v_i^+}{d_3} > 0, \quad (64)$$

which is also positive for $v_i^+ \in (0, 1)$ as $t^2 = 1$ violates the branch condition. \square

3.4.2. Geometric properties of the Hashin–Shtrikman feasible set

For any fixed v_i^+ and strain sample $\boldsymbol{\varepsilon}$, the Hashin–Shtrikman constraint (55) is affine in the entries of \mathbf{E}_i , hence the feasible set in \mathbf{E}_i is convex (see Figure 2); with an outer approximation by a finite set of sampled strains it becomes a polyhedron. However, (55) is nonconvex in (v_i^+, \mathbf{E}_i) , which we show in the following lemma.

Lemma 3.1 (Nonconvexity of the HS-feasible set). *Let $0 < \kappa^- < \kappa^+$ and $0 < \mu^- < \mu^+$. Then, the Hashin–Shtrikman upper bound (55) with $q(t; v_i^+)$ defined in (60) and $t = |\text{Tr}(\boldsymbol{\varepsilon})|$ is nonconvex in (v_i^+, \mathbf{E}_i) .*

Proof. Consider the feasible pairs $(\mathbf{E}^-, 0)$ and $(\mathbf{E}^+, 1)$. By Proposition 3.4, for any strain $\boldsymbol{\varepsilon}$ (and thus t) we have $q(t; 0) = q(t; 1) = 0$, so (55) holds with equality at both endpoints. Fix any $\theta \in (0, 1)$ and set $\hat{v} := \theta$ and $\hat{\mathbf{E}} := (1 - \theta)\mathbf{E}^- + \theta\mathbf{E}^+$. Evaluating (55) at $(\hat{v}, \hat{\mathbf{E}})$ gives, for any strain $\boldsymbol{\varepsilon}$,

$$\langle \hat{\mathbf{E}}\boldsymbol{\varepsilon}, \boldsymbol{\varepsilon} \rangle \leq \langle [(1 - \hat{v})\mathbf{E}^- + \hat{v}\mathbf{E}^+]\boldsymbol{\varepsilon}, \boldsymbol{\varepsilon} \rangle - q(|\text{Tr}(\boldsymbol{\varepsilon})|; \hat{v}). \quad (65)$$

Since $\hat{\mathbf{E}} = (1 - \hat{v})\mathbf{E}^- + \hat{v}\mathbf{E}^+$, the two quadratic terms are identical and the inequality reduces to $0 \leq -q(\boldsymbol{\varepsilon}; \hat{v})$. However, for any interior $\hat{v} \in (0, 1)$ the strains $\hat{\boldsymbol{\varepsilon}} \in \{\boldsymbol{\varepsilon} \in \mathbb{S}^{2 \times 2} : \text{Tr}(\boldsymbol{\varepsilon}) \neq \Delta\mu/\sqrt{\Delta\mu^2 + \Delta\kappa^2}\}$ result in $q(|\text{Tr}(\hat{\boldsymbol{\varepsilon}})|; \hat{v}) > 0$. Hence, the inequality fails for such a strain, and $(\hat{v}, \hat{\mathbf{E}})$ is infeasible. Therefore, although $(0, \mathbf{E}^-)$ and $(1, \mathbf{E}^+)$ are feasible, every interior convex combination $((1 - \theta)\mathbf{E}^- + \theta\mathbf{E}^+, \theta)$ with $\theta \in (0, 1)$ is infeasible. The feasible set in (v_i^+, \mathbf{E}_i) is thus nonconvex. \square

The nonconvexity of the Hashin–Shtrikman bounds in (v_i^+, \mathbf{E}_i) is illustrated in Figure 3, which shows the feasible sets for varying v_i^+ . The figure also suggests that, when combined with the zeroth-order lower bound $\mathbf{E}^- \preceq \mathbf{E}_i$, the Voigt relation $\mathbf{E}_i \preceq \mathbf{E}_i^V(v_i^+)$ describes the closed convex hull of the Hashin–Shtrikman feasible set in (v_i^+, \mathbf{E}_i) , which we prove next.

Lemma 3.2 (Convex hull of the HS-feasible set). *Define the feasible sets $\mathcal{F}_{\text{HS}} := \{(v, \mathbf{E}) \in [0, 1] \times \mathbb{S}^{2 \times 2 \times 2 \times 2} : \mathbf{E} \in \mathcal{A}^{(2)}(v)\}$, and $\mathcal{F}_V := \{(v, \mathbf{E}) \in [0, 1] \times \mathbb{S}^{2 \times 2 \times 2 \times 2} : \mathbf{E} \in \mathcal{A}^{(1)}(v)\}$. Then, taking the convex hull in the product space $[0, 1] \times \mathbb{S}^{2 \times 2 \times 2 \times 2}$ (with coordinates (v, \mathbf{E})), we have $\text{Conv}(\mathcal{F}_{\text{HS}}) = \mathcal{F}_V$.*

Proof. By definition of $\mathcal{A}^{(2)}(v)$ we have $\mathbf{E}^- \preceq \mathbf{E}$ for all $(v, \mathbf{E}) \in \mathcal{F}_{\text{HS}}$. Moreover, since $q \geq 0$ (cf. Proposition 3.4), we obtain

$$f^{\text{HS}}(\boldsymbol{\varepsilon}; v) = \langle \mathbf{E}^V(v)\boldsymbol{\varepsilon}, \boldsymbol{\varepsilon} \rangle - q(\boldsymbol{\varepsilon}; v) \leq \langle \mathbf{E}^V(v)\boldsymbol{\varepsilon}, \boldsymbol{\varepsilon} \rangle \quad \forall \boldsymbol{\varepsilon}, \forall v \in [0, 1]. \quad (66)$$

Hence, every $(v, \mathbf{E}) \in \mathcal{F}_{\text{HS}}$ satisfies $\mathbf{E} \preceq \mathbf{E}^V(v)$, i.e., $\mathcal{F}_{\text{HS}} \subseteq \mathcal{F}_V$. Since \mathcal{F}_V is convex, this implies that $\text{Conv}(\mathcal{F}_{\text{HS}}) \subseteq \mathcal{F}_V$.

For the reverse inclusion, let $(v, \mathbf{E}) \in \mathcal{F}_V$ be arbitrary. If $v = 0$, then $\mathbf{E} = \mathbf{E}^-$ and $(0, \mathbf{E}^-) \in \mathcal{F}_{\text{HS}}$ (cf. the endpoint identity $f^{\text{HS}}(\cdot; 0) = \langle \mathbf{E}^-, \cdot \rangle$, e.g. Proposition 3.4). Assume $v \in (0, 1]$ and define

$$\mathbf{E}_1 := \mathbf{E}^- + \frac{1}{v}(\mathbf{E} - \mathbf{E}^-). \quad (67)$$

From $\mathbf{E} \preceq \mathbf{E}^V(v) = \mathbf{E}^- + v(\mathbf{E}^+ - \mathbf{E}^-)$ we infer $\mathbf{E}_1 \preceq \mathbf{E}^+$ and clearly $\mathbf{E}^- \preceq \mathbf{E}_1$. Using the endpoint identity $f^{\text{HS}}(\cdot; 1) = \langle \mathbf{E}^+, \cdot \rangle$ (Proposition 3.4), it follows that $(1, \mathbf{E}_1) \in \mathcal{F}_{\text{HS}}$. Consequently,

$$(v, \mathbf{E}) = (1 - v)(0, \mathbf{E}^-) + v(1, \mathbf{E}_1) \in \text{Conv}(\mathcal{F}_{\text{HS}}), \quad (68)$$

which shows $\mathcal{F}_V \subseteq \text{Conv}(\mathcal{F}_{\text{HS}})$. Together with $\mathcal{F}_V \supseteq \text{Conv}(\mathcal{F}_{\text{HS}})$ this yields $\text{Conv}(\mathcal{F}_{\text{HS}}) = \mathcal{F}_V$. \square

3.4.3. Eliminating the volume fractions

As in the Voigt case, we show that the Hashin–Shtrikman constraint is active at optimality, which allows us to reformulate (57) by eliminating v_i^+ . By Propositions A.1 and A.2 in the Appendix, for every fixed $\boldsymbol{\varepsilon}$ the map $v \mapsto f^{\text{HS}}(\boldsymbol{\varepsilon}; v)$ is continuous and nondecreasing. Hence, for fixed $(\mathbf{E}_i, \boldsymbol{\varepsilon})$ the feasibility set in v_i^+ is an interval,

$$\{v_i^+ \in [0, 1] : \langle \mathbf{E}_i\boldsymbol{\varepsilon}, \boldsymbol{\varepsilon} \rangle \leq f^{\text{HS}}(\boldsymbol{\varepsilon}; v_i^+)\} = [\hat{v}_i(\boldsymbol{\varepsilon}; \mathbf{E}_i), 1], \quad (69)$$

where $\hat{v}_i(\boldsymbol{\varepsilon}; \mathbf{E}_i) \in [0, 1]$ denotes the minimal admissible volume fraction (equivalently, the smallest v such that the inequality holds; when $\langle \mathbf{E}_i\boldsymbol{\varepsilon}, \boldsymbol{\varepsilon} \rangle$ lies on the graph this means $\langle \mathbf{E}_i\boldsymbol{\varepsilon}, \boldsymbol{\varepsilon} \rangle = f^{\text{HS}}(\boldsymbol{\varepsilon}; \hat{v}_i(\boldsymbol{\varepsilon}; \mathbf{E}_i))$). Imposing the Hashin–Shtrikman inequality for all normalized strains is, therefore, equivalent to

$$v_i^+ \geq \bar{v}_i(\mathbf{E}_i) := \sup_{\boldsymbol{\varepsilon} \in \mathbb{S}^{2 \times 2} : \|\boldsymbol{\varepsilon}\|_F = \sqrt{2}/2} \hat{v}_i(\boldsymbol{\varepsilon}; \mathbf{E}_i). \quad (70)$$

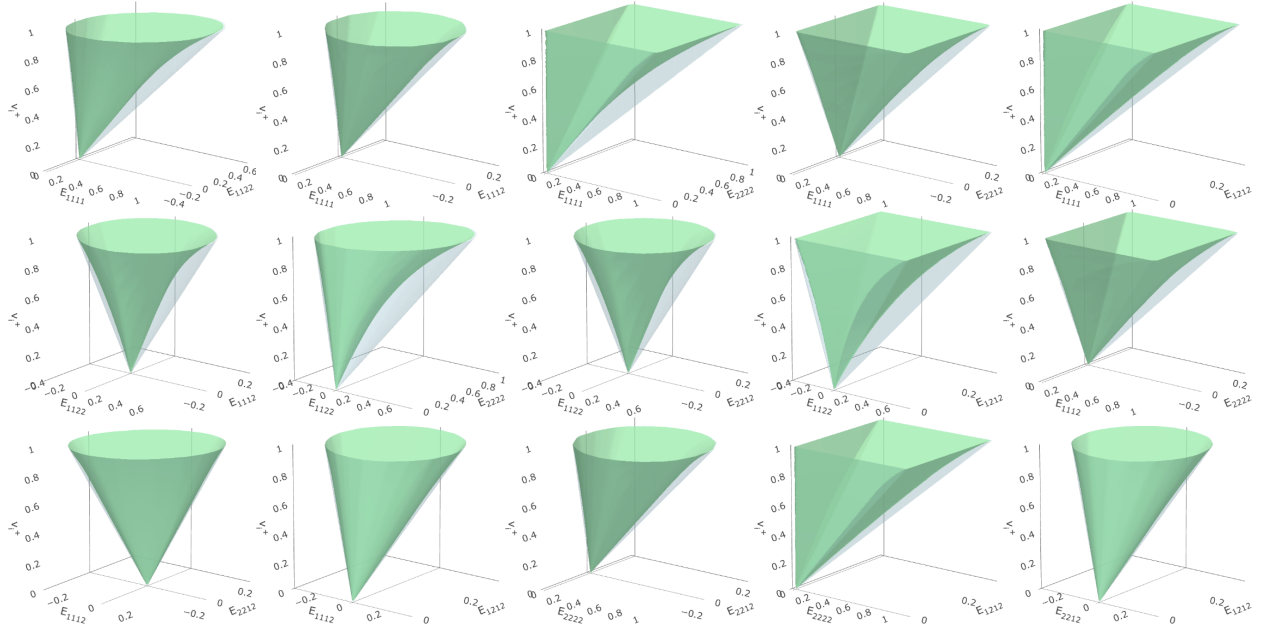


Figure 3: Comparison of the product-space feasible sets \mathcal{F}_{HS} (green) and \mathcal{F}_V (blue), defined in Lemma 3.2. The figure shows projections in (\mathbf{E}_i, v_i^+) for all pairs of selected components of \mathbf{E}_i together with v_i^+ . Each plotted set is shown by its boundary surface, obtained by sampling v_i^+ and taking the outer hull of feasible points, using 250 sampled strains $\boldsymbol{\varepsilon}$ with Frobenius norm $\sqrt{2}/2$. Material parameters: $\kappa^- = 0.714 \times 10^{-9}$, $\kappa^+ = 0.714$, $\mu^- = 0.385 \times 10^{-9}$, and $\mu^+ = 0.385$.

Lemma 3.3 (Elementwise activity of the HS constraint at optimality). *There exists an optimal solution of (57) such that, for every element i , $v_i^+ = \bar{v}_i(\mathbf{E}_i) = \inf\{v \in [0, 1] : \mathbf{E}_i \in \mathcal{A}^{(2)}(v)\}$.*

Proof. Let $(c_j^*, \mathbf{E}_i^*, v_i^{+*})$ be any optimal solution. By monotonicity (Proposition A.2) and continuity (Proposition A.1), for each i we can decrease v_i^{+*} down to

$$\tilde{v}_i^+ := \inf\{v_i^+ \in [0, 1] : \langle \mathbf{E}_i^* \boldsymbol{\varepsilon}, \boldsymbol{\varepsilon} \rangle \leq f^{\text{HS}}(\boldsymbol{\varepsilon}; v_i^+), \forall \boldsymbol{\varepsilon}\} = \bar{v}_i(\mathbf{E}_i^*), \quad (71)$$

without violating (57d). This operation leaves \mathbf{E}_i^* unchanged, so all matrices $\mathbf{K}_j(\{\mathbf{E}_i\})$ and the objective $\sum_{j=1}^{n_{1c}} c_j$ remain the same. It only reduces the left-hand side of the volume constraint (57e), so feasibility is preserved. Hence, $(c_j^*, \mathbf{E}_i^*, \tilde{v}_i^+)$ is also optimal, with each \tilde{v}_i^+ equal to the minimal admissible value for fixed \mathbf{E}_i^* . \square

In particular, activity here is with respect to the design variable v_i^+ for fixed \mathbf{E}_i : v_i^+ is reduced to its minimal admissible value, not interpreted as equality in (55) for every strain. It remains to compute $\hat{v}(\boldsymbol{\varepsilon}; \mathbf{E}_i)$ explicitly. The following result provides closed-form expressions by solving the equality $\langle \mathbf{E}_i \boldsymbol{\varepsilon}, \boldsymbol{\varepsilon} \rangle = f^{\text{HS}}(\boldsymbol{\varepsilon}; v_i^+)$ for each branch of (60).

Proposition 3.5 (Closed-form minimal admissible volume for HS activity). *For any fixed $\mathbf{E}_i \in \{\mathbf{E} : \mathbf{E}^- \preceq \mathbf{E} \preceq \mathbf{E}^+\}$ and strain $\boldsymbol{\varepsilon} \in \mathbb{S}^{2 \times 2}$ with the Frobenius norm $\sqrt{2}/2$, the minimal $v_i^+ \in [0, 1]$ such that the Hashin–Shtrikman upper bound (55) with $q(t; v_i^+)$ defined in (60) is active, i.e., $\langle \mathbf{E}_i \boldsymbol{\varepsilon}, \boldsymbol{\varepsilon} \rangle = f^{\text{HS}}(\boldsymbol{\varepsilon}; v_i^+)$, is given*

by

$$\hat{v}(\boldsymbol{\varepsilon}; \mathbf{E}_i) = \begin{cases} \hat{v}_1(\boldsymbol{\varepsilon}; \mathbf{E}_i) := \frac{1}{2} + \frac{\langle \mathbf{E}_i \boldsymbol{\varepsilon}, \boldsymbol{\varepsilon} \rangle (\Delta\mu + \Delta\kappa) + (2t^2 - 1)(\Delta\kappa\mu^+ - \Delta\mu\kappa^+) - \sqrt{D}}{2\Delta\mu\Delta\kappa(t + \sqrt{1 - t^2})^2} \\ \text{if } \hat{v}_1 \leq \frac{\kappa^+ + \mu^+}{t + \sqrt{1 - t^2}} \min \left\{ \frac{\sqrt{1 - t^2}}{\Delta\kappa}, \frac{t}{\Delta\mu} \right\} \\ \hat{v}_2(\boldsymbol{\varepsilon}; \mathbf{E}_i) := \frac{\kappa^+ + \mu^+}{\Delta\kappa} \left[1 - \frac{t^2(\kappa^- + \mu^+)}{\langle \mathbf{E}_i \boldsymbol{\varepsilon}, \boldsymbol{\varepsilon} \rangle - \mu^+(1 - 2t^2)} \right] & \text{if } \hat{v}_2 > \frac{(\kappa^+ + \mu^+)\sqrt{1 - t^2}}{\Delta\kappa(t + \sqrt{1 - t^2})} \\ \hat{v}_3(\boldsymbol{\varepsilon}; \mathbf{E}_i) := \frac{\kappa^+ + \mu^+}{\Delta\mu} \left[1 - \frac{(1 - t^2)(\kappa^+ + \mu^-)}{\langle \mathbf{E}_i \boldsymbol{\varepsilon}, \boldsymbol{\varepsilon} \rangle + \kappa^+(1 - 2t^2)} \right] & \text{if } \hat{v}_3 > \frac{(\kappa^+ + \mu^+)t}{\Delta\mu(t + \sqrt{1 - t^2})} \end{cases} \quad (72)$$

with

$$D = \left[\langle \mathbf{E}_i \boldsymbol{\varepsilon}, \boldsymbol{\varepsilon} \rangle (\Delta\mu + \Delta\kappa) + (1 - 2t^2)(\Delta\mu\kappa^+ - \Delta\kappa\mu^+) + \Delta\mu\Delta\kappa(\sqrt{1 - t^2} + t)^2 \right]^2 - 4\Delta\mu\Delta\kappa(\kappa^+ + \mu^+)(\sqrt{1 - t^2} + t)^2 (\langle \mathbf{E}_i \boldsymbol{\varepsilon}, \boldsymbol{\varepsilon} \rangle + (t^2 - 1)\mu^- - t^2\kappa^-). \quad (73)$$

Proof. Define, for $t \in [0, 1]$,

$$v_{12}(t) = \frac{\kappa^+ + \mu^+}{\Delta\kappa} \frac{\sqrt{1 - t^2}}{t + \sqrt{1 - t^2}}, \quad v_{13}(t) = \frac{\kappa^+ + \mu^+}{\Delta\mu} \frac{t}{t + \sqrt{1 - t^2}}. \quad (74)$$

Then the branch conditions in (60) are equivalently $v_i^+ \leq \min\{v_{12}(t), v_{13}(t)\}$ in the first branch, $v_i^+ > v_{12}(t)$ in the second branch, and $v_i^+ > v_{13}(t)$ in the third branch.

For the first branch in (60), after unification to a common denominator and grouping powers of v_i^+ , the Hashin–Shtrikman equality reads as

$$0 = \frac{(v_i^+)^2(-\Delta\mu\Delta\kappa(\sqrt{1 - t^2} + t)^2) - [(\kappa^+ + \mu^+)(\langle \mathbf{E}_i \boldsymbol{\varepsilon}, \boldsymbol{\varepsilon} \rangle + \Delta\mu(1 - t^2) + \Delta\kappa t^2 - \kappa^+ t^2 - \mu^+(1 - t^2))]}{\kappa^+ + \mu^+ - (\Delta\kappa + \Delta\mu)v_i^+} + \frac{v_i^+ [\langle \mathbf{E}_i \boldsymbol{\varepsilon}, \boldsymbol{\varepsilon} \rangle (\Delta\mu + \Delta\kappa) + (1 - 2t^2)(\Delta\mu\kappa^+ - \Delta\kappa\mu^+) + \Delta\mu\Delta\kappa(\sqrt{1 - t^2} + t)^2]}{\kappa^+ + \mu^+ - (\Delta\kappa + \Delta\mu)v_i^+}. \quad (75)$$

Thus, we search for the roots of the quadratic polynomial in the numerator, which can be expressed as

$$\frac{1}{2} + \frac{\langle \mathbf{E}_i \boldsymbol{\varepsilon}, \boldsymbol{\varepsilon} \rangle (\Delta\mu + \Delta\kappa) + (2t^2 - 1)(\Delta\kappa\mu^+ - \Delta\mu\kappa^+) \pm \sqrt{D}}{2\Delta\mu\Delta\kappa(t + \sqrt{1 - t^2})^2} \quad (76)$$

with D in (73). Due to uniqueness of the activating volume fraction (Corollary A.1), $D \geq 0$ but only one root can be admissible in $[0, 1]$, so it remains to show which one. To this end, set $\mathbf{E}_i = \mathbf{E}^-$. Then, (76) simplifies to

$$\frac{1}{2} + \frac{(t^2\Delta\kappa + (1 - t^2)\Delta\mu)(\kappa^- + \mu^-) \pm [(t^2\Delta\kappa + (1 - t^2)\Delta\mu)(\kappa^+ + \mu^+) - (\Delta\kappa t - \Delta\mu\sqrt{1 - t^2})^2]}{2\Delta\mu\Delta\kappa(t + \sqrt{1 - t^2})^2} = \begin{cases} 0 \\ 1 + \frac{(\Delta\mu(1 - t^2) + \Delta\kappa t^2)(\kappa^- + \mu^-)}{\Delta\mu\Delta\kappa(t + \sqrt{1 - t^2})^2}. \end{cases} \quad (77)$$

Clearly, the “negative” root gives admissible $v_i^+ = 0$, whereas the “positive” root gives $v_i^+ > 1$. By strict monotonicity in v_i^+ (Proposition A.2), the admissible root for any $\mathbf{E}_i \in [\mathbf{E}^-, \mathbf{E}^+]$ is, therefore, the “negative” root, i.e.,

$$\hat{v}_1(\boldsymbol{\varepsilon}; \mathbf{E}_i) = \frac{1}{2} + \frac{\langle \mathbf{E}_i \boldsymbol{\varepsilon}, \boldsymbol{\varepsilon} \rangle (\Delta\mu + \Delta\kappa) + (2t^2 - 1)(\Delta\kappa\mu^+ - \Delta\mu\kappa^+) - \sqrt{D}}{2\Delta\mu\Delta\kappa(t + \sqrt{1 - t^2})^2}. \quad (78)$$

Consider now the second branch in (60). Rearranging the equality $\langle \mathbf{E}_i \boldsymbol{\varepsilon}, \boldsymbol{\varepsilon} \rangle = f^{\text{HS}}(\boldsymbol{\varepsilon}; v_i^+)$ gives

$$0 = \frac{\Delta\kappa(\mu^+(2t^2 - 1) + \langle \mathbf{E}_i \boldsymbol{\varepsilon}, \boldsymbol{\varepsilon} \rangle) v_i^+ + (\kappa^+ + \mu^+)(\kappa^- t^2 + \mu^+(1 - t^2) - \langle \mathbf{E}_i \boldsymbol{\varepsilon}, \boldsymbol{\varepsilon} \rangle)}{\kappa^+ + \mu^+ - \Delta\kappa v_i^+}. \quad (79)$$

Equating the numerator gives the solution

$$\hat{v}_2(\boldsymbol{\varepsilon}; \mathbf{E}_i) = \frac{\kappa^+ + \mu^+}{\Delta\kappa} \left[1 - \frac{t^2(\kappa^- + \mu^+)}{\langle \mathbf{E}_i \boldsymbol{\varepsilon}, \boldsymbol{\varepsilon} \rangle - \mu^+(1 - 2t^2)} \right]. \quad (80)$$

For the third branch in (60), rearranging the equality $\langle \mathbf{E}_i \boldsymbol{\varepsilon}, \boldsymbol{\varepsilon} \rangle = f^{\text{HS}}(\boldsymbol{\varepsilon}; v_i^+)$ gives

$$0 = \frac{\Delta\mu(\kappa^+(1 - 2t^2) + \langle \mathbf{E}_i \boldsymbol{\varepsilon}, \boldsymbol{\varepsilon} \rangle) v_i^+ + (\kappa^+ + \mu^+)(\kappa^+ t^2 + \mu^-(1 - t^2) - \langle \mathbf{E}_i \boldsymbol{\varepsilon}, \boldsymbol{\varepsilon} \rangle)}{\kappa^+ + \mu^+ - \Delta\mu v_i^+}, \quad (81)$$

with the numerator providing

$$\hat{v}_3(\boldsymbol{\varepsilon}; \mathbf{E}_i) = \frac{\kappa^+ + \mu^+}{\Delta\mu} \left[1 - \frac{(1 - t^2)(\kappa^+ + \mu^-)}{\langle \mathbf{E}_i \boldsymbol{\varepsilon}, \boldsymbol{\varepsilon} \rangle + \kappa^+(1 - 2t^2)} \right]. \quad (82)$$

□

By Lemma 3.3, at optimality one may always take $v_i^+ = \bar{v}_i(\mathbf{E}_i)$, with $\bar{v}_i(\mathbf{E}_i)$ defined in (70) and $\hat{v}(\boldsymbol{\varepsilon}; \mathbf{E}_i)$ given in Proposition 3.5. The free material optimization problem under Hashin–Shtrikman upper bounds (57) can, therefore, be written as

$$\min_{\{c_j\}, \{\mathbf{E}_i\}} \sum_{j=1}^{n_{lc}} c_j \quad (83a)$$

$$\text{s.t.} \quad \begin{pmatrix} c_j & -\mathbf{f}_j^\top \\ -\mathbf{f}_j & \mathbf{K}_j(\{\mathbf{E}_i\}) \end{pmatrix} \succeq 0, \quad j = 1, \dots, n_{lc}, \quad (83b)$$

$$\mathbf{E}^- \preceq \mathbf{E}_i \preceq \mathbf{E}^+, \quad i = 1, \dots, n_e, \quad (83c)$$

$$\frac{1}{n_e} \sum_{i=1}^{n_e} \sup_{\boldsymbol{\varepsilon} \in \mathbb{S}^{2 \times 2}: \|\boldsymbol{\varepsilon}\|_F = \sqrt{2}/2} \hat{v}(\boldsymbol{\varepsilon}; \mathbf{E}_i) \leq \bar{V} \quad (83d)$$

in which (83c) guarantees that the volume given in Proposition 3.5 is in the $[0, 1]$ domain.

3.4.4. Single-loadcase equivalence in the continuum setting

The nonconvexity of the Hashin–Shtrikman upper bounds in (v_i^+, \mathbf{E}_i) (Lemma 3.1) carries over to the nonconvexity of (57) and (83). Moreover, due to the nature of the volume function in Proposition 3.5, both these problems are nonsmooth (this can be seen by evaluating the derivatives at the branch boundaries, we refer to Proposition A.2 in the appendix for explicit formulas). Nevertheless, for the special case of a single-loadcase ($n_{lc} = 1$), we can identify the continuum Hashin–Shtrikman/Allaire–Kohn (HS/AK) relaxation with the relaxed single-loadcase compliance problem of Allaire and Kohn [4], which is attained (in the relaxation sense) by sequential laminates. This result is stated in the following theorem.

Theorem 3.1 (Tightness of the HS/AK relaxation in the single-loadcase continuum setting). *Assume the standing continuum hypotheses of Section 3.1 (in particular, the regularity of Ω , boundary conditions ensuring coercivity on \mathcal{U}_0 , and a bounded linear load functional $\ell := \ell_1$ from (5)), two-dimensional plane stress with well-ordered isotropic phases $\mathbf{0} \prec \mathbf{E}^- \prec \mathbf{E}^+$, and a single-loadcase. Define*

$$\mathcal{V}_{\bar{V}} := \left\{ v^+ \in L^\infty(\Omega; [0, 1]) : \int_{\Omega} v^+(\mathbf{x}) \, d\mathbf{x} \leq \bar{V} |\Omega| \right\}. \quad (84)$$

Let $c_{\text{HS-FMO}}^{\text{cont}}$ be the infimum value of the continuum FMO problem (15) from Section 3.1 (with $n_{1c} = 1$), taken over all pairs $(v^+, \mathbf{E}) \in \mathcal{V}_{\overline{V}} \times L^\infty(\Omega; \mathbb{S}^{2 \times 2 \times 2 \times 2})$ satisfying the pointwise admissibility $\mathbf{E}(\mathbf{x}) \in \mathcal{A}^{(2)}(v^+(\mathbf{x}))$ for a.e. $\mathbf{x} \in \Omega$, where $\mathcal{A}^{(2)}$ is given by (56). We refer to this model as the continuum Hashin–Shtrikman-constrained free material optimization problem (HS-FMO). Define the Allaire–Kohn primal relaxed value by

$$c_{\text{AK,pr}}^{\text{cont}} := \inf_{v^+ \in \mathcal{V}_{\overline{V}}} \sup_{\mathbf{u} \in \mathcal{U}_0} \left\{ 2\ell(\mathbf{u}) - \int_{\Omega} f^{\text{HS}}(\boldsymbol{\varepsilon}(\mathbf{u}); v^+) \, d\mathbf{x} \right\}. \quad (85)$$

Further, define the complementary-energy envelope

$$f_c^{\text{HS}}(\boldsymbol{\sigma}; v) := \sup_{\boldsymbol{\varepsilon} \in \mathbb{S}^{2 \times 2}} \{ 2\langle \boldsymbol{\sigma}, \boldsymbol{\varepsilon} \rangle - f^{\text{HS}}(\boldsymbol{\varepsilon}; v) \}, \quad (86)$$

the statically admissible stress set

$$\Sigma_{\text{ad}} := \left\{ \boldsymbol{\sigma} \in L^2(\Omega; \mathbb{S}^{2 \times 2}) : \int_{\Omega} \langle \boldsymbol{\sigma}, \boldsymbol{\varepsilon}(\mathbf{v}) \rangle \, d\mathbf{x} = \ell(\mathbf{v}), \forall \mathbf{v} \in \mathcal{U}_0 \right\}, \quad (87)$$

and the dual relaxed value

$$c_{\text{AK,du}}^{\text{cont}} := \inf_{v^+ \in \mathcal{V}_{\overline{V}}} \inf_{\boldsymbol{\sigma} \in \Sigma_{\text{ad}}} \int_{\Omega} f_c^{\text{HS}}(\boldsymbol{\sigma}; v^+) \, d\mathbf{x}. \quad (88)$$

Then,

$$c_{\text{HS-FMO}}^{\text{cont}} = c_{\text{AK,pr}}^{\text{cont}} = c_{\text{AK,du}}^{\text{cont}} =: c_{\text{AK}}^{\text{cont}}. \quad (89)$$

Moreover, the common value is attained in the relaxation sense by a sequence of orthotropic sequential laminates (of rank at most two) with vanishing microstructural length scale.

Proof. Fix any HS-FMO admissible pair (v^+, \mathbf{E}) , i.e., $v^+ \in \mathcal{V}_{\overline{V}}$, $\mathbf{E} \in L^\infty(\Omega; \mathbb{S}^{2 \times 2 \times 2 \times 2})$, and $\mathbf{E}(\mathbf{x}) \in \mathcal{A}^{(2)}(v^+(\mathbf{x}))$ for a.e. $\mathbf{x} \in \Omega$. For this fixed pair, the single-loadcase compliance admits the dual representation (24),

$$c(v^+, \mathbf{E}) = \sup_{\mathbf{w} \in \mathcal{U}_0} \left\{ 2\ell(\mathbf{w}) - \int_{\Omega} \langle \mathbf{E} \boldsymbol{\varepsilon}(\mathbf{w}), \boldsymbol{\varepsilon}(\mathbf{w}) \rangle \, d\mathbf{x} \right\}. \quad (90)$$

Because $\mathbf{E}(\mathbf{x}) \in \mathcal{A}^{(2)}(v^+(\mathbf{x}))$, for a.e. $\mathbf{x} \in \Omega$ and all $\boldsymbol{\varepsilon} \in \mathbb{S}^{2 \times 2}$ we have $\langle \mathbf{E}(\mathbf{x}) \boldsymbol{\varepsilon}, \boldsymbol{\varepsilon} \rangle \leq f^{\text{HS}}(\boldsymbol{\varepsilon}; v^+(\mathbf{x}))$. Hence, for every $\mathbf{w} \in \mathcal{U}_0$,

$$2\ell(\mathbf{w}) - \int_{\Omega} \langle \mathbf{E} \boldsymbol{\varepsilon}(\mathbf{w}), \boldsymbol{\varepsilon}(\mathbf{w}) \rangle \, d\mathbf{x} \geq 2\ell(\mathbf{w}) - \int_{\Omega} f^{\text{HS}}(\boldsymbol{\varepsilon}(\mathbf{w}); v^+) \, d\mathbf{x}. \quad (91)$$

Taking supremum in \mathbf{w} yields

$$c(v^+, \mathbf{E}) \geq \sup_{\mathbf{w} \in \mathcal{U}_0} \left\{ 2\ell(\mathbf{w}) - \int_{\Omega} f^{\text{HS}}(\boldsymbol{\varepsilon}(\mathbf{w}); v^+) \, d\mathbf{x} \right\}. \quad (92)$$

Taking infimum over all HS-FMO admissible (v^+, \mathbf{E}) gives

$$c_{\text{HS-FMO}}^{\text{cont}} \geq c_{\text{AK,pr}}^{\text{cont}}. \quad (93)$$

For the converse inequality, fix $\delta > 0$ and define

$$\mathcal{J}(v^+) := \sup_{\mathbf{u} \in \mathcal{U}_0} \left\{ 2\ell(\mathbf{u}) - \int_{\Omega} f^{\text{HS}}(\boldsymbol{\varepsilon}(\mathbf{u}); v^+) \, d\mathbf{x} \right\}, \quad v^+ \in \mathcal{V}_{\overline{V}}. \quad (94)$$

By definition of $c_{\text{AK,pr}}^{\text{cont}}$, there exists $v_\delta^+ \in \mathcal{V}_{\overline{V}}$ such that $\mathcal{J}(v_\delta^+) \leq c_{\text{AK,pr}}^{\text{cont}} + \delta$. Now use the recovery result for the single-loadcase Allaire–Kohn relaxation [3, 4]: there exists a sequence of sequential-laminate microstructures with characteristic scale tending to zero; denote by $(v_{\delta,m}^+, \mathbf{E}_{\delta,m})$ with $m \rightarrow \infty$ their associated homogenized (effective) design fields. In the present 2D, well-ordered isotropic setting, these recovering laminates can be

chosen orthotropic and of rank at most two (rank-one in one branch, rank-two in the others, with layering directions tied to principal directions), cf. [3, 1]. These satisfy $v_{\delta,m}^+ \in \mathcal{V}_{\overline{V}}$, and $\mathbf{E}_{\delta,m}(\mathbf{x}) \in \mathcal{A}^{(2)}(v_{\delta,m}^+(\mathbf{x}))$ for a.e. $\mathbf{x} \in \Omega$, and $c(v_{\delta,m}^+, \mathbf{E}_{\delta,m}) \rightarrow \mathcal{J}(v_{\delta}^+)$. Since $c_{\text{HS-FMO}}^{\text{cont}}$ is the infimum over all such admissible pairs, for every m we have $c_{\text{HS-FMO}}^{\text{cont}} \leq c(v_{\delta,m}^+, \mathbf{E}_{\delta,m})$. Passing to the limit $m \rightarrow \infty$ gives $c_{\text{HS-FMO}}^{\text{cont}} \leq \mathcal{J}(v_{\delta}^+) \leq c_{\text{AK,pr}}^{\text{cont}} + \delta$. Because $\delta > 0$ is arbitrary, we obtain

$$c_{\text{HS-FMO}}^{\text{cont}} \leq c_{\text{AK,pr}}^{\text{cont}}. \quad (95)$$

Combining (93) and (95), $c_{\text{HS-FMO}}^{\text{cont}} = c_{\text{AK,pr}}^{\text{cont}}$.

It remains to identify the primal and dual AK values directly in the fixed-volume setting. By definition (86), for every fixed v^+ , $f_c^{\text{HS}}(\cdot; v^+)$ is the Fenchel conjugate of $f^{\text{HS}}(\cdot; v^+)$. In the homogenized setting, combining the minimum complementary-energy principle [1, Theorem 4.1.9 and Eqs. (4.36)–(4.39)], the local character of the G -closure [1, Theorem 2.1.2], and the explicit Hashin–Shtrikman complementary bound/regularity [1, Proposition 2.3.25 and Remark 2.3.27] yields, for every fixed $v^+ \in \mathcal{V}_{\overline{V}}$,

$$\sup_{\mathbf{u} \in \mathcal{U}_0} \left\{ 2\ell(\mathbf{u}) - \int_{\Omega} f^{\text{HS}}(\boldsymbol{\varepsilon}(\mathbf{u}); v^+) \, d\mathbf{x} \right\} = \inf_{\boldsymbol{\sigma} \in \Sigma_{\text{ad}}} \int_{\Omega} f_c^{\text{HS}}(\boldsymbol{\sigma}; v^+) \, d\mathbf{x}. \quad (96)$$

Taking the infimum over $v^+ \in \mathcal{V}_{\overline{V}}$ on both sides yields $c_{\text{AK,pr}}^{\text{cont}} = c_{\text{AK,du}}^{\text{cont}}$. Hence, $c_{\text{HS-FMO}}^{\text{cont}} = c_{\text{AK,pr}}^{\text{cont}} = c_{\text{AK,du}}^{\text{cont}} = c_{\text{AK}}^{\text{cont}}$. The same recovery construction yields attainment in the relaxation sense by a sequence of orthotropic sequential laminates of rank at most two. \square

Theorem 3.1 is a continuum relaxation statement based on scale separation: the relaxed optimum is attained in the relaxation sense by sequences of sequential laminates whose characteristic length tends to zero. One should therefore not interpret Theorem 3.1 as an exact equivalence for a fixed finite element discretization of (57) or (83). Three issues are relevant.

First, while numerical stabilization (filters, perimeter or gradient penalties on design variables) is often necessary in practice [28], it is not innocuous from the viewpoint of laminate realizability: the set of orthotropic sequential laminate tensors (at fixed v^+) is generally not convex in \mathbf{E} (see Fig. 4). Consequently, regularization mechanisms that enforce local averaging or smoothness of \mathbf{E} may produce tensors that are no longer representable in this class, even if each unregularized pointwise optimum is.

Second, the Hashin–Shtrikman envelope $f^{\text{HS}}(\boldsymbol{\varepsilon}; v)$ is tight in the sense that, for each fixed strain $\boldsymbol{\varepsilon}$, there exist sequential laminates attaining equality in (55). In a discretization with nonconstant strains inside an element (e.g., higher-order elements or multi-point quadrature), the elemental contribution involves multiple strain modes. Optimality then drives \mathbf{E}_i against a superposition of strain directions. There is, in general, no guarantee that a single orthotropic sequential laminate simultaneously saturates all active bounds; thus laminate constructions designed for a single strain direction need not be exact discrete optimizers on a fixed mesh.

Last, Allaire’s continuum duality framework constructs laminates pointwise from the local macroscopic fields. In discrete implementations this is often approximated by designing laminates for an elementwise representative strain/stress (e.g., midpoint or average [1]). Such a replacement is theoretically justified precisely in the scale-separation regime where the macroscopic strain is (approximately) constant at the sampling scale; otherwise it should be viewed as an approximation rather than an exact characterization of the discrete HS-FMO optimum.

In summary, Theorem 3.1 identifies the correct continuum limit of the HS-FMO formulation. In the single-load, well-ordered isotropic case, the HS-relaxed problem is tight: it attains the same optimal value as the relaxed compliance minimization problem of Allaire and Kohn [4], and both optima are attained by sequential laminates. Nevertheless, in our formulation we do not restrict the feasible set of the elasticity tensors to sequential laminates or any other specific microstructure class [2]. Moreover, for a fixed finite element discretization, discrete equivalence with laminate-based constructions is expected only asymptotically, and it may be altered by numerical regularization. For multiple loadcases, the optimal solution of (57) or (83) is generally not tight and therefore provides only a lower bound on the optimal value of compliance minimization over all microstructures; tightness in the multi-loadcase setting would additionally require enforcing Hashin–Shtrikman upper bounds on the sum of elastic energies [5, 6, 9].

3.5. Free orthotropic material optimization under Hashin–Shtrikman upper bound

In what follows, we consider the FMO problem under the Hashin–Shtrikman upper bounds (83), with the additional restriction that $\{\mathbf{E}_i\}$ are orthotropic. We refer to this setting as free-orthotropic material optimization (FOMO), and to its Hashin–Shtrikman-constrained version as HS-FOMO. Orthotropic materials possess three mutually orthogonal planes of symmetry, which in two dimensions implies that the stiffness tensor has four independent components. In a suitable coordinate system, the off-diagonal shear couplings vanish, i.e., $E_{1112} = E_{2212} = 0$.

To make the dependence on the material orientation explicit, for each orthotropic tensor \mathbf{E}_i we denote by \mathbf{E}_i^b its representation in a material (base) coordinate system in which $(\mathbf{E}_i^b)_{1112} = (\mathbf{E}_i^b)_{2212} = 0$. We parametrize its global orientation by an angle $\varphi_i \in [0, \pi)$ and the corresponding planar rotation

$$\mathbf{Q}(\varphi) := \begin{pmatrix} \cos \varphi & -\sin \varphi \\ \sin \varphi & \cos \varphi \end{pmatrix}. \quad (97)$$

The stiffness tensor \mathbf{E}_i in global coordinates is then obtained by the standard tensor rotation rule

$$(\mathbf{E}_i)_{ijkl} = \sum_{p,q,r,s=1}^2 (\mathbf{Q}(\varphi_i))_{ip} (\mathbf{Q}(\varphi_i))_{jq} (\mathbf{Q}(\varphi_i))_{kr} (\mathbf{Q}(\varphi_i))_{ls} (\mathbf{E}_i^b)_{pqrs}. \quad (98)$$

Since the Hashin–Shtrikman envelope $f^{\text{HS}}(\boldsymbol{\varepsilon}; v)$ for isotropic phases is isotropic in $\boldsymbol{\varepsilon}$, and both $\text{Tr}(\boldsymbol{\varepsilon})$ and $\|\boldsymbol{\varepsilon}\|_F$ are rotation-invariant, the minimal activating volume is invariant under simultaneous rotations of the microstructure and the macroscopic strain. In particular, with $\boldsymbol{\varepsilon}^b := \mathbf{Q}(\varphi_i)^\top \boldsymbol{\varepsilon} \mathbf{Q}(\varphi_i)$ we have

$$\hat{v}(\boldsymbol{\varepsilon}; \mathbf{E}_i) = \hat{v}(\boldsymbol{\varepsilon}^b; \mathbf{E}_i^b). \quad (99)$$

Consequently, the worst-case volume fraction $\bar{v}_i(\mathbf{E}_i) = \sup_{\|\boldsymbol{\varepsilon}\|_F = \sqrt{2}/2} \hat{v}(\boldsymbol{\varepsilon}; \mathbf{E}_i)$ is independent of the orientation angle φ_i and depends on \mathbf{E}_i only through its base coefficients.

As described in the previous section, for two-dimensional composites with well-ordered isotropic constituents, the Hashin–Shtrikman upper energy bound (55), with $q(t; v_i^+)$ defined in (60), is tight and admits an explicit form that splits into three regimes [3]: The first regime is attained by rank-one sequential laminates (which are orthotropic), while the other two are realized by rank-two sequential laminates with orthogonal layering directions, so the resulting effective tensors are again orthotropic. Hence, the bound (55) remains tight even when the admissible set of tensors \mathbf{E}_i is restricted to the orthotropic symmetry class with free rotations of the material coordinate system.

Under this restriction, and using (99) to work in the base coordinate system of \mathbf{E}_i , the minimal activating volume $\hat{v}(\boldsymbol{\varepsilon}; \mathbf{E}_i)$ in Proposition 3.5 can be simplified and depends on $\boldsymbol{\varepsilon}$ only through t , as stated in the following proposition.

Proposition 3.6 (Trace-only reduction of the HS activating-volume map for orthotropy). *For any fixed orthotropic, plane stress $\mathbf{E}_i \in \{\mathbf{E} : \mathbf{E}^- \preceq \mathbf{E} \preceq \mathbf{E}^+\}$, let \mathbf{E}_i^b denote its base orientation (so that $(\mathbf{E}_i^b)_{1112} = (\mathbf{E}_i^b)_{2212} = 0$). For any strain $\boldsymbol{\varepsilon} \in \mathbb{S}^{2 \times 2}$ with Frobenius norm $\sqrt{2}/2$, set*

$$E_{\max}(t; \mathbf{E}_i) := \max \left\{ \langle \mathbf{E}_i \boldsymbol{\varepsilon}, \boldsymbol{\varepsilon} \rangle : \boldsymbol{\varepsilon} \in \mathbb{S}^{2 \times 2}, \|\boldsymbol{\varepsilon}\|_F = \sqrt{2}/2, |\text{Tr}(\boldsymbol{\varepsilon})| = t \right\}.$$

Then, the minimal $v_i^+ \in [0, 1]$ for which the Hashin–Shtrikman upper bound (55) with $q(t; v_i^+)$ defined in (60) is active, i.e., $\langle \mathbf{E}_i \boldsymbol{\varepsilon}, \boldsymbol{\varepsilon} \rangle = f^{\text{HS}}(\boldsymbol{\varepsilon}; v_i^+)$, depends on $\boldsymbol{\varepsilon}$ only through t , and is obtained by replacing $\langle \mathbf{E}_i \boldsymbol{\varepsilon}, \boldsymbol{\varepsilon} \rangle$ with $E_{\max}(t; \mathbf{E}_i)$ in the three closed-form branches $\hat{v}_1, \hat{v}_2, \hat{v}_3$ stated in Proposition 3.5, with the same branch-

activation conditions evaluated at $\langle \mathbf{E}_i \boldsymbol{\varepsilon}, \boldsymbol{\varepsilon} \rangle = E_{\max}(t; \mathbf{E}_i)$. Moreover, $E_{\max}(t; \mathbf{E}_i)$ admits the explicit form

$$E_{\max}(t; \mathbf{E}_i) = \begin{cases} \frac{t^2}{4} ((\mathbf{E}_i^b)_{1111} + 2(\mathbf{E}_i^b)_{1122} + (\mathbf{E}_i^b)_{2222}) + (\mathbf{E}_i^b)_{1212}(1-t^2) - \frac{t^2((\mathbf{E}_i^b)_{1111} - (\mathbf{E}_i^b)_{2222})^2}{4\Xi} \\ \quad \text{if } \Xi < 0 \text{ and } t \leq \frac{|\Xi|}{\sqrt{\Xi^2 + ((\mathbf{E}_i^b)_{1111} - (\mathbf{E}_i^b)_{2222})^2}}, \\ \frac{1}{4} ((\mathbf{E}_i^b)_{1111} - 2(\mathbf{E}_i^b)_{1122} + (\mathbf{E}_i^b)_{2222}) + (\mathbf{E}_i^b)_{1122}t^2 + \frac{|(\mathbf{E}_i^b)_{1111} - (\mathbf{E}_i^b)_{2222}|}{2} t \sqrt{1-t^2} \\ \quad \text{otherwise,} \end{cases} \quad (100)$$

where $\Xi := (\mathbf{E}_i^b)_{1111} - 2(\mathbf{E}_i^b)_{1122} + (\mathbf{E}_i^b)_{2222} - 4(\mathbf{E}_i^b)_{1212}$.

Proof. Because $v_i^+ \mapsto f^{\text{HS}}(\boldsymbol{\varepsilon}; v_i^+)$ is nondecreasing by Proposition A.2 for all $\boldsymbol{\varepsilon}$, the minimal zero \hat{v} of $f^{\text{HS}}(\boldsymbol{\varepsilon}; v_i^+) - \langle \mathbf{E}_i \boldsymbol{\varepsilon}, \boldsymbol{\varepsilon} \rangle$ is nondecreasing in the energy $\langle \mathbf{E}_i \boldsymbol{\varepsilon}, \boldsymbol{\varepsilon} \rangle$. Hence, for any fixed t , $\hat{v}(\boldsymbol{\varepsilon}; \mathbf{E}_i)$ is the largest when $\langle \mathbf{E}_i \boldsymbol{\varepsilon}, \boldsymbol{\varepsilon} \rangle$ is the largest. Therefore, for purposes of evaluating the minimal activating volume at that t , it suffices to plug the maximizing energy $E_{\max}(t; \mathbf{E}_i)$ into the explicit branch formulas. This eliminates all dependence on the remaining components of $\boldsymbol{\varepsilon}$ beyond t .

By (99), we may rotate the pair and work with $(\mathbf{E}_i^b, \boldsymbol{\varepsilon}^b)$ instead of $(\mathbf{E}_i, \boldsymbol{\varepsilon})$. In particular $E_{\max}(t; \mathbf{E}_i) = E_{\max}(t; \mathbf{E}_i^b)$. To this goal, we work in the base coordinate system of \mathbf{E}_i and write $\boldsymbol{\varepsilon}$ in components as

$$\boldsymbol{\varepsilon} = \begin{pmatrix} \varepsilon_{11} & \varepsilon_{12} \\ \varepsilon_{12} & \varepsilon_{22} \end{pmatrix} = \begin{pmatrix} \hat{t}/2 + \zeta & r \\ r & \hat{t}/2 - \zeta \end{pmatrix} \quad (101)$$

where $\hat{t} = \text{Tr}(\boldsymbol{\varepsilon})$. Notice that $t = |\hat{t}|$. Then, the strain energy reads as

$$\langle \mathbf{E}_i^b \boldsymbol{\varepsilon}, \boldsymbol{\varepsilon} \rangle = \frac{\hat{t}^2}{4} \left((\mathbf{E}_i^b)_{1111} + 2(\mathbf{E}_i^b)_{1122} + (\mathbf{E}_i^b)_{2222} \right) + \zeta^2 \left((\mathbf{E}_i^b)_{1111} - 2(\mathbf{E}_i^b)_{1122} + (\mathbf{E}_i^b)_{2222} \right) \\ + 4(\mathbf{E}_i^b)_{1212}r^2 + \hat{t}\zeta \left((\mathbf{E}_i^b)_{1111} - (\mathbf{E}_i^b)_{2222} \right). \quad (102)$$

The Frobenius norm constraint on $\boldsymbol{\varepsilon}$ requires $\zeta^2 + r^2 = (1 - \hat{t}^2)/4$. On one hand, this allows us to eliminate r^2 through $r^2 = (1 - \hat{t}^2)/4 - \zeta^2$. On the other hand, it implies $\zeta^2 \leq (1 - \hat{t}^2)/4$ and $\hat{t}^2 \leq 1$. Hence,

$$E_{\max}(\hat{t}; \mathbf{E}_i) = \max_{\zeta^2 \leq \frac{1-\hat{t}^2}{4}} \left[\frac{\hat{t}^2}{4} \left((\mathbf{E}_i^b)_{1111} + 2(\mathbf{E}_i^b)_{1122} + (\mathbf{E}_i^b)_{2222} - 4(\mathbf{E}_i^b)_{1212} \right) \right. \\ \left. + \zeta^2 \left((\mathbf{E}_i^b)_{1111} - 2(\mathbf{E}_i^b)_{1122} + (\mathbf{E}_i^b)_{2222} - 4(\mathbf{E}_i^b)_{1212} \right) + \hat{t}\zeta \left((\mathbf{E}_i^b)_{1111} - (\mathbf{E}_i^b)_{2222} \right) + (\mathbf{E}_i^b)_{1212} \right], \quad (103)$$

which is a quadratic function in ζ . It is strictly concave in ζ iff $\Xi = (\mathbf{E}_i^b)_{1111} - 2(\mathbf{E}_i^b)_{1122} + (\mathbf{E}_i^b)_{2222} - 4(\mathbf{E}_i^b)_{1212} < 0$, i.e., shear has a dominant contribution. Then, the maximum is attained at the stationary point $\zeta^* = -\hat{t}((\mathbf{E}_i^b)_{1111} - (\mathbf{E}_i^b)_{2222})/(2\Xi)$ if $(\zeta^*)^2 \leq (1 - \hat{t}^2)/4$ or, equivalently, if $t = |\hat{t}| \leq |\Xi|/\sqrt{\Xi^2 + ((\mathbf{E}_i^b)_{1111} - (\mathbf{E}_i^b)_{2222})^2}$. Inserting ζ^* into the expression for $E_{\max}(\hat{t}; \mathbf{E}_i)$ gives

$$\frac{\hat{t}^2}{4} ((\mathbf{E}_i^b)_{1111} + 2(\mathbf{E}_i^b)_{1122} + (\mathbf{E}_i^b)_{2222}) + (\mathbf{E}_i^b)_{1212}(1 - \hat{t}^2) - \frac{\hat{t}^2((\mathbf{E}_i^b)_{1111} - (\mathbf{E}_i^b)_{2222})^2}{4\Xi}. \quad (104)$$

Since $\hat{t}^2 = t^2$ and the maximum value is even in \hat{t} , we get the first branch in (100).

In the remaining cases when $\zeta^2 > (1 - \hat{t}^2)/4$ or $\Xi \geq 0$, maximum of (103) occurs at an endpoint, so that $(\zeta^*)^2 = \frac{1-\hat{t}^2}{4}$. Inserting this into (103), we receive the maximum energy

$$\frac{1}{4} ((\mathbf{E}_i^b)_{1111} - 2(\mathbf{E}_i^b)_{1122} + (\mathbf{E}_i^b)_{2222}) + (\mathbf{E}_i^b)_{1122}t^2 + \frac{|(\mathbf{E}_i^b)_{1111} - (\mathbf{E}_i^b)_{2222}|}{2} |\hat{t}| \sqrt{1 - \hat{t}^2}, \quad (105)$$

which is exactly the second branch in (100) when using $t = |\hat{t}|$. \square

By Propositions 3.5 and 3.6, $\hat{v}(t; \mathbf{E}_i^b)$ is univariate on $t \in [0, 1]$, obtained by composing $E_{\max}(t; \mathbf{E}_i)$ with the branchwise formulas in Proposition 3.5, yielding the orthotropic FMO formulation

$$\min_{\{c_j\}, \{\mathbf{E}_i\}} \sum_{j=1}^{n_c} c_j \quad (106a)$$

$$\text{s.t.} \quad \begin{pmatrix} c_j & -\mathbf{f}_j^\top \\ -\mathbf{f}_j & \mathbf{K}_j(\{\mathbf{E}_i\}) \end{pmatrix} \succeq 0, \quad j = 1, \dots, n_c, \quad (106b)$$

$$\mathbf{E}^- \preceq \mathbf{E}_i \preceq \mathbf{E}^+, \quad i = 1, \dots, n_e, \quad (106c)$$

$$\frac{1}{n_e} \sum_{i=1}^{n_e} \sup_{t \in [0, 1]} \hat{v}(t; \mathbf{E}_i^b) \leq \bar{V}, \quad (106d)$$

$$\mathbf{E}_i \text{ orthotropic}, \quad i = 1, \dots, n_e. \quad (106e)$$

in which—for each \mathbf{E}_i —the univariate supremum in (106d) can be computed to approximate global optimality by coarse sampling to bracket candidate intervals, followed by golden-section refinement on each bracket; empirical plots contained at most two maxima.

Problem (106) is again nonconvex due to the volume constraint (106d). For a single-loadcase, its continuum relaxation value is consistent with the HS/AK value from Theorem 3.1; however, this does not imply exact attainment on a fixed finite-element mesh. Laminate attainability should be understood in the continuum relaxation (vanishing-scale) sense.

3.6. Sequential global programming for free-orthotropic material optimization

To solve problem (106), we apply the sequential global programming (SGP) approach, which was first suggested in [45] and later applied in different contexts, see, e.g. [39, 51]. The SGP algorithm is an iterative method in which, in each iteration, a first-order model is established that is separable with respect to the anisotropic material tensors $\mathbf{E}_i, i = 1, \dots, n_e$. To explain this in more detail, we first rewrite problem (106) in the following form:

$$\min_{\{\mathbf{E}_i\}} \sum_{j=1}^{n_c} c_j(\{\mathbf{E}_i\}) \quad (107a)$$

$$\text{s.t.} \quad \mathbf{E}^- \preceq \mathbf{E}_i \preceq \mathbf{E}^+, \quad i = 1, \dots, n_e, \quad (107b)$$

$$\frac{1}{n_e} \sum_{i=1}^{n_e} \sup_{t \in [0, 1]} \hat{v}(t; \mathbf{E}_i^b) = \bar{V}, \quad (107c)$$

$$\mathbf{E}_i \text{ orthotropic}, \quad i = 1, \dots, n_e, \quad (107d)$$

where $c_j(\{\mathbf{E}_i\}) = \mathbf{f}_j^\top \mathbf{K}_j(\{\mathbf{E}_i\})^{-1} \mathbf{f}_j$. We note that we have expressed the volume constraint as an equality constraint, as the volume is fully utilized at an optimal solution (recall Lemma 3.3). Since constraints (107b) and (107d) are formulated element-wise and the volume constraint (107c) is separable with respect to $\{\mathbf{E}_i\}$, it remains to approximate the cost function (107a) by a separable first-order model. Following [51], we use a variant of the separable model introduced in [47] for FMO problems. To do so, we denote by $\{\mathbf{E}_i^M\}$ the corresponding Kelvin–Mandel matrices and, at the expansion point $\{\bar{\mathbf{E}}_i\}$, we define

$$\mathbf{G}_i^j := \frac{\partial c_j(\{\bar{\mathbf{E}}_i\})}{\partial \mathbf{E}_i^M} \in \mathbb{S}^{3 \times 3}. \quad (108)$$

We then approximate the compliance for the loadcase j as

$$\hat{c}_j(\{\mathbf{E}_i\}; \{\bar{\mathbf{E}}_i\}) = C + \sum_{i=1}^{n_e} \left\langle (\bar{\mathbf{E}}_i^M - \mathbf{L}_i^j) \mathbf{G}_i^j (\bar{\mathbf{E}}_i^M - \mathbf{L}_i^j), (\mathbf{E}_i^M - \mathbf{L}_i^j)^{-1} \right\rangle_{\mathbb{S}^{3 \times 3}}, \quad (109)$$

where the constant C is chosen such that the function value of \hat{c}_j coincides with that of c_j at the expansion point $\{\overline{\mathbf{E}}_i\}$ and $\{\mathbf{L}_i^j\}_{i=1,\dots,n_e}^{j=1,\dots,n_{lc}}$ are generalized asymptotes, which are chosen to be zero matrices in the sequel. Using a Lagrangian approach, we obtain the model problem

$$\min_{\{\mathbf{E}^- \preceq \mathbf{E}_i \preceq \mathbf{E}^+, \mathbf{E}_i \text{ orth.}\}} \max_{\lambda} \sum_{j=1}^{n_{lc}} \hat{c}_j(\{\mathbf{E}_i\}; \{\overline{\mathbf{E}}_i\}) + \lambda \left(\frac{1}{n_e} \sum_{i=1}^{n_e} \sup_{t \in [0,1]} \hat{v}(t; \mathbf{E}_i^b) - \overline{V} \right). \quad (110)$$

We note that due to the orthotropy and volume constraints, (110) is a nonconvex optimization problem. Nevertheless, after switching the order of min and max, we obtain the Lagrangian dual problem:

$$\max_{\lambda} \psi(\lambda), \quad (111)$$

where the function value of the dual function ψ for a given λ is computed by solving

$$\min_{\{\mathbf{E}_i\}} \sum_{j=1}^{n_{lc}} \hat{c}_j(\{\mathbf{E}_i\}; \{\overline{\mathbf{E}}_i\}) + \lambda \left(\frac{1}{n_e} \sum_{i=1}^{n_e} \sup_{t \in [0,1]} \hat{v}(t; \mathbf{E}_i^b) - \overline{V} \right) \quad (112a)$$

$$\text{s.t. } \mathbf{E}^- \preceq \mathbf{E}_i \preceq \mathbf{E}^+, \quad i = 1, \dots, n_e, \quad (112b)$$

$$\mathbf{E}_i \text{ orthotropic}, \quad i = 1, \dots, n_e, \quad (112c)$$

to global optimality. From the saddle point theory we see that, if we find a pair $(\{\mathbf{E}_i^*\}, \lambda^*)$, which is a saddle point for the Lagrangian

$$L(\{\mathbf{E}_i\}, \lambda) = \sum_{j=1}^{n_{lc}} \hat{c}_j(\{\mathbf{E}_i\}; \{\overline{\mathbf{E}}_i\}) + \lambda \left(\frac{1}{n_e} \sum_{i=1}^{n_e} \sup_{t \in [0,1]} \hat{v}(t; \mathbf{E}_i^b) - \overline{V} \right),$$

then this pair is also optimal for (112). Obviously this is the case, if for a given λ^* , the corresponding (globally optimal) solution $(\{\mathbf{E}_i(\lambda^*)\})$ is feasible with respect to the volume constraint (stated as equality constraint), which can be easily checked in practice. Thus, we use the following strategy: as in the classical optimality criteria method, we solve the dual problem (111) using a bisection strategy, where we aim to solve (112) to global minimality in each iteration. Rather than solving (112) at once, thanks to separability, we can solve for each \mathbf{E}_i individually, i. e., we solve n_e problems of the form:

$$\min_{\mathbf{E}^- \preceq \mathbf{E}_i \preceq \mathbf{E}^+, \mathbf{E}_i \text{ orth.}} \sum_{j=1}^{n_{lc}} \left\langle \overline{\mathbf{E}}_i^M \mathbf{G}_i^j \overline{\mathbf{E}}_i^M, (\mathbf{E}_i^M)^{-1} \right\rangle_{\mathbb{S}^{3 \times 3}} + \frac{\lambda}{n_e} \sup_{t \in [0,1]} \hat{v}(t; \mathbf{E}_i^b). \quad (113)$$

We note that we skipped the constant $C - \lambda V$ in the objective here and set all asymptotes to zero.

In order to treat the orthotropy constraint, we parametrize each element tensor \mathbf{E}_i by its base coefficients and a rotation angle. In Kelvin–Mandel form, the base orientation reads

$$\mathbf{E}_i^{M,b} := \begin{pmatrix} (\mathbf{E}_i^b)_{1111} & (\mathbf{E}_i^b)_{1122} & 0 \\ (\mathbf{E}_i^b)_{1122} & (\mathbf{E}_i^b)_{2222} & 0 \\ 0 & 0 & 2(\mathbf{E}_i^b)_{1212} \end{pmatrix}, \quad \mathbf{E}_i^M = \mathbf{R}(\varphi_i) \mathbf{E}_i^{M,b} \mathbf{R}(\varphi_i)^T, \quad (114)$$

with $\varphi_i \in [0, \pi)$. The matrix $\mathbf{R}(\varphi) \in \mathbb{R}^{3 \times 3}$ is the Kelvin–Mandel rotation induced by $\mathbf{Q}(\varphi)$ in (97), i.e., for every symmetric strain $\boldsymbol{\varepsilon}$, with Mandel vector $\boldsymbol{\varepsilon}^M := (\varepsilon_{11}, \varepsilon_{22}, \sqrt{2}\varepsilon_{12})^T$, we have $(\mathbf{Q}(\varphi)^T \boldsymbol{\varepsilon} \mathbf{Q}(\varphi))^M = \mathbf{R}(\varphi) \boldsymbol{\varepsilon}^M$.

Since \mathbf{E}^- and \mathbf{E}^+ are isotropic, the Loewner bounds are rotation invariant and can be imposed directly on the base matrix:

$$\begin{pmatrix} (\mathbf{E}^-)_{1111} & (\mathbf{E}^-)_{1122} \\ (\mathbf{E}^-)_{1122} & (\mathbf{E}^-)_{2222} \end{pmatrix} \preceq \begin{pmatrix} (\mathbf{E}_i^{M,b})_{11} & (\mathbf{E}_i^{M,b})_{12} \\ (\mathbf{E}_i^{M,b})_{12} & (\mathbf{E}_i^{M,b})_{22} \end{pmatrix} \preceq \begin{pmatrix} (\mathbf{E}^+)_{1111} & (\mathbf{E}^+)_{1122} \\ (\mathbf{E}^+)_{1122} & (\mathbf{E}^+)_{2222} \end{pmatrix}, \quad (115a)$$

$$2(\mathbf{E}^-)_{1212} \leq (\mathbf{E}_i^{M,b})_{33} \leq 2(\mathbf{E}^+)_{1212}. \quad (115b)$$

With this parametrization, (113) can be written as

$$\min_{\substack{\mathbf{E}_i^{\text{M,b}}, \varphi_i \\ \text{s.t. (115)}}} \sum_{j=1}^{n_{\text{lc}}} \left\langle \overline{\mathbf{E}}_i^{\text{M}} \mathbf{G}_i^j \overline{\mathbf{E}}_i^{\text{M}}, (\mathbf{E}_i^{\text{M}})^{-1} \right\rangle_{\mathbb{S}^{3 \times 3}} + \frac{\lambda}{n_e} \sup_{t \in [0,1]} \hat{v}(t; \mathbf{E}_i^{\text{b}}), \quad (116)$$

where \mathbf{E}_i^{M} depends on $(\mathbf{E}_i^{\text{M,b}}, \varphi_i)$ through (114). Problem (113) is a 5-dimensional optimization problem with semidefinite constraints and, due to the properties of the volume constraint, a nondifferentiable objective. As no global optimization solvers are available, which could treat problems with this structure directly, we have implemented a sampling based solution approach. To do so, we discretized the interval $[0, \pi/2]$ equidistantly by 9001 angles. The resulting discrete set of angles is denoted by Φ^{G} . Similarly, the cuboid $[(\mathbf{E}^-)_{1111}, (\mathbf{E}^+)_{1111}] \times [(\mathbf{E}^-)_{2222}, (\mathbf{E}^+)_{2222}] \times [2(\mathbf{E}^-)_{1212}, 2(\mathbf{E}^+)_{1212}]$ is discretized equidistantly by 101^3 points and the corresponding set of discrete points is denoted by Θ^{G} . Finally, for each grid point $(E_{11}^{\text{G}}, E_{22}^{\text{G}}, E_{33}^{\text{G}})_i \in \Theta^{\text{G}}$ we compute the interval I_i , which contains all choices E_{12}^{G} such that

$$\begin{pmatrix} (\mathbf{E}^-)_{1111} & (\mathbf{E}^-)_{1122}^- \\ (\mathbf{E}^-)_{1122}^- & (\mathbf{E}^-)_{2222}^- \end{pmatrix} \preceq \begin{pmatrix} E_{11}^{\text{G}} & E_{12}^{\text{G}} \\ E_{12}^{\text{G}} & E_{22}^{\text{G}} \end{pmatrix} \preceq \begin{pmatrix} (\mathbf{E}^+)_{1111} & (\mathbf{E}^+)_{1122}^+ \\ (\mathbf{E}^+)_{1122}^+ & (\mathbf{E}^+)_{2222}^+ \end{pmatrix}.$$

Then, if I_i is nonempty, we again discretize this interval by 101 points. We denote the corresponding grid by \mathcal{X}_i . If I_i is empty, the corresponding point $(E_{11}^{\text{G}}, E_{22}^{\text{G}}, E_{33}^{\text{G}})_i$ is eliminated from Θ^{G} . In this way, we sample only points that are feasible. Then, in principle, we could solve (116) approximately, by evaluating the cost function for any sample point and accept the one with lowest function value as approximate solution. However, taking into account that the 5D-grid has about 100 billion points, this strategy would not be tractable. Instead, we use a hierarchical grid approach, which only needs about 10 million function evaluations. Moreover, we would like to emphasize that we pre-compute the inverse tensors as well as estimated volume in formula (116) offline for each grid point.

- Remark 3.2.**
1. We have tested the resolution of our sampling set by projecting a solution we obtained from the algorithm described in Section 3.7 onto our sampling grid. The loss in the objective function value we observed was typically very small.
 2. We cannot guarantee that we find the best point in the grid using our hierarchical grid approach in general. However, in our experiments we observed that the function value for the points we find were either optimal (on the full grid) or at least correct up to at least 5 digits.
 3. Without globalization, the iterative solution strategy we described above for the solution of problem (107) is not guaranteed to converge. A remedy is to add a line-search step after each solution of a sub problem of type (110). However our experiments revealed that for the compliance minimization problems we solve in this article no globalization is needed. Thus, we omit the description here.

3.7. Single-loadcase via alternating minimization and sequential laminates

After introducing the bound-based HS-FOMO models and the SGP solver, we now present the single-loadcase laminate-based alternating minimization baseline used in Section 4. Unlike the primal strain-energy formulation used above, this method updates material through the dual Hashin–Shtrikman complementary-energy envelope using explicit continuum minimizers of the local material subproblem; in 2D and single-loadcase, these minimizers are orthotropic sequential laminates of rank one or two. The complementary-energy envelope is dual to the primal HS envelope, so this viewpoint is consistent with the continuum tightness statement in Theorem 3.1. For completeness, we recall only the formulas needed for implementation; supporting derivations are deferred to Appendix B.

Definition 3.1 (Optimal lower bound on complementary energy [1, Definition 2.3.15]). *Let $\mathbf{E}^- \prec \mathbf{E}^+$ be two well-ordered isotropic elasticity tensors and let $v^+ \in [0, 1]$ be the volume fraction of \mathbf{E}^+ . Denote by G_{v^+} the set of all effective elasticity tensors \mathbf{E}^* obtainable by homogenization of the two phases $(\mathbf{E}^-, \mathbf{E}^+)$ with*

volume fraction v^+ . For all $\boldsymbol{\sigma} \in \mathbb{S}^{2 \times 2}$, the HS lower bound of complementary energy holds: $\langle \mathbf{E}^{*-1} \boldsymbol{\sigma}, \boldsymbol{\sigma} \rangle \geq f_c^{\text{HS}}(\boldsymbol{\sigma}; v^+)$, where

$$f_c^{\text{HS}}(\boldsymbol{\sigma}; v^+) := \langle (\mathbf{E}^+)^{-1} \boldsymbol{\sigma}, \boldsymbol{\sigma} \rangle + (1 - v^+) \max_{\boldsymbol{\varepsilon} \in \mathbb{S}^{d \times d}} \left\{ 2 \langle \boldsymbol{\sigma}, \boldsymbol{\varepsilon} \rangle - \left\langle \left((\mathbf{E}^-)^{-1} - (\mathbf{E}^+)^{-1} \right)^{-1} \boldsymbol{\varepsilon}, \boldsymbol{\varepsilon} \right\rangle - v^+ g^c(\boldsymbol{\varepsilon}) \right\} \quad (117)$$

Here, $g^c(\boldsymbol{\varepsilon})$ is the nonlocal term $g^c(\boldsymbol{\varepsilon}) := \max_{\|\mathbf{e}\|=1} \langle \mathbf{F}_{\mathbf{E}^+}^c(\mathbf{e}) \boldsymbol{\varepsilon}, \boldsymbol{\varepsilon} \rangle$. For each lamination direction $\|\mathbf{e}\| = 1$, the tensor $\mathbf{F}_{\mathbf{E}^+}^c(\mathbf{e}) \in \mathbb{R}^{d \times d \times d \times d}$ satisfies

$$\langle \mathbf{F}_{\mathbf{E}^+}^c(\mathbf{e}) \boldsymbol{\varepsilon}, \boldsymbol{\varepsilon} \rangle = \langle \mathbf{E}^+ \boldsymbol{\varepsilon}, \boldsymbol{\varepsilon} \rangle - \frac{1}{\mu^+} \|(\mathbf{E}^+ \boldsymbol{\varepsilon}) \mathbf{e}\|^2 + \left(\frac{1}{\mu^+} - \frac{1}{\kappa^+ + 2\mu^+(d-1)/d} \right) \langle (\mathbf{E}^+ \boldsymbol{\varepsilon}) \mathbf{e}, \mathbf{e} \rangle^2. \quad (118)$$

The quantity $f_c^{\text{HS}}(\boldsymbol{\sigma}; v^+)$ is the local envelope minimized in the material step of alternating minimization. For two-dimensional mixtures of well-ordered isotropic phases, this lower bound is tight in the relaxation sense, and equality is attained by finite-rank laminates (cf. [1, Proposition 2.3.25] and [20, Theorem 2]). We now state the explicit branch-wise formula used in the algorithm.

Theorem 3.2 (Explicit formula of f_c^{HS} in 2D [20, Theorem 2]). *Assume $d = 2$, $0 \prec \mathbf{E}^- \prec \mathbf{E}^+$, and denote by σ_1, σ_2 the eigenvalues of $\boldsymbol{\sigma}$. Let*

$$\Delta \kappa := \kappa^+ - \kappa^-, \quad \Delta \mu := \mu^+ - \mu^-, \quad (119a)$$

$$s_+ := |\sigma_1 + \sigma_2|, \quad s_- := |\sigma_1 - \sigma_2|, \quad (119b)$$

$$d_1^c(v^+) := (1 - v^+) \kappa^- \mu^- (\kappa^+ + \mu^+) + v^+ \kappa^+ \mu^+ (\kappa^- + \mu^-), \quad (119c)$$

$$d_2^c(v^+) := \kappa^- (\kappa^+ + \mu^+) + v^+ \mu^+ \Delta \kappa, \quad d_3^c(v^+) := \mu^- (\kappa^+ + \mu^+) + v^+ \kappa^+ \Delta \mu, \quad (119d)$$

$$a(\boldsymbol{\sigma}) := \kappa^- \kappa^+ \Delta \mu s_- + \mu^- \mu^+ \Delta \kappa s_+. \quad (119e)$$

Define

$$f_{c,1}^{\text{HS}}(\boldsymbol{\sigma}; v^+) := (1 - v^+) \langle (\mathbf{E}^-)^{-1} \boldsymbol{\sigma}, \boldsymbol{\sigma} \rangle + v^+ \langle (\mathbf{E}^+)^{-1} \boldsymbol{\sigma}, \boldsymbol{\sigma} \rangle - \frac{v^+ (1 - v^+) a(\boldsymbol{\sigma})^2}{4\kappa^- \kappa^+ \mu^- \mu^+ d_1^c(v^+)}, \quad (120a)$$

$$f_{c,2}^{\text{HS}}(\boldsymbol{\sigma}; v^+) := \langle (\mathbf{E}^+)^{-1} \boldsymbol{\sigma}, \boldsymbol{\sigma} \rangle + \frac{(1 - v^+) \Delta \kappa (\kappa^+ + \mu^+) (\sigma_1 + \sigma_2)^2}{4\kappa^+ d_2^c(v^+)}, \quad (120b)$$

$$f_{c,3}^{\text{HS}}(\boldsymbol{\sigma}; v^+) := \langle (\mathbf{E}^+)^{-1} \boldsymbol{\sigma}, \boldsymbol{\sigma} \rangle + \frac{(1 - v^+) \Delta \mu (\kappa^+ + \mu^+) (\sigma_1 - \sigma_2)^2}{4\mu^+ d_3^c(v^+)}. \quad (120c)$$

Then

$$f_c^{\text{HS}}(\boldsymbol{\sigma}; v^+) = \begin{cases} f_{c,1}^{\text{HS}}(\boldsymbol{\sigma}; v^+), & \text{if } v^+ \mu^+ \Delta \kappa s_+ < d_2^c(v^+) s_- \text{ and } v^+ \kappa^+ \Delta \mu s_- < d_3^c(v^+) s_+, \\ f_{c,2}^{\text{HS}}(\boldsymbol{\sigma}; v^+), & \text{if } v^+ \mu^+ \Delta \kappa s_+ \geq d_2^c(v^+) s_-, \\ f_{c,3}^{\text{HS}}(\boldsymbol{\sigma}; v^+), & \text{if } v^+ \kappa^+ \Delta \mu s_- \geq d_3^c(v^+) s_+. \end{cases} \quad (121)$$

Branch-wise attainability is by finite-rank laminates:

1. In case $f_{c,1}^{\text{HS}}$, a simple laminate attains the bound, with lamination direction orthogonal to a principal direction of $\boldsymbol{\sigma}$.
2. In case $f_{c,2}^{\text{HS}}$, a rank-two sequential laminate attains the bound with principal directions of $\boldsymbol{\sigma}$ and

$$m_1 = \frac{1}{2} + \frac{d_2^c(v^+) (\sigma_2 - \sigma_1)}{2v^+ \mu^+ \Delta \kappa (\sigma_1 + \sigma_2)}, \quad m_2 = \frac{1}{2} + \frac{d_2^c(v^+) (\sigma_1 - \sigma_2)}{2v^+ \mu^+ \Delta \kappa (\sigma_1 + \sigma_2)}. \quad (122)$$

3. In case $f_{c,3}^{\text{HS}}$, a rank-two sequential laminate attains the bound with principal directions of $\boldsymbol{\sigma}$ and

$$m_1 = \frac{1}{2} + \frac{d_3^c(v^+) (\sigma_1 + \sigma_2)}{2v^+ \kappa^+ \Delta \mu (\sigma_2 - \sigma_1)}, \quad m_2 = \frac{1}{2} + \frac{d_3^c(v^+) (\sigma_1 + \sigma_2)}{2v^+ \kappa^+ \Delta \mu (\sigma_1 - \sigma_2)}. \quad (123)$$

Figure 4 illustrates the geometric relation between the HS bound and its laminate realizers. The corresponding branch-wise laminate parameters also provide a closed-form local tensor update: for each element i , let $\mathbf{e}_{i,j}$ and $m_{i,j}$ denote the lamination directions and weights, with $p_i = 1$ in case 1 and $p_i = 2$ in cases 2-3. Define

$$\mathbf{R} := ((\mathbf{E}^-)^{-1} - (\mathbf{E}^+)^{-1})^{-1}, \quad \mathbf{B}_i := \mathbf{R} + v_i^+ \sum_{j=1}^{p_i} m_{i,j} \mathbf{F}_{\mathbf{E}^+}^c(\mathbf{e}_{i,j}), \quad (124)$$

and set

$$\mathbf{E}_i = ((\mathbf{E}^+)^{-1} + (1 - v_i^+) \mathbf{B}_i^{-1})^{-1}. \quad (125)$$

This defines the LAMINATEUPDATE map used in Algorithm 1.

Although one-dimensional, the local update problem $\arg \min_{v \in [0,1]} f_c^{\text{HS}}(\boldsymbol{\sigma}_i; v) + \lambda v$ is not immediate. Regularity information on the HS lower bound f_c^{HS} is therefore needed.

Proposition 3.7 (Regularity and convexity of the HS complementary-energy bound). *For all $\boldsymbol{\sigma} \in \mathbb{S}^{2 \times 2}$, the function $v \mapsto f_c^{\text{HS}}(\boldsymbol{\sigma}; v)$ is C^1 and convex over $(0, 1]$.*

Proof. See Appendix B. The derivative $D_v f_c^{\text{HS}}(\boldsymbol{\sigma}; v)$ follows from basic perturbation theory for optimization problems. \square

Accordingly, each local update is computed by bisection on the one-dimensional optimality condition $D_v f_c^{\text{HS}}(\boldsymbol{\sigma}; v) = -\lambda$. Algorithm 1 is a descent method: compliance decreases along iterations, so the objective

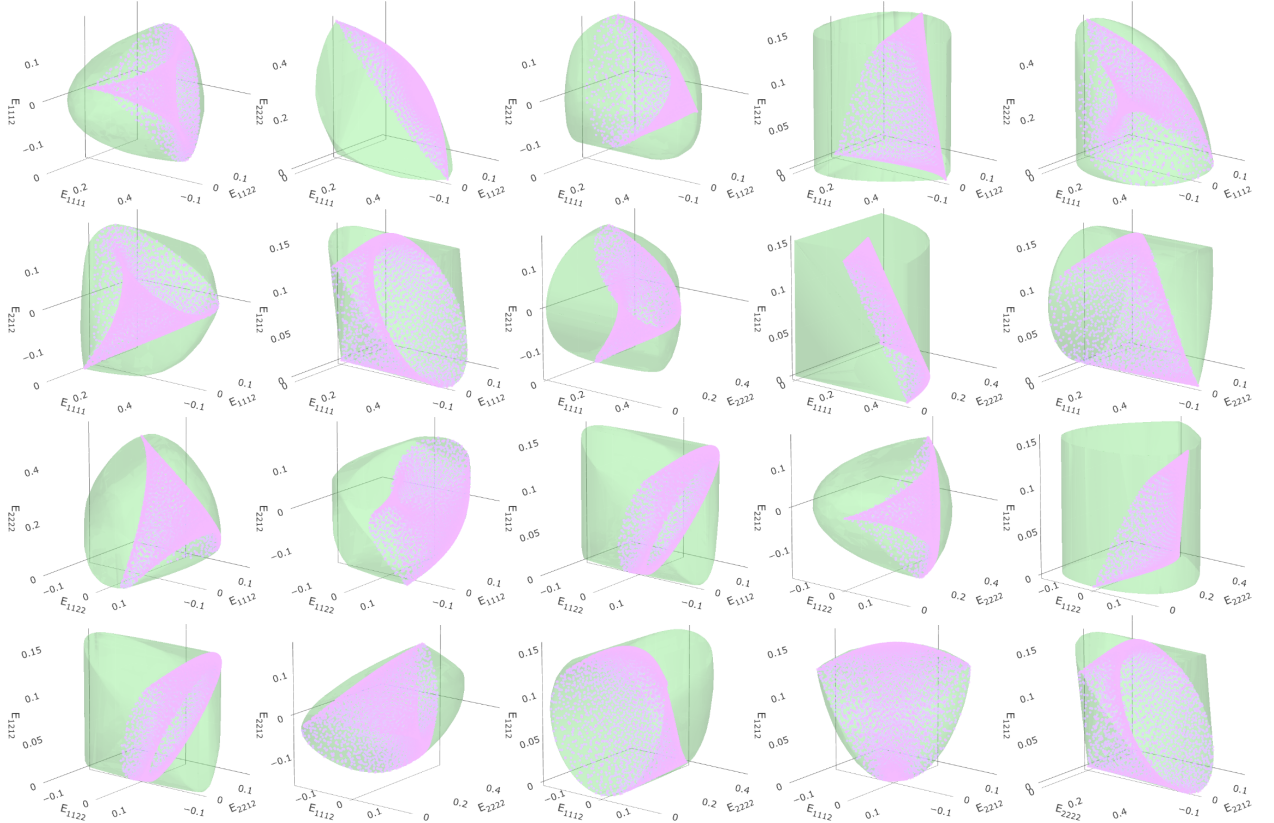


Figure 4: Comparison of the admissible set $\mathcal{A}^{(2)}(0.5)$ (Hashin–Shtrikman, green boundary) and orthotropic sequential-laminate tensors that attain the Hashin–Shtrikman energy bound (pink points). The sets are shown in a selected three-dimensional projection of \mathbf{E} . For fixed $v^+ = 0.5$, the Hashin–Shtrikman boundary was generated using 750 sampled strains $\boldsymbol{\varepsilon}$ with Frobenius norm $\sqrt{2}/2$. The realizing laminate tensors were generated by sampling 5,000 stresses $\boldsymbol{\sigma}$. Material parameters: $\kappa^- = 0.714 \times 10^{-9}$, $\kappa^+ = 0.714$, $\mu^- = 0.385 \times 10^{-9}$, and $\mu^+ = 0.385$.

Algorithm 1: Laminate-based alternating minimization with bisection on λ

Input: Initial $\{v_i^{+,0}\}_{i=1}^{n_e}$, $\{\mathbf{E}_i^0\}_{i=1}^{n_e}$, target volume fraction \bar{V} , tolerance tol .

for $k = 0, 1, 2, \dots$ **do**

Solve state equation for \mathbf{u}^k and compute $\{\boldsymbol{\sigma}_i^k\}$;
 Find λ (by bisection) such that, with

$$v_i^+(\lambda) \in \arg \min_{v \in [0,1]} f_c^{\text{HS}}(\boldsymbol{\sigma}_i^k; v) + \lambda v, \quad \mathbf{E}_i(\lambda) = \text{LAMINATEUPDATE}(\boldsymbol{\sigma}_i^k, v_i^+(\lambda)),$$

the volume constraint $\frac{1}{n_e} \sum_{i=1}^{n_e} v_i^+(\lambda) = \bar{V}$ holds;

Set $v_i^{+,k+1} \leftarrow v_i^+(\lambda)$ and $\mathbf{E}_i^{k+1} \leftarrow \mathbf{E}_i(\lambda)$ for all i ;

values converge. There is no guarantee of convergence to a global minimizer, but Allaire et al. [7] reported low sensitivity to initialization and similar final compliance values.

4. Results

Building on the theoretical developments of the previous sections, we present numerical examples that illustrate the hierarchy of bounds and evaluate the performance of the sequential global programming algorithm for free-orthotropic material optimization. We compare these results for ZO-FMO (Section 3.2), V-FMO (Section 3.3), and finite-rank laminates computed by alternating minimization (Section 3.7).

In all examples, we use dimensionless material parameters with strong phase Young's modulus $E = 1$ and Poisson's ratio $\nu = 0.3$. The weak phase has the same Poisson ratio and a smaller Young modulus (10^{-2} , 10^{-3} or 10^{-6}). The volume constraint is fixed at $\bar{V} = 0.2$. The finite-element discretization is based on Q8 serendipity elements. Since the elasticity tensors are piecewise constant at the element level and the element kinematics are sufficiently rich, no additional regularization is applied, in line with the observation of Jog et al. [28].

For ZO-FMO and V-FMO, the resulting linear semidefinite programs (32) and (54) are solved using the Mosek optimizer with default settings, and we implement elementwise arrow decomposition of the compliance constraints for improved scalability [30].

For the sequential global programming algorithm we stop if the relative change in the merit function

$$\sum_{j=1}^{n_{\text{ic}}} c_j(\{\mathbf{E}_i\}) + \lambda \left(\frac{1}{n_e} \sum_{i=1}^{n_e} \sup_{t \in [0,1]} \hat{v}(t; \mathbf{E}_i^b) - \bar{V} \right) \quad (126)$$

is below 10^{-7} or there is no progress after five consecutive iterations. We note that the second term is not automatically zero after every iteration. Due to the finite-resolution approximation of the feasible set used in the SGP approach, the precision of the volume constraint retrieved from the bisection strategy is typically on the order of 10^{-6} . This is the reason why we monitor the merit function (126) rather than pure compliance. Moreover, the same reason may lead to minimal under- and over-shooting close to the solution. To avoid cycling, we thus include the additional improvement test.

In the alternating-minimization scheme of Allaire et al. [7], orthotropic finite-rank laminates are designed elementwise from average stresses [28]; the volume fraction update follows the compliance optimality condition, and we stop when (i) the maximum density change is below 10^{-5} and (ii) the relative compliance change is below 10^{-8} . The method is initialized with the strong material \mathbf{E}^+ .

4.1. Cantilever problem

As the first example, we consider a cantilever beam of the width 1 and height 1, clamped at the left edge and subjected to a vertical load of magnitude 1 at the bottom right corner, as shown in Fig. 5. The beam is discretized using 30×30 serendipity elements. We solve the optimization problem using the different bounds for three different values of the weak phase Young's modulus: 10^{-2} , 10^{-3} , and 10^{-6} .

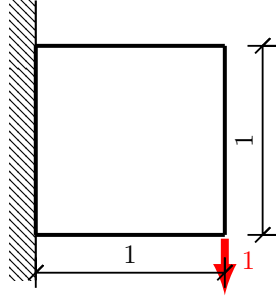


Figure 5: Cantilever beam: geometry and boundary conditions

4.1.1. Phase contrast 10^{-6}

For the 10^{-6} case, the ZO-FMO (32) yields a compliance lower bound of 18.978 with a volume-constraint multiplier $\lambda = 15.038$. The corresponding material distribution and elasticity tensors are shown in the first column of Fig. 6. The tensors are visualized by rosette plots, i.e., polar plots of the directional strain energy $(\mathbf{E}\boldsymbol{\varepsilon}, \boldsymbol{\varepsilon})$ for $\|\boldsymbol{\varepsilon}\|_F = 1$. As seen from these plots, the tensors are nearly orthotropic, although orthotropy is not enforced in this formulation.

The V-FMO (54) gives a substantially tighter compliance lower bound of 39.843, and the volume multiplier increases to $\lambda = 165.438$. The increase in both compliance and λ reflects the tighter coupling between elasticity tensors and element-wise volume estimates; consequently, a larger λ is required to satisfy the volume constraint. This is also reflected in the material distribution: the resulting isotropic tensors are more localized than in the ZO-FMO case (compare first and second columns of Fig. 6).

Solving the HS-FOMO problem (107) with the sequential global programming algorithm yields a compliance of 43.152 with $\lambda = 193.117$, so the objective increases by only 8.31% relative to V-FMO. The multiplier λ likewise increases only moderately. The relative-volume distribution is very similar to the V-FMO case (compare the second and third columns of Fig. 6), but the tensors are now orthotropic and have distinguishably smaller norms; the V-FMO tensors would require more material volume to be realizable.

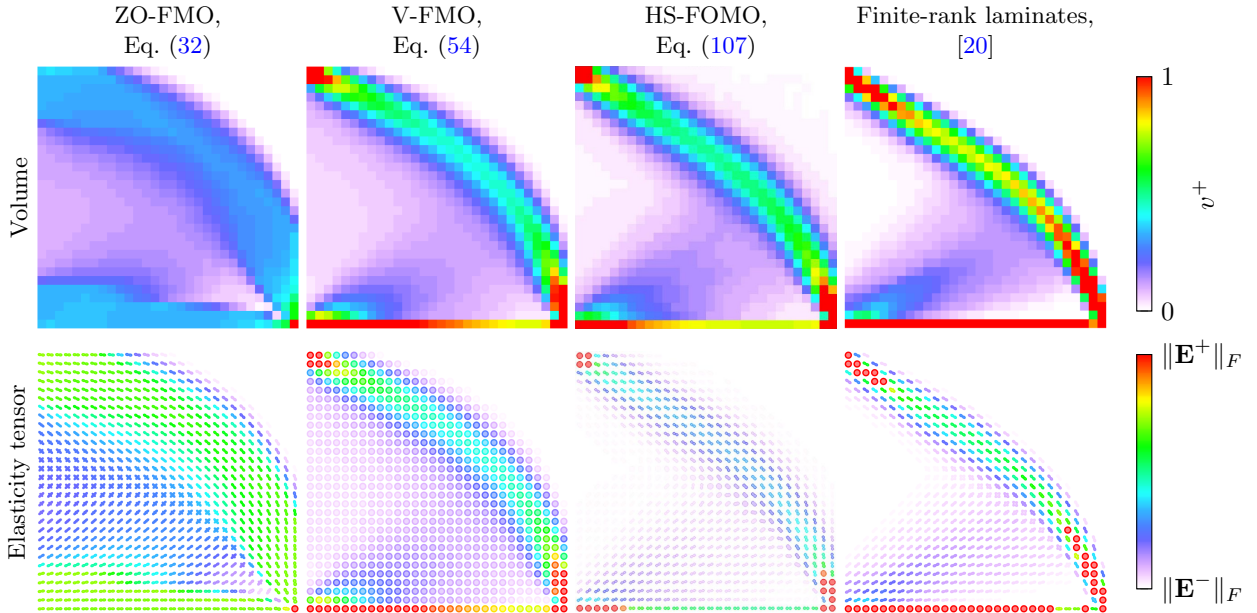


Figure 6: Cantilever beam optimization for $\mathbf{E}^- = 10^{-6}\mathbf{E}^+$: volume fraction (top row) and elasticity tensor rosettes (bottom row) for ZO-FMO, V-FMO, HS-FOMO, and sequential laminate designs.

Finally, we compare the HS-FOMO compliance with the result of alternating minimization using sequential laminates. Sequential laminates provide a realizable upper bound in the present setting because the discretization is finite and element stresses are nonconstant. The resulting compliance is 43.699, i.e., 1.27% higher than in the HS-FOMO setting, with $\lambda = 175.291$. In this case, alternating minimization converged very slowly due to the high contrast between the strong and weak phases, requiring 198,953 iterations. Comparing the third and fourth columns of Fig. 6, the finite-rank laminate design shows a more localized volume distribution, likely due to a narrower admissible class of elasticity tensors. The higher multiplier in the HS-FOMO solution can be interpreted as a larger shadow price of volume: because HS-FOMO resolves the full finite-element response (including stress peaks), it predicts a stronger marginal compliance reduction from additional material, whereas stress averaging in alternating minimization smooths these peaks and yields a smaller effective marginal value, hence a lower λ .

4.1.2. Phase contrast 10^{-3}

For the phase-contrast setting 10^{-3} , the same qualitative picture as in the 10^{-6} case is preserved, so we focus only on what changes. All compliance values are slightly lower, which is expected for the milder contrast between phases: ZO-FMO gives 18.954, V-FMO gives 39.721, HS-FOMO gives 42.456, and sequential laminates give 42.968. Compared with the 10^{-6} case, the relative gap between V-FMO and HS-FOMO is smaller (about 6.89% instead of 8.31%), suggesting that for 10^{-3} contrast V-FMO already captures more of the attainable improvement.

The HS-FOMO and sequential-laminate results remain very close, with only a 1.21% difference in compliance, so the near-tight agreement observed before still holds. The multipliers follow the same pattern as in the high-contrast case: λ increases from ZO-FMO to V-FMO and then to HS-FOMO, while the alternating minimization value stays below HS-FOMO (14.937, 164.027, 184.948, and 173.626, respectively). This is consistent with the same interpretation as before: HS-FOMO sees the full element-wise finite-element response, including local stress peaks, whereas alternating minimization with sequential laminates uses stress averaging, which smooths sensitivities and leads to a lower effective shadow price of volume.

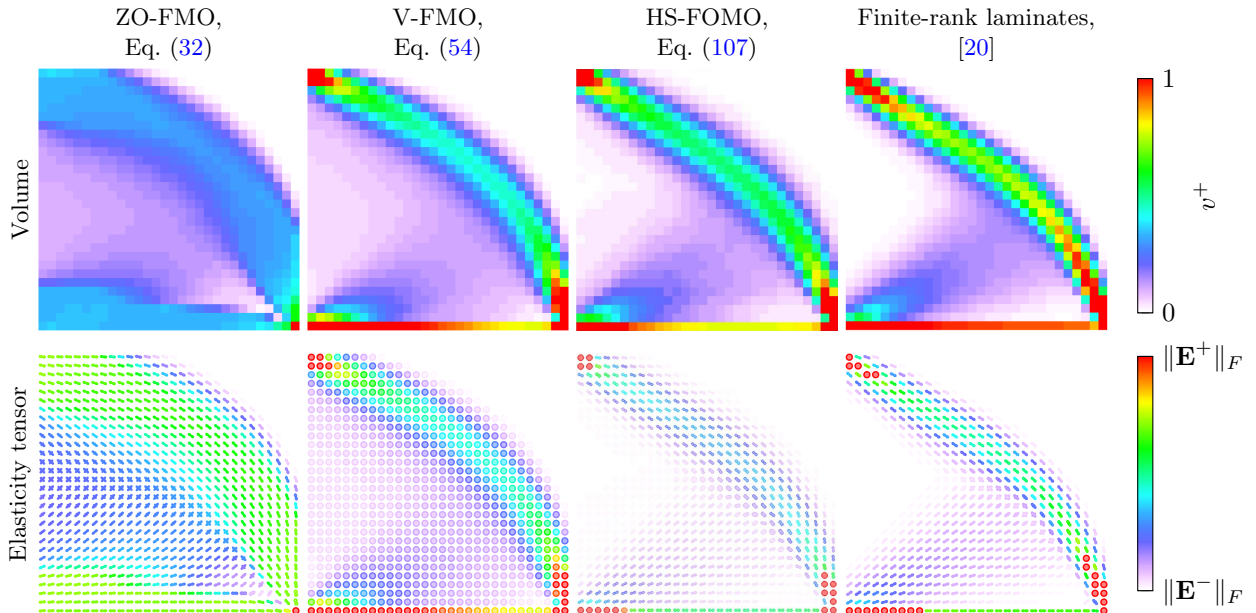


Figure 7: Cantilever beam optimization for $\mathbf{E}^- = 10^{-3}\mathbf{E}^+$: volume fraction (top row) and elasticity tensor rosettes (bottom row) for ZO-FMO, V-FMO, HS-FOMO, and sequential laminate designs.

For the 10^{-3} contrast, the visual trends in Fig. 7 are largely consistent with the 10^{-6} case in Fig. 6. The ZO-FMO model again produces a diffused distribution, while the V-FMO, HS-FOMO, and finite-rank

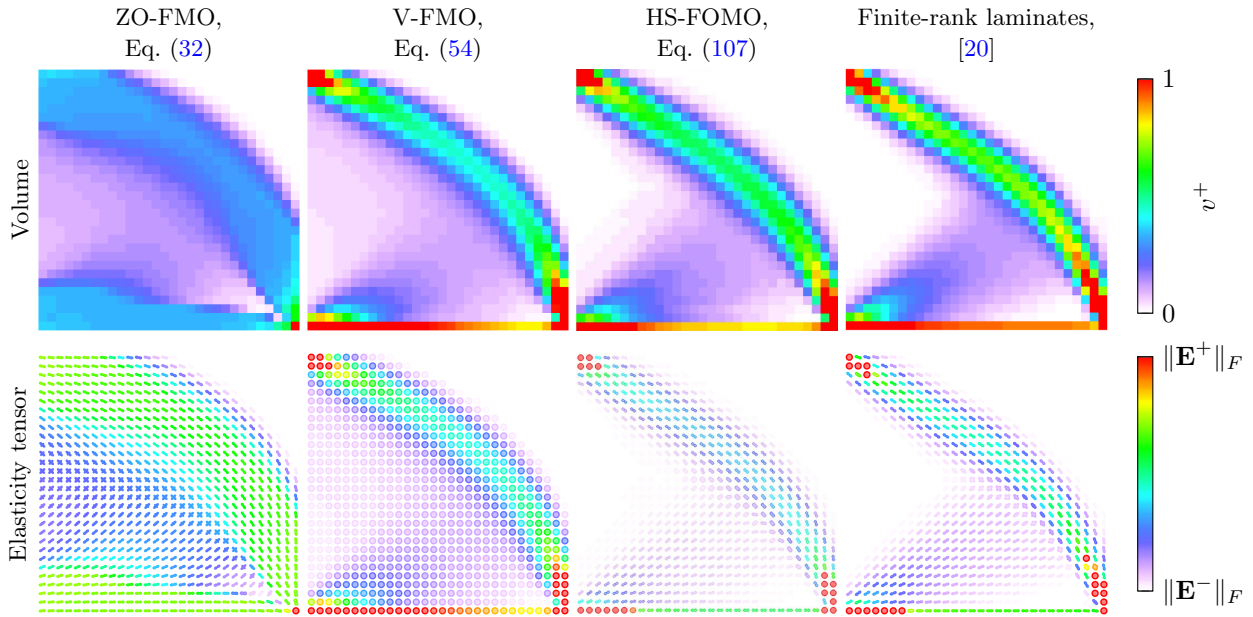


Figure 8: Cantilever beam optimization for $\mathbf{E}^- = 10^{-2}\mathbf{E}^+$: volume fraction (top row) and elasticity tensor rosettes (bottom row) for ZO-FMO, V-FMO, HS-FOMO, and sequential laminate designs.

laminate solutions concentrate material along the same main load-carrying arc. As before, the V-FMO column shows isotropic tensors, whereas HS-FOMO and sequential laminates recover orthotropic tensors with very similar orientation fields. Compared with 10^{-6} , the 10^{-3} designs appear slightly less extreme (smoother transitions and marginally weaker localization), which is consistent with the milder phase contrast and the slightly smaller quantitative gaps reported above.

4.1.3. Phase contrast 10^{-2}

For the 10^{-2} phase contrast in Fig. 8, the same qualitative ordering is preserved as in Figs. 6 and 7, but the differences between models become smaller. The compliance values are 18.827 (ZO-FMO), 38.675 (V-FMO), 40.787 (HS-FOMO), and 41.106 (finite-rank laminates), so all values decrease further as the contrast weakens. The V-FMO-to-HS-FOMO gap drops to 5.46% (from 6.89% at 10^{-3} and 8.31% at 10^{-6}), and the laminate-to-HS-FOMO gap drops to 0.78% (from 1.21% and 1.27%), indicating progressive convergence of the formulations for milder contrast.

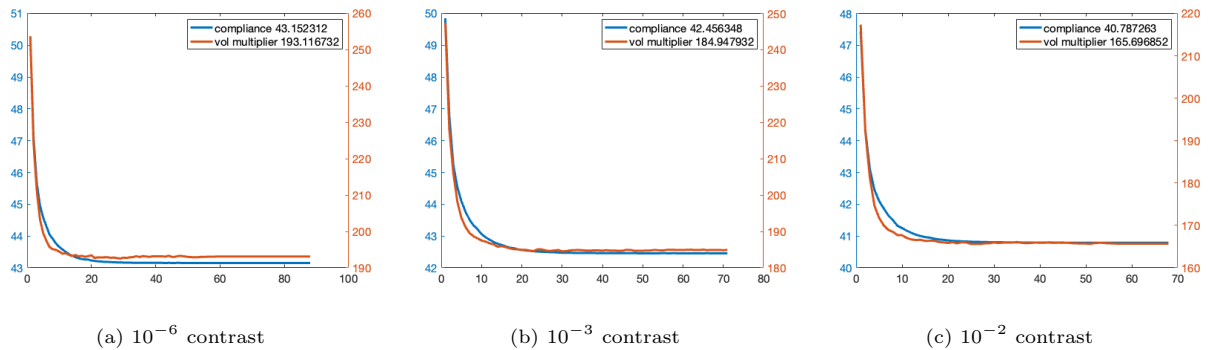


Figure 9: Convergence of the sequential global programming algorithm for the HS-FOMO problem across different phase contrasts. The blue curve shows compliance and the orange curve shows the volume multiplier λ .

Contrast $\mathbf{E}^-/\mathbf{E}^+$	Model	Problem	Compliance	λ
10^{-6}	ZO-FMO	Eq. (32)	18.978	15.038
	V-FMO	Eq. (54)	39.843	165.439
	HS-FOMO	Eq. (107)	43.152	193.117
	Finite-rank laminates	Sec. 3.7	43.699	175.291
10^{-3}	ZO-FMO	Eq. (32)	18.954	14.937
	V-FMO	Eq. (54)	39.721	164.027
	HS-FOMO	Eq. (107)	42.456	184.948
	Finite-rank laminates	Sec. 3.7	42.968	173.626
10^{-2}	ZO-FMO	Eq. (32)	18.827	14.527
	V-FMO	Eq. (54)	38.675	152.165
	HS-FOMO	Eq. (107)	40.787	165.697
	Finite-rank laminates	Sec. 3.7	41.106	158.800

Table 1: Cantilever problem results across phase contrasts and different formulations.

The visual comparison supports this trend: the main load-carrying arc remains in the same location, but the distributions are slightly smoother and less sharply localized than in the 10^{-6} and 10^{-3} cases. As before, the V-FMO column remains isotropic, while HS-FOMO and sequential laminates show closely aligned orthotropic orientation fields. The multipliers also decrease (14.527, 152.165, 165.697, and 158.800, respectively), while retaining the same pattern, including a higher λ for HS-FOMO than for sequential laminates.

For completeness, Table 1 summarizes the compliance and volume multipliers corresponding to the designs shown in Figs. 6–8. As the SGP method is less known compared to the other approaches, we present convergence plots in Fig. 9. It is seen that objective function values decrease almost monotonically and that typically between 60 and 90 iterations are required.

4.2. Multi-loadcase problem

As the second illustration, we consider a multi-loadcase compliance problem on a rectangular domain of width 2 and height 1, see Fig. 10. The structure is supported at the four corner points, and two independent unit point loads are applied: a downward load at the midpoint of the top edge (first loadcase) and an upward load at the midpoint of the bottom edge (second loadcase). In contrast to the cantilever problem, the objective is now the sum of compliances, $c_1 + c_2$, under the same global volume constraint 0.2. We report results for the phase contrasts of \mathbf{E}^+ and \mathbf{E}^- 10^{-6} , 10^{-3} , and 10^{-2} on 40×20 and 60×30 discretizations, and compare the ZO-FMO, V-FMO, and HS-FOMO formulations. The alternating-minimization results are not included in this example because its multi-loadcase extension [6] does not enforce orthotropic microstructures.

4.2.1. Quantitative overview

Table 2 summarizes the quantitative comparison of ZO-FMO, V-FMO, and HS-FOMO formulations for all considered contrasts and both discretizations. Across all cases, the compliance values follow the consistent

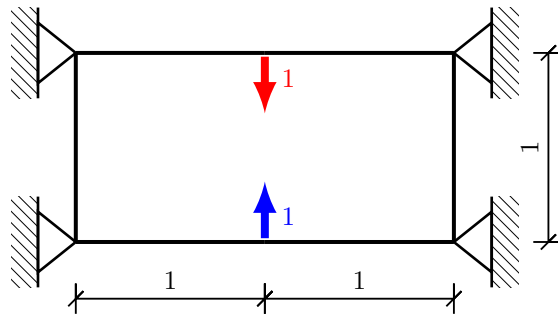


Figure 10: Multi-loadcase problem: geometry and boundary conditions

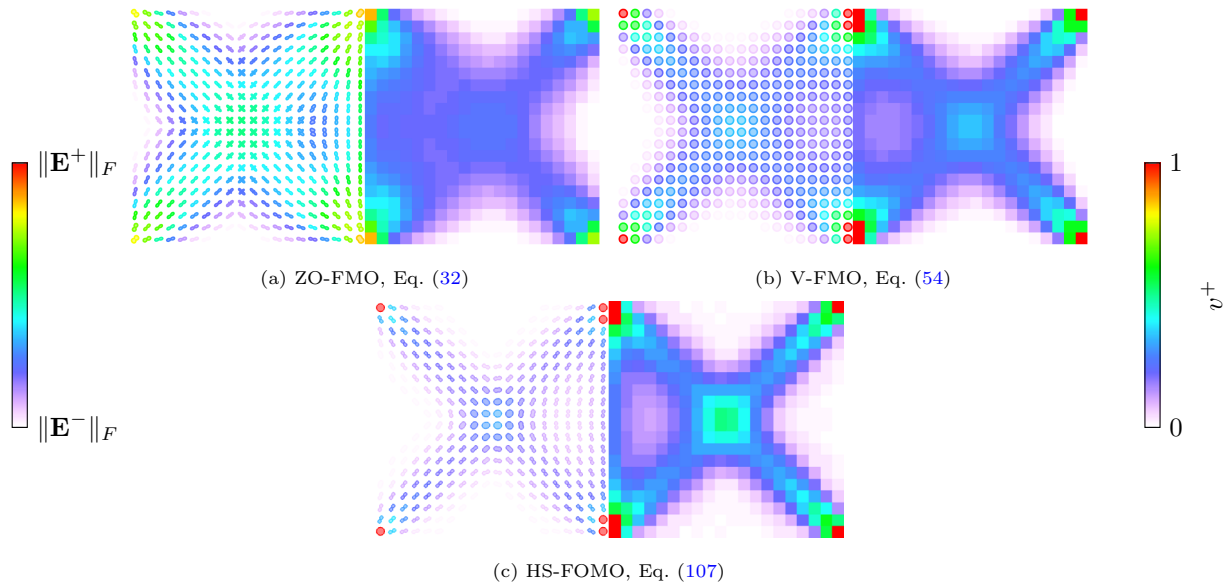


Figure 11: Multi-loadcase optimization for discretization 40×20 and $\mathbf{E}^- = 10^{-6}\mathbf{E}^+$. In each image, the left half shows the elasticity-tensor rosettes and the right half shows the volume fraction v^+ .

ordering $c^{\text{ZO-FMO}} < c^{\text{V-FMO}} < c^{\text{HS-FOMO}}$, with a large increase from ZO-FMO to V-FMO and a smaller, but still systematic, increase from V-FMO to HS-FOMO.

The volume multipliers show the same hierarchy, $\lambda^{\text{ZO-FMO}} < \lambda^{\text{V-FMO}} < \lambda^{\text{HS-FOMO}}$, indicating progressively tighter coupling between stiffness admissibility and effective material usage from ZO-FMO to V-FMO and further to HS-FOMO. Detailed trend interpretations are discussed separately in Section 4.2.2 (phase-contrast effects) and Section 4.2.3 (discretization and convergence effects).

Discretization	Contrast $\mathbf{E}^-/\mathbf{E}^+$	Model	Problem	Compliance	λ
40×20	10^{-6}	ZO-FMO	Eq. (32)	14.213	13.743
		V-FMO	Eq. (54)	28.459	123.643
		HS-FOMO	Eq. (107)	32.017	154.212
60×30	10^{-6}	ZO-FMO	Eq. (32)	14.710	13.101
		V-FMO	Eq. (54)	28.992	121.908
		HS-FOMO	Eq. (107)	32.256	150.620
40×20	10^{-3}	ZO-FMO	Eq. (32)	14.189	13.652
		V-FMO	Eq. (54)	28.361	122.476
		HS-FOMO	Eq. (107)	31.498	146.766
60×30	10^{-3}	ZO-FMO	Eq. (32)	14.687	13.012
		V-FMO	Eq. (54)	28.897	120.811
		HS-FOMO	Eq. (107)	31.693	144.232
40×20	10^{-2}	ZO-FMO	Eq. (32)	14.007	13.006
		V-FMO	Eq. (54)	27.534	112.883
		HS-FOMO	Eq. (107)	30.104	131.556
60×30	10^{-2}	ZO-FMO	Eq. (32)	14.524	12.419
		V-FMO	Eq. (54)	28.092	111.756
		HS-FOMO	Eq. (107)	30.357	129.209

Table 2: Multi-loadcase problem results across phase contrasts, discretizations, and formulations.

4.2.2. Effect of phase contrast

To isolate the role of phase contrast, we compare results at fixed mesh for $\mathbf{E}^-/\mathbf{E}^+ \in \{10^{-6}, 10^{-3}, 10^{-2}\}$ using Table 2 and the field plots in Figs. 11–16. For both discretizations, all compliance values decrease monotonically as the contrast weakens: on 40×20 , from $14.213 \rightarrow 14.189 \rightarrow 14.007$ (ZO-FMO), $28.459 \rightarrow 28.361 \rightarrow 27.534$ (V-FMO), and $32.017 \rightarrow 31.498 \rightarrow 30.104$ (HS-FOMO); on 60×30 , from $14.710 \rightarrow 14.687 \rightarrow 14.524$, $28.992 \rightarrow 28.897 \rightarrow 28.092$, and $32.256 \rightarrow 31.693 \rightarrow 30.357$, respectively.

The magnitude of this decrease is model-dependent. From 10^{-6} to 10^{-2} , the reduction is largest for HS-FOMO (about 6%), intermediate for V-FMO (about 3%), and smallest for ZO-FMO (1.5%). This is consistent with model fidelity: as \mathbf{E}^- increases, the weak phase carries load more effectively, and tighter formulations capture this gain more directly, whereas ZO-FMO is comparatively less sensitive. The same mechanism explains the shrinking V-FMO-to-HS-FOMO gap with weaker contrast (from 12.50% \rightarrow 11.06% \rightarrow 9.33% on 40×20 and from 11.26% \rightarrow 9.68% \rightarrow 8.06% on 60×30), because the Hashin–Shtrikman correction terms are driven by phase-stiffness contrast.

The figures indicate that phase contrast affects the amplitude of localization more than the topology of load-transfer paths. Here, amplitude refers to how pronounced the high-value regions are in the volume field v^+ and in the rosette-magnitude colors (i.e., how close local values are to the $\|\mathbf{E}^+\|_F$ end of the scale). For each model, the dominant load-transfer pattern is preserved across contrasts: ZO-FMO remains comparatively diffused, V-FMO solutions retain isotropic tensors, as confirmed by circular rosettes, and HS-FOMO preserves the orthotropic pattern with similar orientation fields. As contrast weakens, peaks near loads, supports and along the main transfer paths are reduced, and the volume field becomes slightly more evenly distributed, reflecting reduced stiffness mismatch and, consequently, reduced need for strongly concentrated stiff-phase routing.

The multipliers in Table 2 also decrease monotonically with weaker contrast for all formulations. This follows the same physical interpretation: when the weak phase is less compliant (i.e., \mathbf{E}^- increases), the marginal compliance gain from additional stiff material decreases, and the shadow price of the volume constraint is lower.

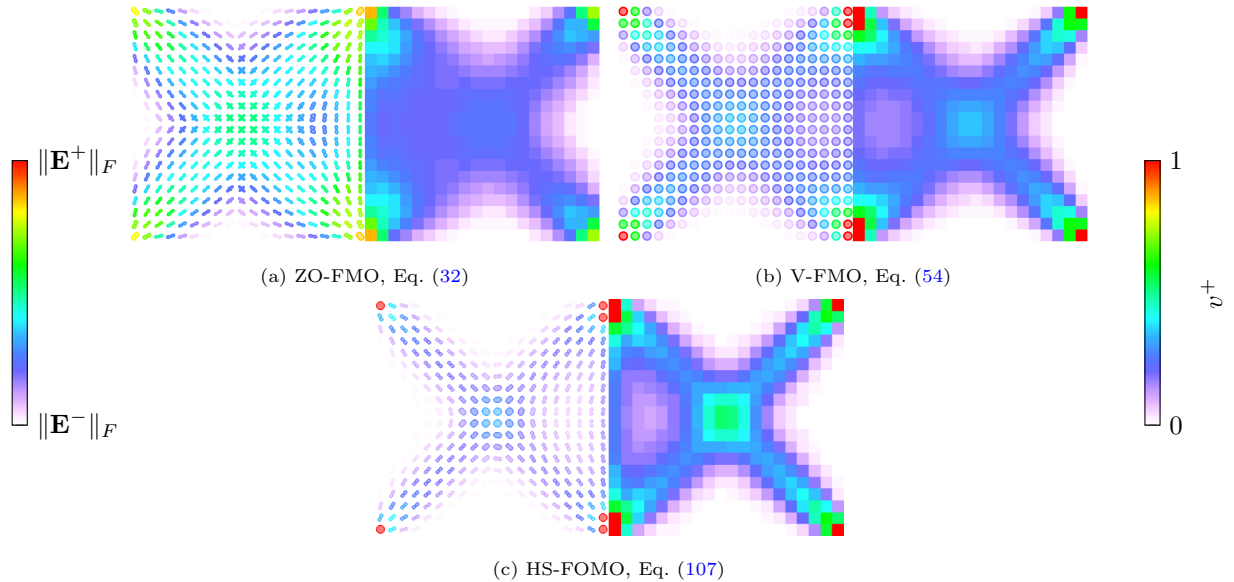


Figure 12: Multi-loadcase optimization for discretization 40×20 and $\mathbf{E}^- = 10^{-3}\mathbf{E}^+$. In each image, the left half shows the elasticity-tensor rosettes and the right half shows the volume fraction v^+ .

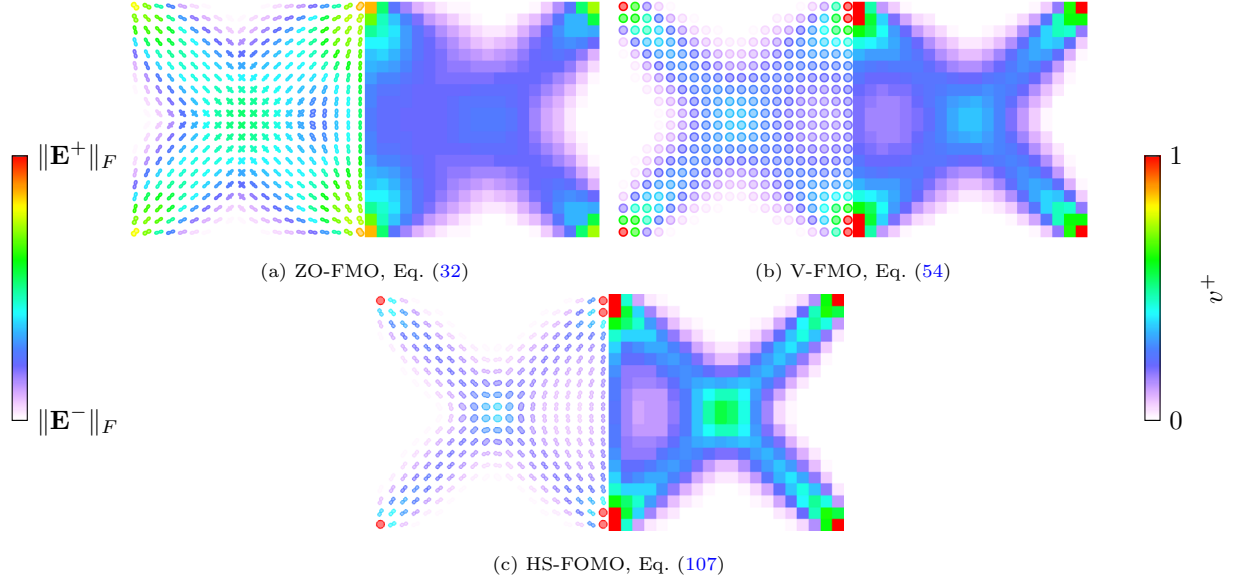


Figure 13: Multi-loadcase optimization for discretization 40×20 and $\mathbf{E}^- = 10^{-2}\mathbf{E}^+$. In each image, the left half shows the elasticity-tensor rosettes and the right half shows the volume fraction v^+ .

4.2.3. Effect of discretization and convergence

To assess discretization effects, we compare the two meshes at fixed phase contrast using Table 2. Defining

$$\Delta_h c := \frac{c_{60 \times 30} - c_{40 \times 20}}{c_{40 \times 20}}, \quad (127)$$

the compliance increase under refinement is moderate: about 3.5–3.7% for ZO-FMO, 1.9–2.0% for V-FMO, and 0.6–0.9% for HS-FOMO.

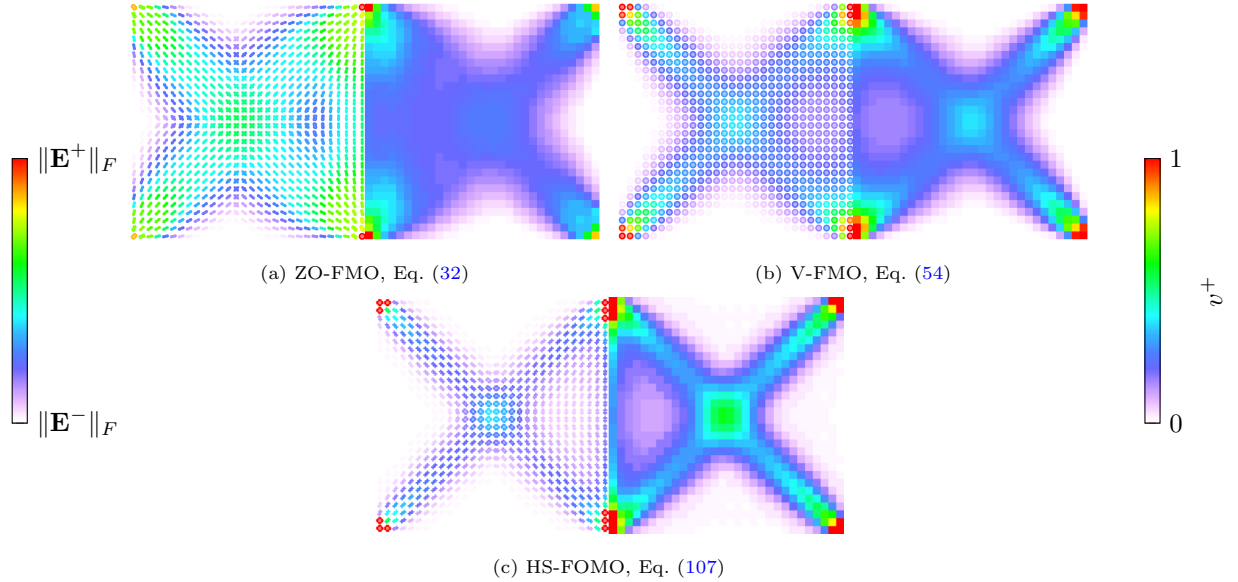


Figure 14: Multi-loadcase optimization for discretization 60×30 and $\mathbf{E}^- = 10^{-6}\mathbf{E}^+$. In each image, the left half shows the elasticity-tensor rosettes and the right half shows the volume fraction v^+ .

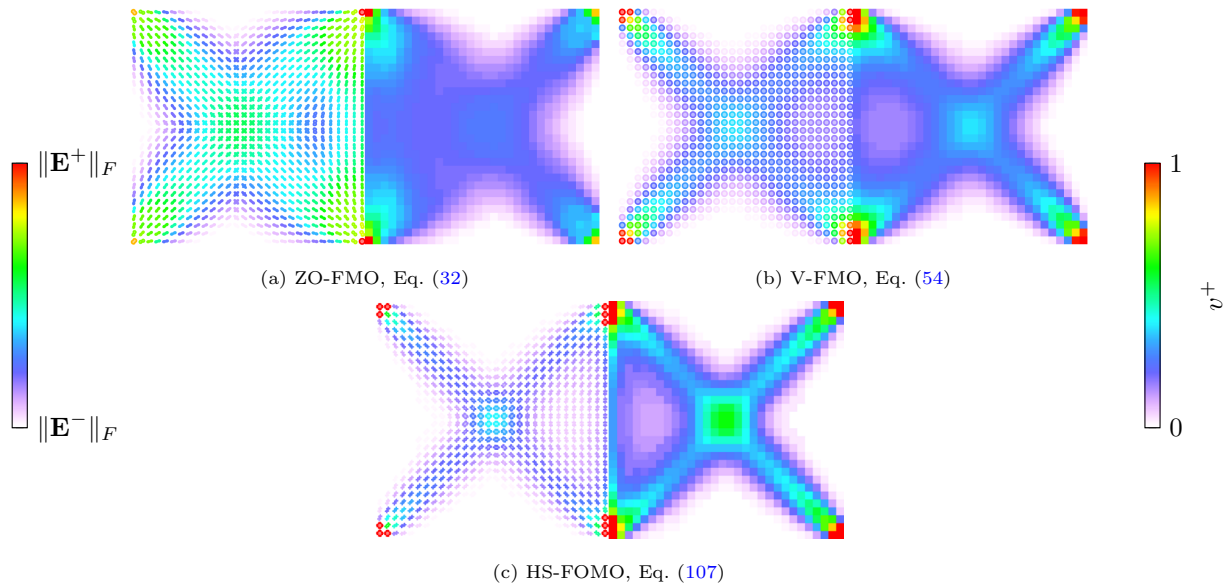


Figure 15: Multi-loadcase optimization for discretization 60×30 and $\mathbf{E}^- = 10^{-3}\mathbf{E}^+$. In each image, the left half shows the elasticity-tensor rosettes and the right half shows the volume fraction v^+ .

The sign of this change is explained by two competing mechanisms. On one hand, finite element modeling correction tends to increase compliance, because coarse displacement-based meshes are typically over-stiff and therefore underestimate the objective. On the other hand, discretization refinement enlarges the admissible design space by allowing finer spatial variation of \mathbf{E}_i , which tends to reduce the objective. In the present results, the former effect dominates. This tendency is further amplified by point loads and point supports, since refinement resolves stress concentrations more sharply and reduces artificial coarse-mesh stiffening.

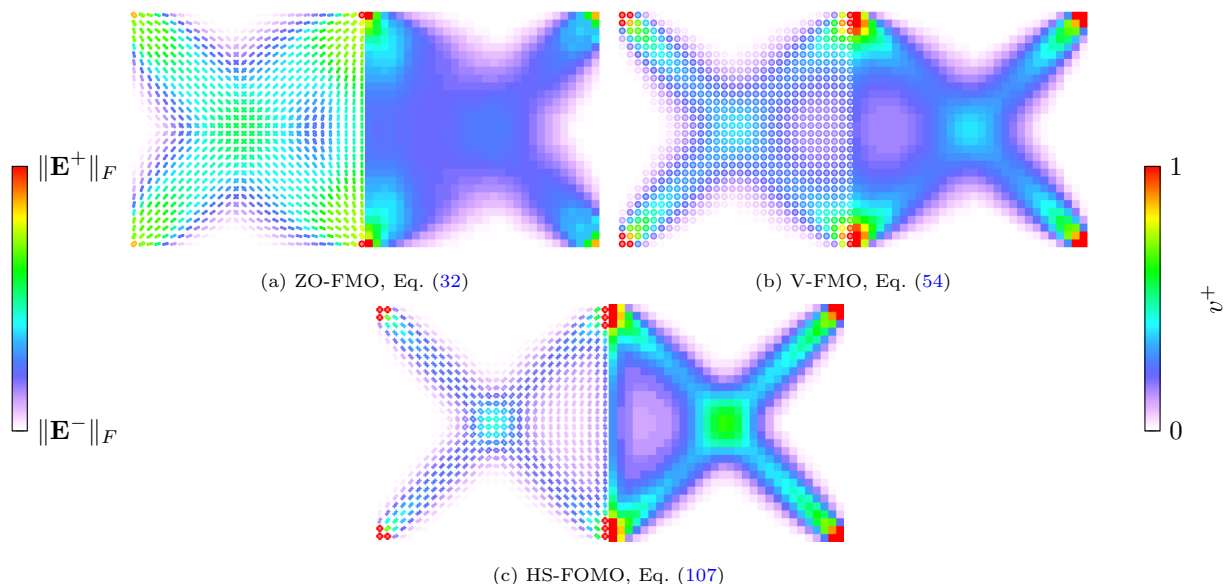


Figure 16: Multi-loadcase optimization for discretization 60×30 and $\mathbf{E}^- = 10^{-2}\mathbf{E}^+$. In each image, the left half shows the elasticity-tensor rosettes and the right half shows the volume fraction v^+ .

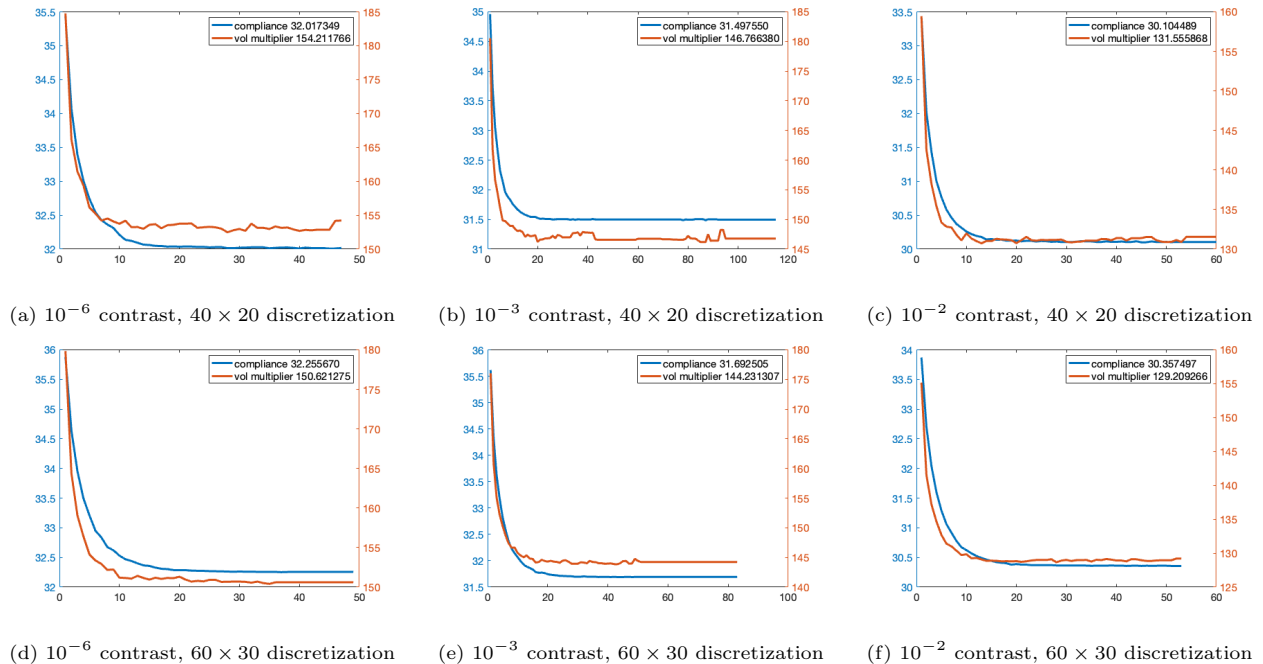


Figure 17: Convergence of the sequential global programming algorithm for the HS-FOMO problem across different phase contrasts. The blue curve shows compliance and the orange curve shows the volume multiplier λ .

The refinement trend is also consistent in the relative gap between V-FMO and HS-FOMO compliances. Moving from 40×20 to 60×30 , this gap decreases from 12.50% to 11.26% at contrast 10^{-6} , from 11.06% to 9.68% at 10^{-3} , and from 9.33% to 8.06% at 10^{-2} , i.e., by about 1.0–1.4 percentage points in all three cases. The multipliers show the same refinement direction: they are reduced by approximately 4.5–4.7% for ZO-FMO, 1.0–1.4% for V-FMO, and 1.7–2.3% for HS-FOMO, consistent with a lower marginal value of additional stiff material on the refined discretization.

The field plots in Figs. 11–16 indicate robust topology under mesh refinement: the same global transfer paths are preserved, while the 60×30 solutions mainly sharpen interfaces and load paths. Convergence curves in Fig. 17 exhibit a common two-stage behavior for HS-FOMO, with a rapid initial compliance drop followed by a shallow tail with small multiplier oscillations; practical stabilization is achieved in roughly 50–120 iterations.

5. Summary

This paper considers the two-dimensional plane-stress setting with well-ordered isotropic weak and strong phases. In this setting, we establish a clear hierarchy of free material optimization models based on increasingly tight energy bounds, from zeroth-order to Voigt and then to Hashin–Shtrikman. The continuum problem (15) is used as a theoretical reference that organizes this hierarchy through (13) and supports existence statements. Within the convex formulations considered here, the Voigt model is the strongest relaxation. It is strictly tighter than the zeroth-order model for $0 < \bar{V} < 1$ (Proposition 3.2) and coincides with it at $\bar{V} \in \{0, 1\}$. It also admits an optimal isotropic representation, which reduces the problem to variable-thickness-sheet optimization with one scalar variable per element (Proposition 3.3 and (54)). In addition, for the single-loadcase continuum zeroth-order model, at least one optimal solution can be chosen orthotropic (Proposition 3.1). For continuum well-posedness, minimizers exist directly for the zeroth-order and Voigt models, while for Hashin–Shtrikman bounds we obtain existence in the H -relaxed sense (Section 3.1).

For the Hashin–Shtrikman model, the results clarify both its strength and its algorithmic implications. The HS correction is nonnegative and vanishes at endpoints (Proposition 3.4). For every interior volume

fraction $v_i^\pm \in (0, 1)$, there exist strains for which this correction is strictly positive (while equality can still occur for a specific invariant relation), giving strict interior improvement over Voigt and leading to nonconvexity of the feasible set in (v_i^\pm, \mathbf{E}_i) (Lemma 3.1). At the same time, its convex hull is exactly the Voigt feasible set (Lemma 3.2), which explains why no tighter convex alternative is available in the same setting. Geometric visualizations of the admissible sets (Figs. 1, 2, and 3) make these relations directly visible. Separately, we show that the local HS volume variables can be eliminated through active-constraint characterization and explicit activating-volume formulas (Lemma 3.3, Proposition 3.5), giving the reduced model (83). A key by-product is an explicit volume estimator that, for a given effective elasticity tensor, quantifies the minimum stiff-phase fraction required for realizability through a worst-case strain evaluation. For orthotropic tensors this further reduces to a one-parameter search in $t = |\text{Tr}(\boldsymbol{\varepsilon})|$ (Proposition 3.6 and (106)).

To connect the discrete HS-FMO model with classical homogenization theory, we additionally analyze the single-loadcase continuum limit: in that setting, the HS-FMO relaxation is tight and has the same optimal value as the Allaire–Kohn relaxed formulation (Theorem 3.1). The corresponding laminate-construction viewpoint is illustrated in Fig. 4. The tightness statement should be interpreted as a continuum relaxation result, not as exact equivalence on a fixed finite-element mesh. For multiple loadcases, HS-FOMO is generally not tight and should be interpreted as a lower bound unless additional coupled energy bounds are enforced.

Computationally, the nonconvex orthotropic HS problem is handled with sequential global programming (Section 3.6). Numerically, both benchmarks confirm the predicted ordering $c^{\text{ZO-FMO}} < c^{\text{V-FMO}} < c^{\text{HS-FOMO}}$ (Tables 1 and 2). In the cantilever test, HS-FOMO remains close to finite-rank laminate solutions (compliance gap about 0.78–1.27%), while in the multi-loadcase test the ordering $c^{\text{ZO-FMO}} < c^{\text{V-FMO}} < c^{\text{HS-FOMO}}$ is preserved across phase contrasts and mesh refinements, with stable SGP empirical convergence behavior (Figs. 9 and 17).

Natural extensions of this work include several directions. A first step is to build inner approximations of the realizability set by designing connectable microstructures via inverse homogenization [46] and by sampling the energy-bound feasible set. A second direction is to move beyond compliance minimization and consider other objectives and constraints within the same free material framework [50]. A third direction is to further analyze the sequential global programming approach from both computational and theoretical viewpoints, in particular with respect to numerical efficiency, scalability, and convergence behavior. Finally, on the modeling side, it is important to investigate tighter energy bounds, broader material symmetry classes, and fully three-dimensional formulations [19].

Funding. The authors acknowledge support from the mobility project 8J24DE005, “Free material optimization for manufacturable modular structures,” funded jointly by the German Academic Exchange Service (DAAD) and the Ministry of Education, Youth and Sports of the Czech Republic (MŠMT). Marek Tyburec and Shen Yuan Ma were additionally co-funded by the European Union through the ROBOPROX project (reg. no. CZ.02.01.01/00/22 008/000459).

Declaration of generative AI use. During the preparation of this work, Marek Tyburec used ChatGPT to improve manuscript clarity. After using this tool, the authors reviewed and edited the content as needed and take full responsibility for the content of the published article.

Data availability. The code and data used to produce the results in this paper are available on request from the corresponding author.

CRedit authorship contribution statement. MT: Conceptualization, Methodology, Software, Formal analysis, Investigation, Writing – original draft, Visualization. MS: Conceptualization, Methodology, Software, Formal analysis, Investigation, Writing – original draft, Visualization. SM: Investigation, Writing – original draft.

A. Properties of the Hashin–Shtrikman upper bound function

This section collects regularity properties of the one-dimensional map $v_i^+ \mapsto f^{\text{HS}}(\boldsymbol{\varepsilon}; v_i^+)$ (for fixed $\boldsymbol{\varepsilon}$) that are used in the main text when eliminating local volume fractions and characterizing activating volumes. We first prove continuity, then monotonicity, and finally derive existence and uniqueness of the activating volume fraction solving $\langle \mathbf{E}_i \boldsymbol{\varepsilon}, \boldsymbol{\varepsilon} \rangle = f^{\text{HS}}(\boldsymbol{\varepsilon}; v_i^+)$.

Proposition A.1 (Continuity of the HS upper-bound function in v_i^+). *For any fixed strain $\boldsymbol{\varepsilon} \in \mathbb{S}^{2 \times 2}$ with the Frobenius norm $\sqrt{2}/2$ and $t = |\text{Tr}(\boldsymbol{\varepsilon})|$, the Hashin–Shtrikman upper bound function $f^{\text{HS}}(v_i^+) = \langle [(1 - v_i^+) \mathbf{E}^- + v_i^+ \mathbf{E}^+] \boldsymbol{\varepsilon}, \boldsymbol{\varepsilon} \rangle - q(t; v_i^+)$ with $q(t; v_i^+)$ defined in (60) is continuous in the volume fraction $v_i^+ \in [0, 1]$.*

Proof. The Voigt part is affine in v_i^+ , hence continuous. Thus, it suffices to show that $q(\boldsymbol{\varepsilon}; v_i^+)$ is continuous.

For the denominators in (60), set

$$d_1 = \kappa^+ + \mu^+ - (\Delta\kappa + \Delta\mu)v_i^+, \quad (\text{A.1a})$$

$$d_2 = \kappa^+ + \mu^+ - \Delta\kappa v_i^+, \quad (\text{A.1b})$$

$$d_3 = \kappa^+ + \mu^+ - \Delta\mu v_i^+. \quad (\text{A.1c})$$

Because $\Delta\kappa = \kappa^+ - \kappa^- > 0$ and $\Delta\mu = \mu^+ - \mu^- > 0$ with $v_i^+ \in [0, 1]$, we have $d_1, d_2, d_3 > 0$. Hence, the branch formulas are rational with strictly positive denominators, so $q(t; v_i^+)$ is continuous in v_i^+ on each branch interior. It remains to match the boundary values.

Define the branch-separation sets

$$\Gamma_{12} : v_i^+ \Delta\kappa t = d_2 \sqrt{1 - t^2}, \quad (\text{A.2a})$$

$$\Gamma_{13} : v_i^+ \Delta\mu \sqrt{1 - t^2} = d_3 t, \quad (\text{A.2b})$$

$$\Gamma_{23} : \frac{d_3 t}{v_i^+ \Delta\mu} < \sqrt{1 - t^2} < \frac{v_i^+ \Delta\kappa t}{d_2}. \quad (\text{A.2c})$$

On Γ_{12} , substituting $v_i^+ \Delta\kappa t = d_2 \sqrt{1 - t^2}$ into the formulas for q_1 and q_2 from (60) gives

$$q_1(t; v_i^+) = q_2(t; v_i^+) = \frac{\Delta\kappa^2 v_i^+ (1 - v_i^+) t^2 d_1}{d_2^2} \quad \text{on } \Gamma_{12}. \quad (\text{A.3})$$

On Γ_{13} , substituting $v_i^+ \Delta\mu \sqrt{1 - t^2} = d_3 t$ into q_1 and q_3 yields

$$q_1(t; v_i^+) = q_3(t; v_i^+) = \frac{\Delta\mu^2 v_i^+ (1 - v_i^+) (1 - t^2) d_1}{d_3^2} \quad \text{on } \Gamma_{13}. \quad (\text{A.4})$$

Finally, let (A.2c) hold. Multiplying the strict inequalities gives $t d_2 d_3 < (v_i^+)^2 \Delta\mu \Delta\kappa t$, which is equivalent to

$$t(d_1 + v_i^+ \Delta\kappa)(d_1 + v_i^+ \Delta\mu) < (v_i^+)^2 t \Delta\kappa \Delta\mu. \quad (\text{A.5})$$

However, this cannot hold for any $v_i^+ \in (0, 1)$ since $d_1 > 0$. Thus, $\Gamma_{23} = \emptyset$.

At $v_i^+ = 0$ we have $q(t; 0) = 0$ (the first branch applies), and at $v_i^+ = 1$ each branch carries a factor $(1 - v_i^+)$, so $q(t; 1) = 0$. Moreover, using the explicit boundary expressions above and $v_i^+ (1 - v_i^+) \rightarrow 0$ as $v_i^+ \rightarrow 0^+$ or 1^- , we see $\lim_{v_i^+ \rightarrow 0^+} q(t; v_i^+) = q(t; 0)$ and $\lim_{v_i^+ \rightarrow 1^-} q(t; v_i^+) = q(t; 1)$. Therefore, q is continuous on $[0, 1]$, and so is f^{HS} . \square

With continuity established, we next prove monotonicity with respect to v_i^+ .

Proposition A.2 (Monotonicity of the HS upper-bound function in v_i^+). *For any fixed strain $\boldsymbol{\varepsilon} \in \mathbb{S}^{2 \times 2}$ with the Frobenius norm $\sqrt{2}/2$, the Hashin–Shtrikman upper bound function $f^{\text{HS}}(v_i^+) = \langle [(1 - v_i^+) \mathbf{E}^- + v_i^+ \mathbf{E}^+] \boldsymbol{\varepsilon}, \boldsymbol{\varepsilon} \rangle - q(t; v_i^+)$ with $q(t; v_i^+)$ defined in (60) is nondecreasing in the volume fraction $v_i^+ \in [0, 1]$.*

Proof. By Proposition A.1, $f^{\text{HS}}(v_i^+)$ is continuous in v_i^+ . It, therefore, suffices to show $\partial f^{\text{HS}}(v_i^+)/\partial v_i^+ \geq 0$ on the interior of each branch and then pass to the boundary by continuity.

Write the Voigt term as

$$\langle [(1 - v_i^+)\mathbf{E}^- + v_i^+\mathbf{E}^+]\boldsymbol{\varepsilon}, \boldsymbol{\varepsilon} \rangle = (\kappa^- + v_i^+\Delta\kappa)t^2 + (\mu^- + v_i^+\Delta\mu)(1 - t^2), \quad (\text{A.6})$$

whose derivative in v_i^+ is $\Delta\kappa t^2 + \Delta\mu(1 - t^2) \geq 0$.

For the first branch in (60), let $\eta_1 = d_2\sqrt{1 - t^2} - v_i^+t\Delta\kappa$, $\eta_2 = d_3t - v_i^+\sqrt{1 - t^2}\Delta\mu$. A direct computation yields

$$\frac{\partial f_1^{\text{HS}}(v_i^+)}{\partial v_i^+} = \frac{\Delta\mu\eta_1^2 + \Delta\kappa\eta_2^2 - \frac{(\Delta\kappa\eta_2 - \Delta\mu\eta_1)^2}{\kappa^+ + \mu^+}}{d_1^2}. \quad (\text{A.7})$$

Using the elementary identity

$$(\Delta\kappa + \Delta\mu)(\Delta\kappa\eta_2^2 + \Delta\mu\eta_1^2) - (\Delta\kappa\eta_2 - \Delta\mu\eta_1)^2 = \Delta\mu\Delta\kappa(\eta_1 + \eta_2)^2 \geq 0. \quad (\text{A.8})$$

and since $\kappa^+ + \mu^+ > \kappa^- + \mu^- > 0$, we may write

$$\frac{\partial f_1^{\text{HS}}(v_i^+)}{\partial v_i^+} = \frac{(\Delta\kappa\eta_2^2 + \Delta\mu\eta_1^2)(\kappa^- + \mu^-) + \Delta\mu\Delta\kappa(\eta_1 + \eta_2)^2}{d_1^2(\kappa^+ + \mu^+)} \geq 0. \quad (\text{A.9})$$

For the second and third branch in (60), differentiation gives

$$\frac{\partial f_2^{\text{HS}}(v_i^+)}{\partial v_i^+} = \frac{t^2(\kappa^- + \mu^+)(\kappa^+ + \mu^+)\Delta\kappa}{d_2^2} > 0, \quad (\text{A.10a})$$

$$\frac{\partial f_3^{\text{HS}}(v_i^+)}{\partial v_i^+} = \frac{(1 - t^2)(\kappa^+ + \mu^-)(\kappa^+ + \mu^+)\Delta\mu}{d_3^2} > 0, \quad (\text{A.10b})$$

with the strict inequality due to the branch conditions. Since the three expressions are nonnegative on the interiors and the branch values of q agree on $\Gamma_{12} \cup \Gamma_{13}$ (Proposition A.1), continuity implies that $f^{\text{HS}}(v_i^+)$ is globally nondecreasing in $v_i^+ \in [0, 1]$. \square

Combining endpoint values with continuity and monotonicity gives the following existence and uniqueness consequence.

Corollary A.1 (Existence and uniqueness of the activating HS volume fraction). *For any fixed strain $\boldsymbol{\varepsilon} \in \mathbb{S}^{2 \times 2}$ with the Frobenius norm $\sqrt{2}/2$ and elasticity tensor $\mathbf{E}_i \in \mathbb{S}^{2 \times 2 \times 2 \times 2}$ with $\mathbf{E}^- \preceq \mathbf{E}_i \preceq \mathbf{E}^+$, there exists a unique volume fraction $v_i^+ \in [0, 1]$ such that $\langle \mathbf{E}_i \boldsymbol{\varepsilon}, \boldsymbol{\varepsilon} \rangle = f^{\text{HS}}(\boldsymbol{\varepsilon}; v_i^+)$.*

Proof. Since $\mathbf{E}^- \preceq \mathbf{E}_i \preceq \mathbf{E}^+$, we have $\langle \mathbf{E}^- \boldsymbol{\varepsilon}, \boldsymbol{\varepsilon} \rangle \leq \langle \mathbf{E}_i \boldsymbol{\varepsilon}, \boldsymbol{\varepsilon} \rangle \leq \langle \mathbf{E}^+ \boldsymbol{\varepsilon}, \boldsymbol{\varepsilon} \rangle$. Moreover, by the endpoint evaluation in Proposition 3.4, $q(\boldsymbol{\varepsilon}; 0) = q(\boldsymbol{\varepsilon}; 1) = 0$. Hence, $f^{\text{HS}}(\boldsymbol{\varepsilon}; 0) = \langle \mathbf{E}^- \boldsymbol{\varepsilon}, \boldsymbol{\varepsilon} \rangle$, $f^{\text{HS}}(\boldsymbol{\varepsilon}; 1) = \langle \mathbf{E}^+ \boldsymbol{\varepsilon}, \boldsymbol{\varepsilon} \rangle$, and $f^{\text{HS}}(\boldsymbol{\varepsilon}; \cdot)$ is continuous on $[0, 1]$ by Proposition A.1. Therefore, the intermediate value theorem gives a (possibly nonunique) $v_i^+ \in [0, 1]$ with $\langle \mathbf{E}_i \boldsymbol{\varepsilon}, \boldsymbol{\varepsilon} \rangle = f^{\text{HS}}(\boldsymbol{\varepsilon}; v_i^+)$.

By Proposition A.2, $f^{\text{HS}}(\boldsymbol{\varepsilon}; \cdot)$ is nondecreasing on $[0, 1]$. We now show it is in fact strictly increasing, which implies uniqueness. On each branch interior, the derivative $\partial f^{\text{HS}}(\boldsymbol{\varepsilon}; v_i^+)/\partial v_i^+$ is nonnegative, and in the second and third branches the derivatives are strictly positive (cf. Eq. (A.10)). In the first branch, the derivative is nonnegative and vanishes only at points where $\eta_1 = \eta_2 = 0$, which occurs exactly on the branch boundaries $\Gamma_{12} \cup \Gamma_{13}$ (see the proof of Proposition A.2). Thus, $f^{\text{HS}}(\boldsymbol{\varepsilon}; \cdot)$ cannot be flat on any nontrivial interval contained in a branch interior. At the boundaries, adjacent-branch formulas coincide, and $\Gamma_{23} = \emptyset$. Hence, any interval $[v_1, v_2] \subset [0, 1]$ decomposes into finitely many subintervals lying in branch interiors, separated by isolated boundary points. Integrating the (strictly) positive derivatives over each interior subinterval shows $v_2 > v_1 \Rightarrow f^{\text{HS}}(\boldsymbol{\varepsilon}; v_2) > f^{\text{HS}}(\boldsymbol{\varepsilon}; v_1)$. Therefore, $f^{\text{HS}}(\boldsymbol{\varepsilon}; \cdot)$ is strictly increasing on $[0, 1]$, and the solution to $\langle \mathbf{E}_i \boldsymbol{\varepsilon}, \boldsymbol{\varepsilon} \rangle = f^{\text{HS}}(\boldsymbol{\varepsilon}; v_i^+)$ is unique. \square

B. Regularity of the Hashin–Shtrikman lower complementary-energy bound

Following Burazin et al. [20], the cell-wise material update contains the one-dimensional volume-fraction subproblem

$$\text{find } v^+ \in \arg \min_{v \in [0,1]} f_c^{\text{HS}}(\boldsymbol{\sigma}; v) + \lambda v. \quad (\text{B.1})$$

In this section, for fixed $\boldsymbol{\sigma}$, we establish regularity properties of the map $v \mapsto f_c^{\text{HS}}(\boldsymbol{\sigma}; v)$. These properties justify an efficient and globally optimal solution strategy for this one-dimensional minimization problem.

Definition B.1 (Optimal lower bound on complementary energy [1, Definition 2.3.15]). *Let $\mathbf{E}^- \preceq \mathbf{E}^+$ be two well-ordered isotropic elasticity tensors and let $v^+ \in [0, 1]$ be the volume fraction of \mathbf{E}^+ . Denote by G_{v^+} the set of all effective elasticity tensors \mathbf{E}^* obtainable by homogenization of the two phases $(\mathbf{E}^-, \mathbf{E}^+)$ with volume fraction v^+ .*

A function $f(\boldsymbol{\sigma}; v^+)$ is called a (complementary-energy) lower bound if, for every $\boldsymbol{\sigma} \in \mathbb{S}^{d \times d}$ and every $\mathbf{E}^ \in G_{v^+}$,*

$$\langle (\mathbf{E}^*)^{-1} \boldsymbol{\sigma}, \boldsymbol{\sigma} \rangle \geq f(\boldsymbol{\sigma}; v^+).$$

The lower bound is optimal if, for every $\boldsymbol{\sigma} \in \mathbb{S}^{d \times d}$, there exists $\mathbf{E}^(\boldsymbol{\sigma}) \in G_{v^+}$ such that equality holds, i.e.,*

$$\langle (\mathbf{E}^*(\boldsymbol{\sigma}))^{-1} \boldsymbol{\sigma}, \boldsymbol{\sigma} \rangle = f(\boldsymbol{\sigma}; v^+).$$

The Hashin–Shtrikman lower complementary-energy bound is optimal. Let κ^+ and μ^+ denote the bulk and shear moduli of \mathbf{E}^+ , and let $\mathbf{e} \in \mathbb{R}^d$ satisfy $\|\mathbf{e}\| = 1$. Define $\mathbf{F}_{\mathbf{E}^+}^c(\mathbf{e}) \in \mathbb{S}^{d \times d \times d \times d}$ by, for all $\boldsymbol{\varepsilon} \in \mathbb{S}^{d \times d}$,

$$\langle \mathbf{F}_{\mathbf{E}^+}^c(\mathbf{e}) \boldsymbol{\varepsilon}, \boldsymbol{\varepsilon} \rangle = \langle \mathbf{E}^+ \boldsymbol{\varepsilon}, \boldsymbol{\varepsilon} \rangle - \frac{1}{\mu^+} \|\mathbf{E}^+ \boldsymbol{\varepsilon}\|^2 + \left(\frac{1}{\mu^+} - \frac{1}{\kappa^+ + 2\mu^+(d-1)/d} \right) \langle (\mathbf{E}^+ \boldsymbol{\varepsilon}) \mathbf{e}, \mathbf{e} \rangle^2. \quad (\text{B.2})$$

The tensor $\mathbf{F}_{\mathbf{E}^+}^c(\mathbf{e})$ admits a geometric interpretation. For a fixed unit direction \mathbf{e} , define the subspaces of $\mathbb{S}^{d \times d}$:

$$V(\mathbf{e}) := \text{span}\{\mathbf{e} \hat{\mathbf{e}}^\top + \hat{\mathbf{e}} \mathbf{e}^\top; \hat{\mathbf{e}} \in \mathbb{R}^d\}, \quad (\text{B.3})$$

$$W(\mathbf{e}) := \{\boldsymbol{\varepsilon} \in \mathbb{S}^{d \times d} : \boldsymbol{\varepsilon} \mathbf{e} = \mathbf{0}\}. \quad (\text{B.4})$$

Since \mathbf{E}^+ is positive definite, it admits a unique square root $(\mathbf{E}^+)^{\frac{1}{2}}$, and $\mathbb{S}^{d \times d}$ has the orthogonal decomposition

$$\mathbb{S}^{d \times d} = (\mathbf{E}^+)^{\frac{1}{2}} V(\mathbf{e}) \oplus (\mathbf{E}^+)^{-\frac{1}{2}} W(\mathbf{e}).$$

Let $\pi_{\mathcal{W}}$ be the projection onto a subspace $\mathcal{W} \subset \mathbb{S}^{d \times d}$. Then,

$$\langle \mathbf{F}_{\mathbf{E}^+}^c(\mathbf{e}) \boldsymbol{\varepsilon}, \boldsymbol{\varepsilon} \rangle = \left\| \pi_{(\mathbf{E}^+)^{-\frac{1}{2}} W(\mathbf{e})} \left((\mathbf{E}^+)^{\frac{1}{2}} \boldsymbol{\varepsilon} \right) \right\|_F^2 = \left\| (\mathbf{E}^+)^{\frac{1}{2}} \boldsymbol{\varepsilon} \right\|_F^2 - \left\| \pi_{(\mathbf{E}^+)^{\frac{1}{2}} V(\mathbf{e})} \left((\mathbf{E}^+)^{\frac{1}{2}} \boldsymbol{\varepsilon} \right) \right\|_F^2.$$

Theorem B.1 (HS lower bound on complementary energy; optimality [1, Proposition 2.3.25]). *Assume two well-ordered isotropic phases $\mathbf{E}^- \preceq \mathbf{E}^+$ and let $v^+ \in [0, 1]$. Let G_{v^+} be the corresponding G-closure. Define, for $\boldsymbol{\sigma} \in \mathbb{S}^{d \times d}$,*

$$f_c^{\text{HS}}(\boldsymbol{\sigma}; v^+) := \langle (\mathbf{E}^+)^{-1} \boldsymbol{\sigma}, \boldsymbol{\sigma} \rangle + (1 - v^+) \max_{\boldsymbol{\varepsilon} \in \mathbb{S}^{d \times d}} \left\{ 2 \langle \boldsymbol{\sigma}, \boldsymbol{\varepsilon} \rangle - \langle ((\mathbf{E}^-)^{-1} - (\mathbf{E}^+)^{-1})^{-1} \boldsymbol{\varepsilon}, \boldsymbol{\varepsilon} \rangle - v^+ g^c(\boldsymbol{\varepsilon}) \right\}, \quad (\text{B.5})$$

where $g^c(\boldsymbol{\varepsilon}) := \max_{\|\mathbf{e}\|=1} \langle \mathbf{F}_{\mathbf{E}^+}^c(\mathbf{e}) \boldsymbol{\varepsilon}, \boldsymbol{\varepsilon} \rangle$. Then, f_c^{HS} is a (complementary-energy) lower bound in the sense of Definition B.1: for all $\boldsymbol{\sigma} \in \mathbb{S}^{d \times d}$ and all $\mathbf{E}^* \in G_{v^+}$, $\langle (\mathbf{E}^*)^{-1} \boldsymbol{\sigma}, \boldsymbol{\sigma} \rangle \geq f_c^{\text{HS}}(\boldsymbol{\sigma}; v^+)$. Moreover, the bound is optimal: for every $\boldsymbol{\sigma}$ there exists $\mathbf{E}^*(\boldsymbol{\sigma}) \in G_{v^+}$ generated by a finite-rank sequential laminate such that equality holds. In $d = 2$, orthotropic rank-two laminates aligned with the principal stress directions are sufficient.

The nonlocal term g^c admits a closed-form expression.

Lemma B.1 ([4, Eq. (4.15)]). *Let $\varepsilon_1, \varepsilon_2$ be the two eigenvalues of $\varepsilon \in \mathbb{S}^{2 \times 2}$, and let μ^+ and κ^+ be the shear and bulk moduli of \mathbf{E}^+ . Then,*

$$g^c(\varepsilon) = \frac{4\kappa^+\mu^+}{\kappa^+ + \mu^+} \max\{\varepsilon_1^2, \varepsilon_2^2\}. \quad (\text{B.6})$$

Moreover, if $\mathbf{e}_1, \mathbf{e}_2$ are eigenvectors of ε associated with the eigenvalues $\varepsilon_1, \varepsilon_2$, then $\max_{\|\mathbf{e}\|=1} (\mathbf{F}_{\mathbf{E}^+}^c(\mathbf{e})\varepsilon, \varepsilon)$ is attained by choosing $\mathbf{e} = \mathbf{e}_i$, where $i \in \{1, 2\}$ satisfies $\varepsilon_i = \max\{\varepsilon_1^2, \varepsilon_2^2\}$.

The Fenchel conjugate of g^c is explicitly known.

Lemma B.2 ([4]). *Let σ_1, σ_2 be the two eigenvalues of σ , let $v^+ > 0$, and let μ^+ and κ^+ be the shear and bulk moduli of \mathbf{E}^+ . Then,*

$$\max_{\varepsilon \in \mathbb{S}^{2 \times 2}} \{2\langle \sigma, \varepsilon \rangle - v^+ g^c(\varepsilon)\} = \frac{\kappa^+ + \mu^+}{4\kappa^+ \mu^+ v^+} (|\sigma_1| + |\sigma_2|)^2. \quad (\text{B.7})$$

Identity (B.7) can be interpreted as the convex (Fenchel) conjugate of the function $\varepsilon \mapsto v^+ g^c(\varepsilon)$, evaluated at 2σ . More precisely,

$$[v^+ g^c]^*(2\sigma) = \frac{\kappa^+ + \mu^+}{4\kappa^+ \mu^+ v^+} (|\sigma_1| + |\sigma_2|)^2. \quad (\text{B.8})$$

Moreover, for any convex function ϕ and $v^+ > 0$, one has the scaling identity $(v^+ \phi)^*(\tau) = v^+ \phi^*(\tau/v^+)$. Applying this with $\phi = g^c$ gives

$$[v^+ g^c]^*(2\tau) = v^+ [g^c]^*\left(\frac{2\tau}{v^+}\right). \quad (\text{B.9})$$

Hence, $(\tau, v^+) \mapsto [v^+ g^c]^*(2\tau)$ is the perspective of $[g^c]^*$ and is jointly convex in (τ, v^+) .

Define $\mathbf{R} = ((\mathbf{E}^-)^{-1} - (\mathbf{E}^+)^{-1})^{-1}$. By standard convex duality, we obtain:

$$\max_{\varepsilon \in \mathbb{S}^{2 \times 2}} \{2\langle \sigma, \varepsilon \rangle - \langle \mathbf{R}\varepsilon, \varepsilon \rangle - v^+ g^c(\varepsilon)\} = \inf_{\tau \in \mathbb{S}^{2 \times 2}} \langle \mathbf{R}^{-1}(\sigma - \tau), (\sigma - \tau) \rangle + [v^+ g^c]^*(2\tau) \quad (\text{B.10})$$

We now analyze the regularity of $v^+ \mapsto f_c^{\text{HS}}(\sigma; v^+)$ for fixed $\sigma \neq \mathbf{0}$. Define

$$\psi(\tau; v^+) := \langle \mathbf{R}^{-1}(\sigma - \tau), (\sigma - \tau) \rangle + [v^+ g^c]^*(2\tau) \quad (\text{B.11})$$

$$\Psi(v^+) := \inf_{\tau \in \mathbb{S}^{2 \times 2}} \psi(\tau; v^+) \quad (\text{B.12})$$

$$\mathcal{S}(v^+) := \arg \min_{\tau \in \mathbb{S}^{2 \times 2}} \psi(\tau; v^+) \quad (\text{B.13})$$

so that

$$f_c^{\text{HS}}(\sigma; v^+) = \langle (\mathbf{E}^+)^{-1} \sigma, \sigma \rangle + (1 - v^+) \Psi(v^+). \quad (\text{B.14})$$

By the explicit expression of $[v^+ g^c]^*(2\tau)$ (cf. (B.7)), for each fixed τ the map $v^+ \mapsto \psi(\tau; v^+)$ is differentiable on $(0, 1]$, with

$$D_{v^+} \psi(\tau; v^+) = -\frac{\kappa^+ + \mu^+}{4\kappa^+ \mu^+ (v^+)^2} (|\tau_1| + |\tau_2|)^2. \quad (\text{B.15})$$

In particular, $(\tau, v^+) \mapsto D_{v^+} \psi(\tau; v^+)$ is continuous on $\mathbb{S}^{2 \times 2} \times (0, 1]$. Hence, regularity of $f_c^{\text{HS}}(\sigma; v^+)$ reduces to regularity of the value function Ψ .

To apply the Danskin-type results of Bonnans and Shapiro [15] to $\Psi(v^+) = \inf_{\tau} \psi(\tau; v^+)$, we need two ingredients: (i) inf-compactness, ensuring bounded minimizing sequences, and (ii) uniqueness of the minimizer for each fixed $v^+ > 0$. We prove these next.

Proposition B.1. *For all $0 < v_0^+ \leq 1$, ψ has the inf-compactness property at v_0^+ .*

Proof. It is enough to construct a compact set $C \subset \mathbb{S}^{2 \times 2}$, a constant $\alpha \in \mathbb{R}$, and a neighborhood V of v_0^+ such that, for every $v^+ \in V$, the sublevel set $\{\boldsymbol{\tau} \in \mathbb{S}^{2 \times 2} : \psi(\boldsymbol{\tau}; v^+) \leq \alpha\}$ is contained in C .

Set $V = (\frac{v_0^+}{2}, v_0^+ + 1)$. By the explicit expression of $[v^+ g^c]^*(2\boldsymbol{\tau})$ (cf. (B.7)), the map $v^+ \mapsto [v^+ g^c]^*(2\boldsymbol{\tau})$ is decreasing on $(0, 1]$ for each fixed $\boldsymbol{\tau}$, hence $\psi(\boldsymbol{\tau}; v^+) \leq \psi(\boldsymbol{\tau}; \frac{v_0^+}{2})$ for all $v^+ \in V$ and $\boldsymbol{\tau} \in \mathbb{S}^{2 \times 2}$. Now fix $\boldsymbol{\tau}_0 \in \mathbb{S}^{2 \times 2}$ and set $\alpha = \psi(\boldsymbol{\tau}_0; \frac{v_0^+}{2})$, so that the above sublevel set is nonempty. Let $r > 0$ be the smallest eigenvalue of \mathbf{R}^{-1} and define $C := \left\{ \boldsymbol{\tau} \in \mathbb{S}^{2 \times 2} : r\|\boldsymbol{\sigma} - \boldsymbol{\tau}\|_F^2 + \frac{\kappa^+ + \mu^+}{4\kappa^+ \mu^+ (v_0^+ + 1)} (|\tau_1| + |\tau_2|)^2 \leq \alpha \right\}$. The set C is closed and bounded in finite dimension, hence compact. Finally, if $v^+ \in V$ and $\psi(\boldsymbol{\tau}; v^+) \leq \alpha$, then using $r\|\boldsymbol{\sigma} - \boldsymbol{\tau}\|_F^2 \leq \langle \mathbf{R}^{-1}(\boldsymbol{\sigma} - \boldsymbol{\tau}), (\boldsymbol{\sigma} - \boldsymbol{\tau}) \rangle$ and $v^+ \leq v_0^+ + 1$ we obtain

$$\begin{aligned} r\|\boldsymbol{\sigma} - \boldsymbol{\tau}\|_F^2 + \frac{\kappa^+ + \mu^+}{4\kappa^+ \mu^+ (v_0^+ + 1)} (|\tau_1| + |\tau_2|)^2 \\ \leq \langle \mathbf{R}^{-1}(\boldsymbol{\sigma} - \boldsymbol{\tau}), (\boldsymbol{\sigma} - \boldsymbol{\tau}) \rangle + \frac{\kappa^+ + \mu^+}{4\kappa^+ \mu^+ v^+} (|\tau_1| + |\tau_2|)^2 = \psi(\boldsymbol{\tau}; v^+) \leq \alpha, \end{aligned} \quad (\text{B.16})$$

which implies $\boldsymbol{\tau} \in C$. □

The strong convexity of the quadratic term then gives uniqueness of the minimizer.

Proposition B.2. *For all $0 < v_0^+ \leq 1$, $\mathcal{S}(v_0^+)$ is single valued.*

Proof. This follows from the strong convexity of $\boldsymbol{\tau} \mapsto \psi(\boldsymbol{\tau}; v_0^+)$. □

With inf-compactness and uniqueness established, we can invoke Danskin's theorem to differentiate Ψ with respect to v^+ .

Theorem B.2. *Ψ is Fréchet differentiable in $(0, 1]$.*

Proof. Fix $v_0^+ > 0$. We verify the assumptions of Bonnans and Shapiro [15, Theorem 4.13]:

1. $\forall \boldsymbol{\tau} \in \mathbb{S}^{2 \times 2}$, $\psi(\boldsymbol{\tau}; \cdot)$ is Gâteaux differentiable near v_0^+ ,
2. $(\boldsymbol{\tau}, v^+) \mapsto \psi(\boldsymbol{\tau}; v^+)$ and $(\boldsymbol{\tau}, v^+) \mapsto D_{v^+} \psi(\boldsymbol{\tau}; v^+)$ are continuous near v_0^+ ,
3. ψ has the inf-compactness property at v_0^+

Since $\mathcal{S}(v_0^+)$ is single valued, Fréchet differentiability and the gradient formula follow (cf. [15, Remark 4.14]):

$$D_{v^+} \Psi(v_0^+) = -\frac{\kappa^+ + \mu^+}{4\kappa^+ \mu^+ (v_0^+)^2} (|\tau_1(v_0^+)| + |\tau_2(v_0^+)|)^2. \quad (\text{B.17})$$

□

Consequently, for fixed $\boldsymbol{\sigma}$, the map $v^+ \mapsto f_c^{\text{HS}}(\boldsymbol{\sigma}; v^+)$ is differentiable on $(0, 1]$. Using (B.14),

$$D_{v^+} f_c^{\text{HS}}(\boldsymbol{\sigma}; v^+) = -\Psi(v^+) + (1 - v^+) D_{v^+} \Psi(v^+). \quad (\text{B.18})$$

We now prove convexity of f_c^{HS} with respect to v^+ .

Theorem B.3. *The lower bound f_c^{HS} is convex in v^+ on $(0, 1]$ for fixed $\boldsymbol{\sigma}$.*

Proof. By (B.14), it suffices to prove that $v^+ \mapsto (1 - v^+) \Psi(v^+)$ is convex on $(0, 1]$. We first note that Ψ is nonincreasing on $(0, 1]$: for each fixed $\boldsymbol{\tau}$, the map $v^+ \mapsto \psi(\boldsymbol{\tau}; v^+)$ is nonincreasing (cf. the explicit expression (B.7)), and taking the infimum over $\boldsymbol{\tau}$ preserves monotonicity. Next, Ψ is convex as a partial minimization of a jointly convex function: indeed, $[v^+ g^c]^*(2\boldsymbol{\tau}) = v^+ (g^c)^* \left(\frac{2\boldsymbol{\tau}}{v^+} \right)$ for $v^+ > 0$, which is the perspective of $(g^c)^*$ and therefore jointly convex in $(\boldsymbol{\tau}, v^+)$; hence $\Psi(v^+) = \inf_{\boldsymbol{\tau}} \psi(\boldsymbol{\tau}; v^+)$ is convex.

Finally, let $v_\theta = \theta v_1 + (1 - \theta) v_2$ with $v_1, v_2 \in (0, 1]$ and $\theta \in [0, 1]$. By convexity of Ψ , $(1 - v_\theta) \Psi(v_\theta) \leq (1 - v_\theta) (\theta \Psi(v_1) + (1 - \theta) \Psi(v_2))$. Since Ψ is nonincreasing, the latter is bounded above by $\theta(1 - v_1) \Psi(v_1) + (1 - \theta)(1 - v_2) \Psi(v_2)$, because the difference equals $\theta(1 - \theta)(v_2 - v_1)(\Psi(v_1) - \Psi(v_2)) \geq 0$. □

Since $v^+ \mapsto f_c^{\text{HS}}(\boldsymbol{\sigma}; v^+)$ is convex and differentiable on $(0, 1]$, the elementwise update

$$v^+ \in \arg \min_{v \in [0, 1]} (f_c^{\text{HS}}(\boldsymbol{\sigma}; v) + \lambda v) \quad (\text{B.19})$$

can be performed efficiently. Since $v^+ \mapsto D_{v^+} f_c^{\text{HS}}(\boldsymbol{\sigma}; v^+) + \lambda$ is nondecreasing, we use bisection: if $D_{v^+} f_c^{\text{HS}}(\boldsymbol{\sigma}; 1) < -\lambda$, set $v^+ = 1$; otherwise, bracket a root of $D_{v^+} f_c^{\text{HS}}(\boldsymbol{\sigma}; v^+) = -\lambda$ by dyadic steps (or set $v^+ = 0$ at tolerance) and bisect on $[v^{+,1}, v^{+,0}]$.

References

- [1] G. Allaire. *Shape optimization by the homogenization method*. Springer New York, 2002. ISBN 9781468492866. [10.1007/978-1-4684-9286-6](https://doi.org/10.1007/978-1-4684-9286-6).
- [2] G. Allaire and S. Aubry. On optimal microstructures for a plane shape optimization problem. *Structural Optimization*, 17(2–3):86–94, 1999. [10.1007/bf01195933](https://doi.org/10.1007/bf01195933).
- [3] G. Allaire and R. V. Kohn. Explicit optimal bounds on the elastic energy of a two-phase composite in two space dimensions. *Quarterly of Applied Mathematics*, 51(4):675–699, 1993. [10.1090/qam/1247434](https://doi.org/10.1090/qam/1247434).
- [4] G. Allaire and R. V. Kohn. Optimal design for minimum weight and compliance in plane stress using extremal microstructures. *European Journal of Mechanics. A. Solids*, 12(6):839–878, 1993.
- [5] G. Allaire and R. V. Kohn. Optimal bounds on the effective behavior of a mixture of two well-ordered elastic materials. *Quarterly of Applied Mathematics*, 51(4):643–674, 1993. [10.1090/qam/1247433](https://doi.org/10.1090/qam/1247433).
- [6] G. Allaire, Z. Belhachmi, and F. Jouve. The homogenization method for topology and shape optimization. Single and multiple loads case. *Revue Européenne des Éléments Finis*, 5(5–6):649–672, 1996. [10.1080/12506559.1996.10511241](https://doi.org/10.1080/12506559.1996.10511241).
- [7] G. Allaire, E. Bonnetier, G. Francfort, and F. Jouve. Shape optimization by the homogenization method. *Numerische Mathematik*, 76(1):27–68, 1997. [10.1007/s002110050253](https://doi.org/10.1007/s002110050253).
- [8] G. Allaire, P. Geoffroy-Donders, and O. Pantz. Topology optimization of modulated and oriented periodic microstructures by the homogenization method. *Computers & Mathematics with Applications*, 78(7):2197–2229, 2019. [10.1016/j.camwa.2018.08.007](https://doi.org/10.1016/j.camwa.2018.08.007).
- [9] M. Avellaneda. Optimal bounds and microgeometries for elastic two-phase composites. *SIAM Journal on Applied Mathematics*, 47(6):1216–1228, 1987. [10.1137/0147082](https://doi.org/10.1137/0147082).
- [10] A. Ben-Tal, M. Kočvara, A. Nemirovski, and J. Zowe. Free material design via semidefinite programming: The multiload case with contact conditions. *SIAM Review*, 42(4):695–715, 2000. [10.1137/s0036144500372081](https://doi.org/10.1137/s0036144500372081).
- [11] M. P. Bendsøe and N. Kikuchi. Generating optimal topologies in structural design using a homogenization method. *Computer Methods in Applied Mechanics and Engineering*, 71(2):197–224, 1988. [10.1016/0045-7825\(88\)90086-2](https://doi.org/10.1016/0045-7825(88)90086-2).
- [12] M. P. Bendsøe and O. Sigmund. Material interpolation schemes in topology optimization. *Archive of Applied Mechanics (Ingenieur Archiv)*, 69(9–10):635–654, 1999. [10.1007/s004190050248](https://doi.org/10.1007/s004190050248).
- [13] M. P. Bendsøe, J. M. Guedes, R. B. Haber, P. Pedersen, and J. E. Taylor. An analytical model to predict optimal material properties in the context of optimal structural design. *Journal of Applied Mechanics*, 61(4):930–937, 1994. [10.1115/1.2901581](https://doi.org/10.1115/1.2901581).
- [14] M. P. Bendsøe, A. R. Díaz, R. Lipton, and J. E. Taylor. Optimal design of material properties and material distribution for multiple loading conditions. *International Journal for Numerical Methods in Engineering*, 38(7):1149–1170, 1995. [10.1002/nme.1620380705](https://doi.org/10.1002/nme.1620380705).

- [15] J. F. Bonnans and A. Shapiro. *Perturbation analysis of optimization problems*. Springer Science & Business Media, 2013. [10.1007/978-1-4612-1394-9](https://doi.org/10.1007/978-1-4612-1394-9).
- [16] S. Boyd and L. Vandenberghe. *Convex optimization*. Cambridge University Press, 2004. ISBN 9780511804441. [10.1017/cbo9780511804441](https://doi.org/10.1017/cbo9780511804441).
- [17] K. Bołbotowski and T. Lewiński. Setting the free material design problem through the methods of optimal mass distribution. *Calculus of Variations and Partial Differential Equations*, 61(2), 2022. [10.1007/s00526-022-02186-8](https://doi.org/10.1007/s00526-022-02186-8).
- [18] H. Brezis. *Functional analysis, Sobolev spaces and partial differential equations*. Springer New York, 2011. ISBN 9780387709147. [10.1007/978-0-387-70914-7](https://doi.org/10.1007/978-0-387-70914-7).
- [19] K. Burazin and I. Crnjac. Application of explicit energy bounds in optimization of 3D elastic structures. *Optimization and Engineering*, 25(3):1179–1202, 2023. [10.1007/s11081-023-09840-w](https://doi.org/10.1007/s11081-023-09840-w).
- [20] K. Burazin, I. Crnjac, and M. Vrdoljak. Optimality criteria method in 2D linearized elasticity problems. *Applied Numerical Mathematics*, 160:192–204, 2021. [10.1016/j.apnum.2020.10.002](https://doi.org/10.1016/j.apnum.2020.10.002).
- [21] K. Burazin, I. Crnjac, and M. Vrdoljak. Explicit Hashin–Shtrikman bounds in 3D linearized elasticity. *Filomat*, 38(17):6033–6048, 2024. [10.2298/fil2417033b](https://doi.org/10.2298/fil2417033b).
- [22] S. Czarnecki and T. Lewiński. A stress-based formulation of the free material design problem with the trace constraint and single loading condition. *Bulletin of the Polish Academy of Sciences: Technical Sciences*, 60(2):191–204, 2012. [10.2478/v10175-012-0026-5](https://doi.org/10.2478/v10175-012-0026-5).
- [23] S. Czarnecki and T. Lewiński. A stress-based formulation of the free material design problem with the trace constraint and multiple load conditions. *Structural and Multidisciplinary Optimization*, 49(5):707–731, 2014. [10.1007/s00158-013-1023-5](https://doi.org/10.1007/s00158-013-1023-5).
- [24] J. P. Groen and O. Sigmund. Homogenization-based topology optimization for high-resolution manufacturable microstructures. *International Journal for Numerical Methods in Engineering*, 113(8):1148–1163, 2017. [10.1002/nme.5575](https://doi.org/10.1002/nme.5575).
- [25] Z. Hashin and S. Shtrikman. A variational approach to the theory of the elastic behaviour of multiphase materials. *Journal of the Mechanics and Physics of Solids*, 11(2):127–140, 1963. [10.1016/0022-5096\(63\)90060-7](https://doi.org/10.1016/0022-5096(63)90060-7).
- [26] J. Haslinger, M. Kočvara, G. Leugering, and M. Stingl. Multidisciplinary free material optimization. *SIAM Journal on Applied Mathematics*, 70(7):2709–2728, 2010. [10.1137/090774446](https://doi.org/10.1137/090774446).
- [27] R. Hill. Elastic properties of reinforced solids: Some theoretical principles. *Journal of the Mechanics and Physics of Solids*, 11(5):357–372, 1963. [10.1016/0022-5096\(63\)90036-x](https://doi.org/10.1016/0022-5096(63)90036-x).
- [28] C. S. Jog, R. B. Haber, and M. P. Bendsøe. Topology design with optimized, self-adaptive materials. *International Journal for Numerical Methods in Engineering*, 37(8):1323–1350, 1994. [10.1002/nme.1620370805](https://doi.org/10.1002/nme.1620370805).
- [29] M. Kočvara and J. Zowe. Free material optimization: An overview. In A. H. Siddiqi and M. Kočvara, editors, *Trends in Industrial and Applied Mathematics*, pages 181–215. Kluwer Academic Publishers, Dordrecht, 2002. [10.1007/978-1-4613-0263-6_9](https://doi.org/10.1007/978-1-4613-0263-6_9).
- [30] M. Kočvara. Decomposition of arrow type positive semidefinite matrices with application to topology optimization. *Mathematical Programming*, 190(1–2):105–134, 2021. [10.1007/s10107-020-01526-w](https://doi.org/10.1007/s10107-020-01526-w).
- [31] M. Kočvara and M. Stingl. Free material optimization for stress constraints. *Structural and Multidisciplinary Optimization*, 33(4–5):323–335, 2007. [10.1007/s00158-007-0095-5](https://doi.org/10.1007/s00158-007-0095-5).

- [32] M. Kočvara and M. Stingl. Solving stress constrained problems in topology and material optimization. *Structural and Multidisciplinary Optimization*, 46(1):1–15, 2012. [10.1007/s00158-012-0762-z](https://doi.org/10.1007/s00158-012-0762-z).
- [33] M. Kočvara, M. Stingl, and J. Zowe. Free material optimization: Recent progress. *Optimization*, 57(1):79–100, 2008. [10.1080/02331930701778908](https://doi.org/10.1080/02331930701778908).
- [34] T. Lewiński. Optimum design of elastic moduli for the multiple load problems. *Archives of Mechanics*, 73:27–66, 2021. [10.24423/AOM.3607](https://doi.org/10.24423/AOM.3607).
- [35] R. Lipton. Optimal bounds on effective elastic tensors for orthotropic composites. *Proceedings of the Royal Society of London. Series A: Mathematical and Physical Sciences*, 444(1921):399–410, 1994. [10.1098/rspa.1994.0028](https://doi.org/10.1098/rspa.1994.0028).
- [36] M. Lobos and T. Böhlke. On optimal zeroth-order bounds of linear elastic properties of multiphase materials and application in materials design. *International Journal of Solids and Structures*, 84:40–48, 2016. [10.1016/j.ijsolstr.2015.12.015](https://doi.org/10.1016/j.ijsolstr.2015.12.015).
- [37] G. W. Milton. *The Theory of Composites*. Society for Industrial and Applied Mathematics, 2022. ISBN 9781611977486. [10.1137/1.9781611977486](https://doi.org/10.1137/1.9781611977486).
- [38] G. W. Milton and A. V. Cherkaev. Which elasticity tensors are realizable? *Journal of Engineering Materials and Technology*, 117(4):483–493, 1995. [10.1115/1.2804743](https://doi.org/10.1115/1.2804743).
- [39] N. Nees, L. Pflug, B. Mann, and M. Stingl. Multi-material design optimization of optical properties of particulate products by discrete dipole approximation and sequential global programming. *Structural and Multidisciplinary Optimization*, 66, 2023. [10.1007/s00158-022-03376-w](https://doi.org/10.1007/s00158-022-03376-w).
- [40] J. Nečas and I. Hlaváček. *Mathematical theory of elastic and elasto-plastic bodies: An introduction*. Elsevier Scientific Pub. Co., 1981.
- [41] O. Pantz and K. Trabelsi. A post-treatment of the homogenization method for shape optimization. *SIAM Journal on Control and Optimization*, 47(3):1380–1398, 2008. [10.1137/070688900](https://doi.org/10.1137/070688900).
- [42] P. Pedersen. On optimal orientation of orthotropic materials. *Structural Optimization*, 1(2):101–106, 1989. [10.1007/bf01637666](https://doi.org/10.1007/bf01637666).
- [43] U. T. Ringertz. On finding the optimal distribution of material properties. *Structural Optimization*, 5(4):265–267, 1993. [10.1007/bf01743590](https://doi.org/10.1007/bf01743590).
- [44] M. P. Rossow and J. E. Taylor. A finite element method for the optimal design of variable thickness sheets. *AIAA Journal*, 11(11):1566–1569, 1973. [10.2514/3.50631](https://doi.org/10.2514/3.50631).
- [45] J. Semmler, L. Pflug, and M. Stingl. Material optimization in transverse electromagnetic scattering applications. *SIAM Journal on Scientific Computing*, 40(1):B85–B109, 2018. [10.1137/17M1127569](https://doi.org/10.1137/17M1127569).
- [46] O. Sigmund. Materials with prescribed constitutive parameters: An inverse homogenization problem. *International Journal of Solids and Structures*, 31(17):2313–2329, 1994. [10.1016/0020-7683\(94\)90154-6](https://doi.org/10.1016/0020-7683(94)90154-6).
- [47] M. Stingl, M. Kočvara, and G. Leugering. A sequential convex semidefinite programming algorithm with an application to multiple-load free material optimization. *SIAM Journal on Optimization*, 20(1):130–155, 2009. [10.1137/070711281](https://doi.org/10.1137/070711281).
- [48] M. Stingl, M. Kočvara, and G. Leugering. Free material optimization with fundamental eigenfrequency constraints. *SIAM Journal on Optimization*, 20(1):524–547, 2009. [10.1137/080717122](https://doi.org/10.1137/080717122).
- [49] M. Tyburec, M. Doškář, J. Zeman, and M. Kružík. Modular-topology optimization of structures and mechanisms with free material design and clustering. *Computer Methods in Applied Mechanics and Engineering*, 395:114977, 2022. [10.1016/j.cma.2022.114977](https://doi.org/10.1016/j.cma.2022.114977).

- [50] M. Tyburec, M. Doškář, M. Somr, M. Kružík, and J. Zeman. Modular-topology optimization for additive manufacturing of reusable mechanisms. *Computers & Structures*, 307:107630, 2025. [10.1016/j.compstruc.2024.107630](https://doi.org/10.1016/j.compstruc.2024.107630).
- [51] B. N. Vu, V. Lukeš, M. Stingl, and E. Rohan. A sequential global programming approach for two-scale optimization of homogenized multiphysics problems with application to Biot porous media. *Structural and Multidisciplinary Optimization*, 66, 2023. [10.1007/s00158-023-03659-w](https://doi.org/10.1007/s00158-023-03659-w).
- [52] J. Wu, O. Sigmund, and J. P. Groen. Topology optimization of multi-scale structures: A review. *Structural and Multidisciplinary Optimization*, 63(3):1455–1480, 2021. [10.1007/s00158-021-02881-8](https://doi.org/10.1007/s00158-021-02881-8).
- [53] X. Yang and M. Li. Free isotropic material optimization via second order cone programming. *Computer-Aided Design*, 115:52–63, 2019. [10.1016/j.cad.2019.05.002](https://doi.org/10.1016/j.cad.2019.05.002).
- [54] J. Zowe, M. Kočvara, and M. P. Bendsøe. Free material optimization via mathematical programming. *Mathematical Programming*, 79(1–3):445–466, 1997. [10.1007/bf02614328](https://doi.org/10.1007/bf02614328).